Large Polymers that Behave Like Small Polymers

Meredith Pomfret

A dissertation submitted in partial fulfillment of the requirements for the degree of

Doctor of Philosophy

University of Washington

2024

Reading Committee:

Matthew Golder, Chair

Alshakim Nelson

Forrest Michael

Program Authorized to Offer Degree:

Chemistry

University of Washington

Abstract

Large Polymers that Behave Like Small Polymers

Meredith Pomfret

Chair of the Supervisory Committee:
Matthew Golder
Department of Chemistry

Polymer architecture dictates the physical properties and therefore the function of a material. Consequently, structural changes in the polymer backbone have drastic influences on macromolecular physical properties. For example, rigid monomer units create stiff polymer chains with excellent thermal and mechanical properties, at the expense of processability. Meanwhile, flexible monomer units like ethylenes and siloxanes create soft, flexible plastics at the expense of thermal and mechanical robustness. Synthesizing polymers with novel architectures can overcome these challenges by creating materials with a unique set of properties and thus eliminating the trade-off between chain flexibility and desirable macromolecular physical properties. Detailed within this thesis are our reports of modulating backbone architecture of linear polymers using fluxional monomer units. Additionally, we explore the synthesis of cyclic polymer architectures using ring expansion metathesis polymerization (REMP) through catalyst design and mechanistic studies. First, we demonstrate that small molecule pericyclic rearrangements in bullvalene monomer units creates stochastic kinks in an otherwise rigid polymer backbone. This unique chain architecture results in lower hydrodynamic volumes and decreased thermal transitions. Next, we

investigate a different, but also compact, polymer architecture by investigating the REMP mechanism and the role of chain transfer events in molecular weight evolution and size of the cyclic polymer products. Finally, we investigate the structure-function relationship of REMP catalysts by modifying tether length and studying the resulting polymerization profiles. Tether length was found to have a significant effect on REMP rate, providing further understanding on these processes. Through these studies, we elucidate valuable information on REMP polymerization profiles and catalyst behavior, providing insight for future optimization of the synthesis of cyclic polymers.

Acknowledgements

None of this work would have been possible without the endless support from my family, friends, and mentors. The best science comes from a strong community and a strong team. I am incredibly grateful for everyone who has provided guidance, encouragement, and joy in the past five years.

First, I want to thank my wonderful team in the Golder group, both past and current members. I feel so lucky that I got to work with such excellent scientists and people. You have challenged me, taught me so much, and helped me create memories I will cherish for the rest of my life. I am so proud of the team we have built and am excited to see all your future successes. Sarah, I couldn't imagine going through this journey with anyone else. Your kindness, generosity and intelligence has always been an inspiration to me and I am grateful to have a friend like you. From building Schlenk lines and desks to becoming doctors, I am thankful that you have been with me the whole way!

Matt, thank you for going above and beyond as a mentor to me for the past five years. Thank you for seeing potential in me even when I was at my lowest points and encouraging me when I needed it the most. Your enthusiasm about science is contagious, and I always look forward to our science chats and brainstorming sessions. I feel lucky to be a part of this team and am excited to see where it goes in the future.

To my mentors at Stonehill, thank you for providing the strongest foundation I could ask for, encouraging me to achieve my goals, and providing support long after I graduated. Professor Liotta, thanks for showing me how awesome organic chemistry is. Thank you for always holding me to a high standard and showing me that I am capable of more than I believe. Prof. Lombardi, Prof. Hall, Prof. Harris, Prof. Hinkle and Prof. Pederson, thank you for being amazing role models and inspiring me as strong and powerful women in chemistry. Prof. Del Sesto, Prof Tilley, and Prof. Rogers, thank you for everything you have taught me, both inside and outside the lab, and providing endless encouragement.

To my friends in Massachusetts, thank you all for showing me that 3,000 miles has nothing on the strength of our friendship. I feel lucky that every time we see each other, it's like we never had any time apart. Zahra and Jullian, thank you for staying by my side since we were literal children, always making me laugh, and loving me through some of my most embarrassing phases. Gavin, Erin, Stephanie, and Katie, thank you for making everything fun, all the adventures at Shields and beyond, and showing me that our friendship is stronger than any physical distance. I love you all!

To new and old friends in Washington, thank you for being a source of joy during a very intense time in my life. Nick, thank you for taking us on adventures and making sure I spend some time outside of the lab. Ari and Greg, thank you for being a solid support system for us and making

sure we touch grass once in awhile! Alex D., thank you for talking shop with me and arguing about initiators and catalysts- these are some of my fondest memories from grad school. Mercie, I am so grateful our friendship has developed and flourished outside of the lab. Thank you for being such a wonderful person and brilliant scientist. To my church family at the Hallows, thank you for showing me unconditional acceptance and welcoming me in with open arms, and reminding me of what is truly important. Your love and support got me through the end of grad school and I will always cherish that.

To my parents, thank you for everything you have done to get me where I am now. You inspire me to take risks, follow my dreams, and enjoy life through it all. Thank you for visiting me and always being so accommodating through this phase of my life. I love you so much. Garret, thank you for making my life lighter with your wit and sense of humor. Mikaela, thank you for inspiring me by being a strong, independent, and intelligent woman. You both are my best friends. Thank you to all four of my grandparents for being one of the most important parts of my life. You bring me so much joy and I am so thankful that you helped build a foundation for where I am now.

Alex, my husband and most important person in my life, thank you for your unconditional love and support. Thank you for always being by my side, supporting me through the low points and celebrating with me though the highs. Thank you for your patience, your sense of humor, and your willingness to support my craziest ideas and lofty goals. Thank you for grounding me and reminding me of what is most important in life. I truly could not have accomplished this without you. I love you and am grateful for you every day.

Table of Contents

Table of Figures

Table of Schemes

Table of Tables

Chapter 1: Introduction

1.1 Structure-function relationships in polymers

Polymer architecture influences their physical properties and functions. This can be observed in both natural and synthetic polymers; for example the amino acid sequence of enzymes allows for unique folding through non-covalent bonds. The complex topologies of natural polymers have long served as inspiration to polymer scientists to develop novel architectures in synthetic polymers for a broad range of applications (Figure 1.1).[1] While synthetic polymer architecture is not as intricate and complex as those of natural polymers, emerging synthetic methodology and polymerization methods allows for some topological control. For example, in polymer networks individual chains are connected by physical or covalent cross-links, resulting in superior mechanical strength and thermal stability.[2] Multifunctional monomer units can also be used to create branching in polymer chains, allowing for the formation of dendrimers, star polymers, and brush polymers.[3]

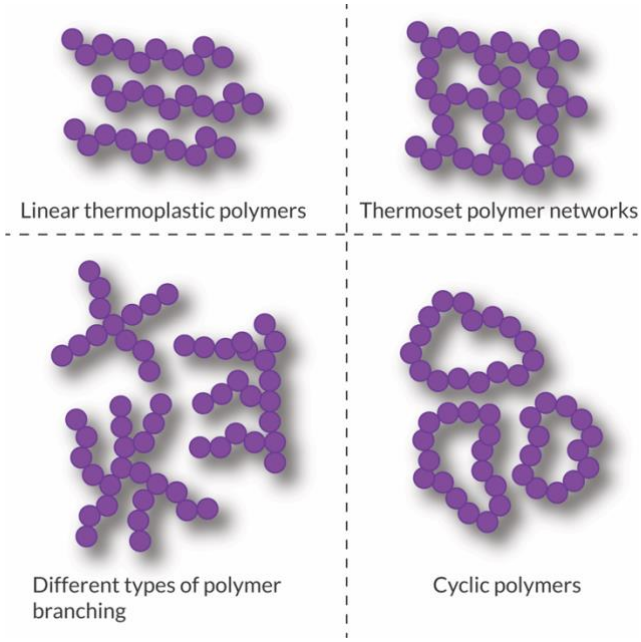

Figure 1.1. Structural complexities in synthetic polymers

In these hyperbranched polymers, high chain density leads to opportunities in post-polymerization functionalization, surface modification, and applications in coatings, drug delivery, medicine, and electronics.[4] On the other hand, cyclic polymers have no chain ends, resulting in decreased viscosity along with superior thermal stability. Polymer architecture can also be controlled by harnessing supramolecular interactions. Brush and block copolymers spontaneously self-assemble into unique morphologies through non-covalent interactions. Similarly, single chain nanoparticles experience intramolecular bonding that drives folding of the polymer chain into a compact nanostructure. Despite these recent advances, synthetic polymers do not approach the topological complexity of natural polymers and further work is needed in designing novel macromolecular structure

1.2 Tuning polymer architecture in linear polymers

In linear polymers, chain architecture and macromolecular physical properties can be dictated by the rigidity of each monomer unit. For semiflexible polymers (e.g., polydimethylsiloxane, polyethylene), covalent bond rotational freedom allows for segmental chain motion to increase solubility and depress glass transition temperatures (T_g) via an increase in free volume.[5] These flexible polymers are useful as plastics, rubbers, and textiles. On the other hand, rigid π-rich materials have extended backbones and decreased free volumes which manifest in higher T_gs alongside superior thermal and mechanical stability.[6] Related high T_g saturated analogs can be accessed from hydrocarbon isosteres[7] such as adamantane,[8] propellane,[9] cubane,[10] norbornadiene.[11] Because of their desirable physical properties, rigid polymers are

useful in electronics, solar cells, aerospace, construction, and impact-resistant materials. For these polymers, rigidity comes at the

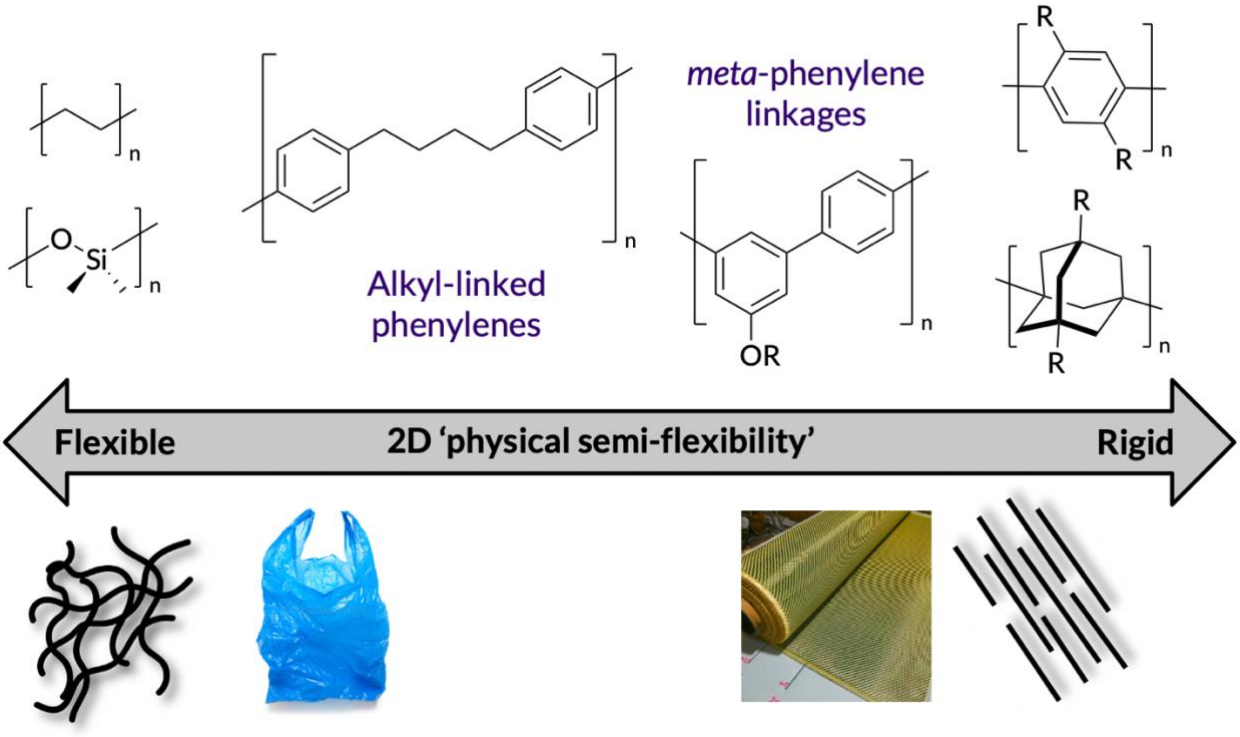

Figure 1.2. Macromolecular architectures of linear polymers

expense of low solubility, high thermal transitions, and chain immobility, leading to harsh synthetic conditions and difficulties in processing these materials.[12] Therefore, there is a need for flexible and processable materials that also display robust mechanical properties. Adding solubilizing size chains to conjugated polymers can help overcome difficulties in processing and synthesis, however this is at the expense of effective charge transport and mechanical stability.[13] Adding conformational freedom to rigid backbones through conjugation break spacers is another approach to modulate physical properties. Alkyl chains can bridge rigid domains in hydrocarbon materials to increase solubility and decrease T_g (e.g., stretchable

electronics).[14] This molecular design relies on the conformational flexibility of alkyl chains to modulate accessible backbone geometries, however these materials still exhibit high melting temperatures, low solubility, and potentially unwanted crystalline domains (Table 1.1).[15]

Polymer	Name	$\frac{T_m(\text{exp})}{^\circ C}$	$\frac{T_m(\text{calc})}{^\circ C}$	Processability
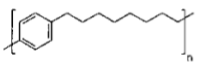	**PPPO**	90	n.a.[a)]	Tractable
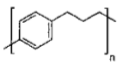	**PPPPr**	110–130	n.a.[b)]	Tractable
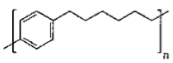	**PPPH**	120	127[c)]	Tractable
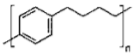	**PPPB**	200–225	202[c)]	Tractable
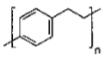	**PPX**	425	n.a.[a)]	Intractable
	**PPPM**	n.a.[d)]	>1 000[e)]	Intractable
	**PPP**	n.a.[d)]	>1 000[e)]	Intractable

Table 1.1. Poly(phenylenes) with conjugation break spacers of varying lengths with high melting temperatures. Adapted with permission from De Rosa, C.; Malafronte, A.; Auriemma, F.; Scoti, M.; Di Girolamo, R.; D'Alterio, M. C.; Ricci, G.; Zanchin, G.; Leone, G. Synthesis, Chain Conformation and Crystal Structure of Poly(Norbornadiene) Having Repeating 3,5-Enchained Nortricyclene Units. *Polym. Chem.* **2019**, *10* (33), 4593. Copyright RSC journals 2019.

Regardless, these flexible linkers have been introduced to polyphenylene vinylene to gain control over conjugation length and the self-assembly of these polymers into crystalline domains; changing the length of the flexible segment resulted in varied interchain interactions in these polymers.[16] This approach has also been used in other semiconducting polymers tune viscoelastic properties to enable melt processing of these materials; large flexible domains create amorphous regions in the material.[17,18] However, higher ratios of amorphous domains lead to lower charge

mobility, decreasing the performance of these materials.[19] Another use of conjugation break spacers involves the incorporation of adamantane and diadamantanes to direct chains into bent and linear morphologies, respectively.[20] Atomic force microscopy showed that thin film morphologies were drastically different between the two polymers, with diadamantanes producing a more ordered structure. This example highlights how small structural changes in a polymer chain can influence macromolecular properties and self-assembly.

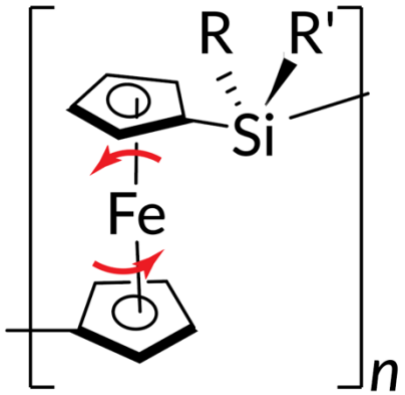

Figure 1.3. Poly(ferrocenosilane) structure

Poly(ferrocenosilanes) are another class of polymer that relies on bond rotation to achieve conformational flexibility in a polymer backbone.[21,22] The freely-rotating ferrocene monomer unit creates an easily polymer with unique self-assembly, charge transport, and magnetic properties.[23–26] An alternative approach relies on combining rigid monomers with different bonding angles (e.g., phenylene regioisomers) to achieve backbone kinks without sacrificing thermal stability.[27] For poly(m-phenylene)s, solubility increases relative to poly(p-phenylene)s due to diminished π-stacking but T_gs remain high (e.g., Mw=27 kDa, T_g=149 °C).[28] For poly(o-phenylenes), intramolecular pi-stacking drives self-assembly into well-defined helices, introducing a new class of polymers called foldamers.[29,30]

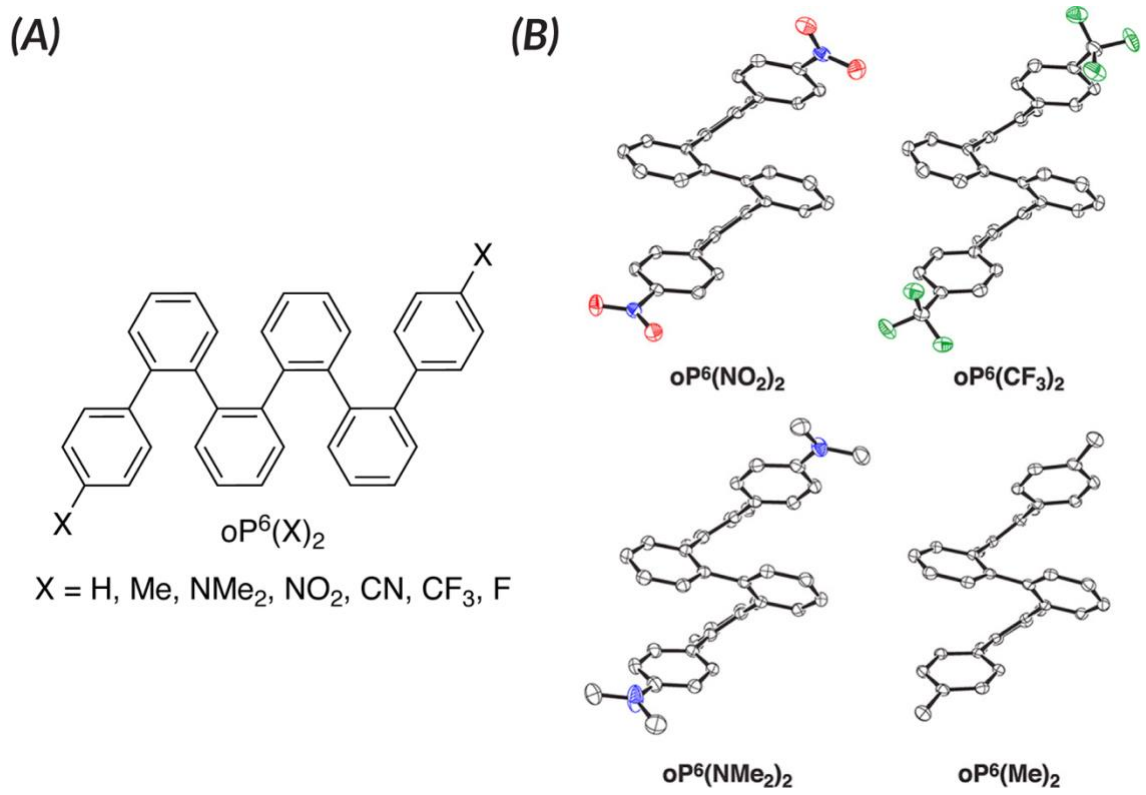

Figure 1.4. (A) General structure of poly(*o*-phenylene) model compounds and (B) ORTEP representations (50% ellipsoid probability) of the crystal structures of oP6(NO2)2, oP6(CF3)2, oP6(NMe2)2, and oP6(Me2)2. Reprinted (adapted) with permission from Mathew, S. M.; Engle, J. T.; Ziegler, C. J.; Hartley, C. S. The Role of Arene-Arene Interactions in the Folding of Ortho-Phenylenes. *J. Am. Chem. Soc.* **2013**, *135* (17), 6714.

All of the examples above rely on *physical* transformations (e.g., bond rotation) to achieve conformational freedom, which usually results in a trade-off between backbone flexibility and desirable thermal and mechanical properties. *Chemical* transformations (e.g., pericyclic rearrangements) could provide an alternative approach to access unique polymer architectures that are not reliant on the conformational freedom of the system.

1.3 Cyclic polymers

Cyclic polymers are another unique and captivating macromolecular topology due to their unusual physical properties.[31] Cyclic polymers were first identified in nature as cyclic DNA and peptides and have remained a resource for studying structure-function relationships in macromolecules and designing new materials.[32–34] The lack of chain ends in these polymers result in a lower hydrodynamic radii,[35] slower degradation profile,[27] and unique self-assembly behavior[37–39] compared to their linear counterparts. For example, cyclic polystyrene and polyisoprene block polymers have been shown to assemble into spherical, worm-like, or flower-like structures, while cyclic brush polymers have been shown to assemble into supramolecular tubes.[40–43] Due to their unique properties, these polymers have emerging applications in drug-delivery,[44] biomaterials,[45] semiconducting materials,[46] and nanolithography,[47]. Despite recent advancements in the synthesis of these polymers, the full potential of their applications have not yet been realized; there is still work to be done in determining efficient, controlled methods to make these polymers.

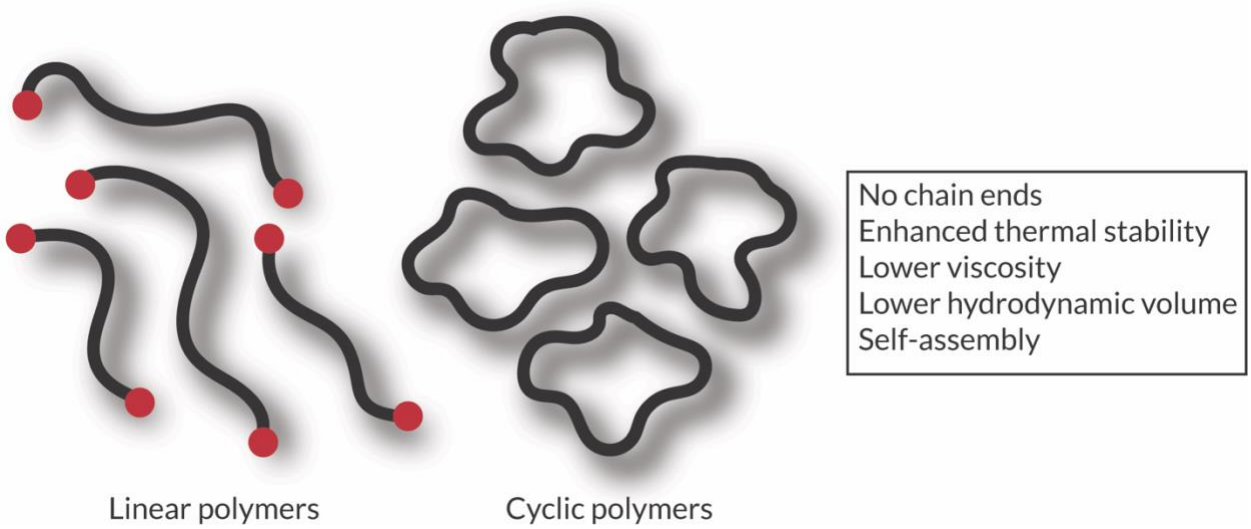

Figure 1.5. Cyclic polymers have different properties than their linear counterparts

Cyclic topologies can be accessed through acyclic ring closure or ring expansion polymerization (REP). Using the acyclic ring closure approach, polymers are usually prepared through a controlled polymerization followed by a bimolecular or unimolecular ring closure. In a bimolecular ring closure, cyclization occurs when a bifunctional coupling agent couples to functionalized polymer chain ends. Cyclic polytetrahydrofuran was synthesized using this approach; the chain ends of linear polytetrahydrofuran were functionalized with a strained N-phenylpyrrolidinium cation and were coupled with an anionic dicarboxylate.[36] In a unimolecular ring closure, functionalized chain ends are coupled directly in an intramolecular reaction. For example, cyclic polystyrene (PS) can be synthesized using ATRP to generate linear PS followed by chain end functionalization and a 'click' cyclization.[48] Unfortunately, the size of cyclic polymers that can be made using acyclic ring closure is limited and requires dilute conditions to avoid intermolecular chain coupling and linear impurities.

REP involves the repeated addition of monomer into a cyclic initiator, maintaining the cyclic topology throughout the polymerization. This strategy is advantageous because it avoids the entropic penalties involved in ring closing strategies, allowing access to high molecular weight polymers with high topological purity. Examples of REP include polymerizations of lactones and

lactides using cyclic tin initiators[49]. One disadvantage of these approaches is that the initiator is retained in the final polymer structure.

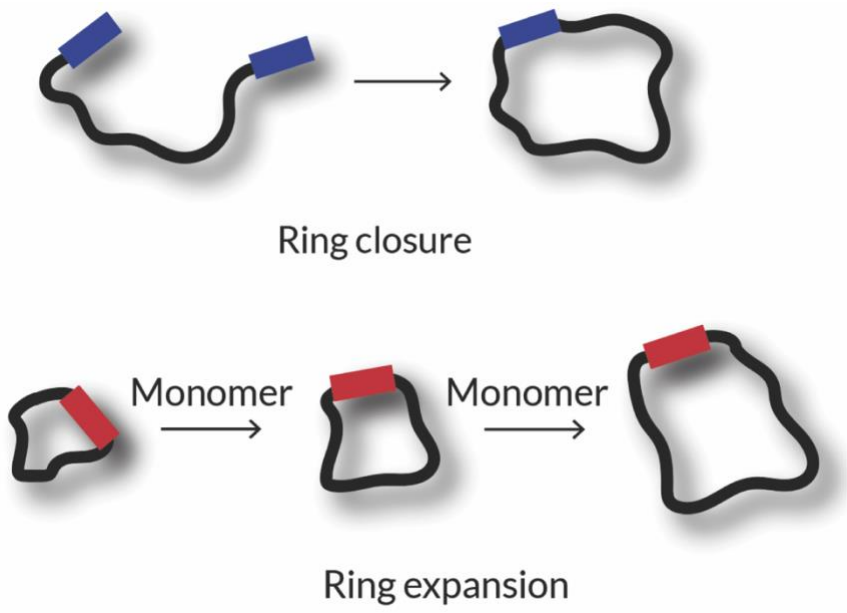

Figure 1.6. Ring expansion and ring closure approaches to making cyclic polymers

1.4 Ring Expansion Metathesis Polymerization

One of the most notable methods of REP is ring expansion metathesis polymerization, which involves a cyclic metal carbene complex that can undergo metathesis with strained cyclic monomers, followed by a backbiting termination event producing high purity cyclic polymer without initiator incorporation. This approach is based on ring opening metathesis polymerization, which produces primarily linear polymers, but can produce some cyclic byproducts through intramolecular backbiting. One of the first reports from Grubbs uses a six-carbon tethered Ru-alkylidene complex to synthesize cyclic polycyclooctene.[50] Since then, subsequent versions of this initiator have been made with varying tether length and saturation of the N-heterocyclic carbene resulting in differences in REMP kinetics between the initiators.[51] However, the Ru-alkylidene

initiators suffer from lack of stability, slow initiation rates, and poor molecular weight control of resulting polymers. Commercially available Hoveyda-Grubbs II catalyst has also been used to produce cyclic polymers due to its propensity for backbiting during ROMP. Sampson first demonstrated that alternating ROMP of cyclohexenes and cyclobutenes using Hoveyda Grubbs II produces primarily cyclic polymers.[52] Subsequently, Qiao showed that Hoveyda Grubbs' II produced cyclic oligocyclooctenes in high purity under the critical monomer concentration.[53]

Inspired by design principles of Grubbs' G2 and G3 catalysts, our group designed a novel cyclic benzylidene initiator (CB6) featuring a bulky NHC to address shortcomings present in previous state-of-the-art REMP initiators.[54] These features enhanced initiator stability and enabled more control over polymerizations of norbornene derivatives. Installing pyridine as a more labile ancillary ligand introduced further improvements by eliminating molar mass evolution leading to lower dispersities and decreasing overall reaction time.[55] However, these Ru-benzylidenes have not been optimized to the same extent as state-of-the-art ROMP initiators; more investigation needs to be done to determine how small structural changes in these initiators can impact the overall REMP polymerization profile.

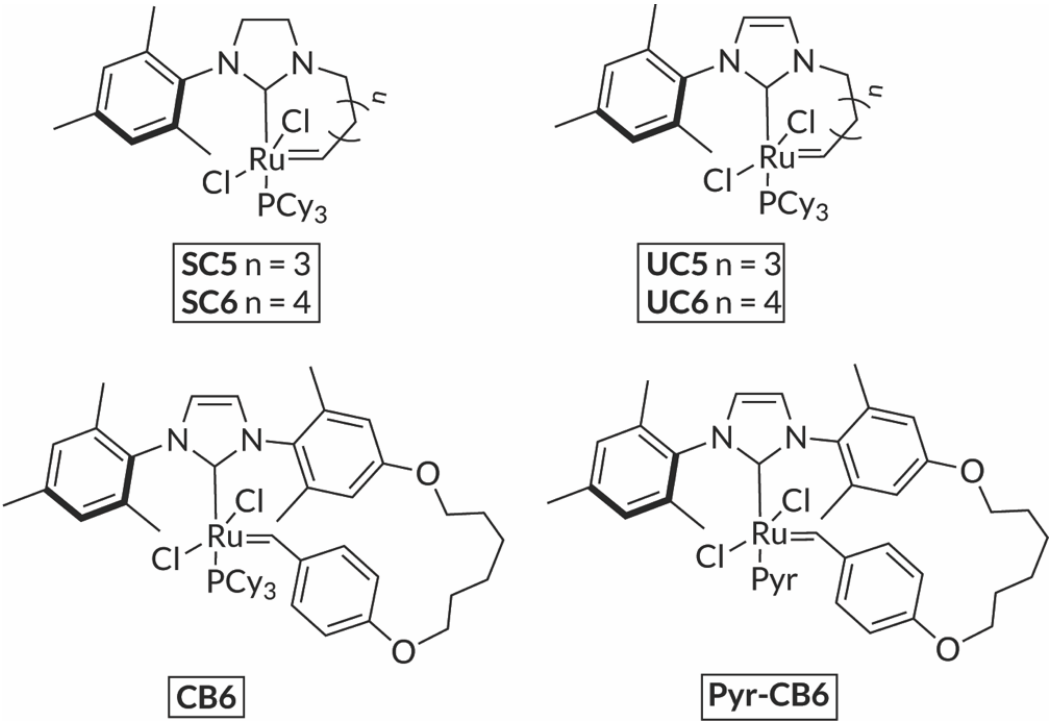

Figure 1.7. Structures of different Ru-based REMP catalysts

Cyclic Mo[56] and W[57–60] initiators have also been used to polymerize both alkenes and alkynes, albeit with low functional group tolerance. Sumerlin and Veige designed a tethered W alkylidyne initiator capable of polymerizing alkynes[57] or undergoing ynene metathesis,[59] producing cyclic polymers with high stereoregularity. Post-polymerization modification of these cyclic polymers produced cyclic poly(propylene).[61] These tungsten initiators have also been used to synthesize the first cyclic poly(acetylene), opening up the opportunity for applications in flexible electronics.[62] Similarly, Fisher developed a tethered Mo carbyne to polymerize strained alkynes, enabling access to a fully conjugated cyclic poly(o-phenylene ethynylene).[56] While Mo and W initiators provide an opportunity for alkyne metathesis and access to a variety of conjugated cyclic polymers, they are limited to mainly hydrocarbon feedstocks.

1.5 Dissertation summary

In this dissertation I will outline the work I have conducted in the Golder lab to contribute to the growing field of polymers with unique architectures.

First, we investigate how fluxional building blocks can modulate the architecture of linear polymers. We incorporate bullvalene, a molecule capable of undergoing room temperature Hardy-Cope rearrangements, into a poly(phenylene) chain. We measure how these building blocks affect the bulk thermal transitions, thermal stability, and solution-state processability of the resulting polymers. We reveal that bullvalene introduces stochastic kinks in the polymer backbone, resulting in lower hydrodynamic volumes than expected for a given molecular weight. Other attempts at bullvalene containing polymers will be highlighted along with ongoing work on investigating the origin of the thermal stability of bullvalene.

Next, we investigate cyclic polymers, which are another unique topology that appear smaller in solution than they actually are. To gain a deeper understanding of REMP processes to make these polymers, we conduct mechanistic studies using the CB6 catalyst. We examine molecular weight evolution profiles and initiator consumption over the course of the polymerization to gain more insight on the mechanistic steps and relative rates of different REMP events. We also investigate concentration dependence of REMP with CB6 to gain more control of equilibrium molecular weight of the resulting cyclic polymers. This work expands our knowledge of the different factors at play in determining the polymerization profiles, laying groundwork for future developments in this field. Deeper mechanistic understanding of REMP provides insight for work in initiator design and methods of controlling polymerizations.

To follow up on our mechanistic studies, we begin to investigate the structure-function relationship of cyclic benzylidene REMP catalysts by synthesizing a series of catalysts with

different tether lengths. We measured structural differences between the catalysts along with time studies to measure molecular weight evolution. We measured stark differences in REMP rates between the three catalysts, demonstrating that small changes in initiator structure can affect the overall polymerization profile. Advancements in initiator design will further deeper our understanding of REMP processes and expand the scope of cyclic polymers that can be made. Overall, this work highlights how small structural changes can have a large-scale impact in macromolecular properties.

1.6 References

(1) Romio, M.; Trachsel, L.; Morgese, G.; Ramakrishna, S. N.; Spencer, N. D.; Benetti, E. M. Topological Polymer Chemistry Enters Materials Science: Expanding the Applicability of Cyclic Polymers. *ACS Macro Lett.* **2020**, *9* (7), 1024–1033. https://doi.org/10.1021/acsmacrolett.0c00358.

(2) Gu, Y.; Zhao, J.; Johnson, J. A. Polymer Networks: From Plastics and Gels to Porous Frameworks. *Angew. Chemie Int. Ed.* **2020**, *59* (13), 5022–5049. https://doi.org/10.1002/anie.201902900.

(3) Zheng, Y.; Li, S.; Weng, Z.; Gao, C. Hyperbranched Polymers: Advances from Synthesis to Applications. *Chem. Soc. Rev.* **2015**, *44* (12), 4091–4130. https://doi.org/10.1039/c4cs00528g.

(4) Gao, C.; Yan, D. Hyperbranched Polymers: From Synthesis to Applications. *Prog. Polym. Sci.* **2004**, *29* (3), 183–275. https://doi.org/10.1016/J.PROGPOLYMSCI.2003.12.002.

(5) Lodge, T. P.; Hiemenz, P. C. *Polymer Chemistry*, 3rd ed.; CRC Press, 2020.

(6) Chae, H. G.; Kumar, S. Rigid-Rod Polymeric Fibers. *J. Appl. Polym. Sci.* **2006**, *100* (1), 791–802. https://doi.org/10.1002/app.22680.

(7) Locke, G. M.; Bernhard, S. S. R.; Senge, M. O. Nonconjugated Hydrocarbons as Rigid-Linear Motifs: Isosteres for Material Sciences and Bioorganic and Medicinal Chemistry. *Chem. - A Eur. J.* **2019**, *25* (18), 4590–4647. https://doi.org/10.1002/chem.201804225.

(8) Inomata, S.; Matsuoka, S. I.; Sakai, S.; Tajima, H.; Ishizone, T. Ring-Opening Polymerizations of 1,3-Dehydroadamantanes: Synthesis of Novel Thermally Stable Poly(1,3-Adamantane)S. *Macromolecules* **2012**, *45* (10), 4184–4195. https://doi.org/10.1021/ma300395s.

(9) Schlüter, A. D. Poly([1.1.1]Propellane).1 A Novel Rigid-Rod Polymer Obtained by Ring-Opening Polymerization Breaking a Carbon-Carbon σ-Bond. *Macromolecules* **1988**, *21* (5), 1208–1211. https://doi.org/10.1021/ma00183a004.

(10) Eaton, P. E. Cubanes: Starting Materials for the Chemistry of the 1990s and the New Century. *Angew. Chemie Int. Ed. English* **1992**, *31* (11), 1421–1436. https://doi.org/10.1002/anie.199214211.

(11) De Rosa, C.; Malafronte, A.; Auriemma, F.; Scoti, M.; Di Girolamo, R.; D'Alterio, M. C.;

Ricci, G.; Zanchin, G.; Leone, G. Synthesis, Chain Conformation and Crystal Structure of Poly(Norbornadiene) Having Repeating 3,5-Enchained Nortricyclene Units. *Polym. Chem.* **2019**, *10* (33), 4593–4603. https://doi.org/10.1039/c9py00757a.

(12) Wang, D. H.; Jiang, H.; Adams, W. W. Rigid-Rod Polymers. In *Encyclopedia of Polymer Science and Technology*; John Wiley & Sons, Inc.: Hoboken, NJ, USA, 2011. https://doi.org/10.1002/0471440264.pst323.pub2.

(13) Xie, R.; Weisen, A. R.; Lee, Y.; Aplan, M. A.; Fenton, A. M.; Masucci, A. E.; Kempe, F.; Sommer, M.; Pester, C. W.; Colby, R. H.; Gomez, E. D. Glass Transition Temperature from the Chemical Structure of Conjugated Polymers. *Nat. Commun.* **2020**, *11* (1), 4–11. https://doi.org/10.1038/s41467-020-14656-8.

(14) Galuska, L. A.; McNutt, W. W.; Qian, Z.; Zhang, S.; Weller, D. W.; Dhakal, S.; King, E. R.; Morgan, S. E.; Azoulay, J. D.; Mei, J.; Gu, X. Impact of Backbone Rigidity on the Thermomechanical Properties of Semiconducting Polymers with Conjugation Break Spacers. *Macromolecules* **2020**, *53* (14), 6032–6042. https://doi.org/10.1021/acs.macromol.0c00889.

(15) Steiger, D.; Tervoort, T.; Weder, C.; Smith, P. Poly(p-Phenylene Alkylene)s – A Forgotten Class of Polymers. *Macromol. Rapid Commun.* **2000**, *21* (8), 405–422. https://doi.org/10.1002/(SICI)1521-3927(20000501)21:8<405::AID-MARC405>3.0.CO;2-J.

(16) Zhu, X.; Traub, M. C.; Vanden Bout, D. A.; Plunkett, K. N. Well-Defined Alternating Copolymers of Oligo(Phenylenevinylene)s and Flexible Chains. *Macromolecules* **2012**, *45* (12), 5051–5057. https://doi.org/10.1021/ma300430e.

(17) Zhao, Y.; Zhao, X.; Roders, M.; Gumyusenge, A.; Ayzner, A. L.; Mei, J. Melt-Processing of Complementary Semiconducting Polymer Blends for High Performance Organic Transistors. *Adv. Mater.* **2017**, *29* (6). https://doi.org/10.1002/adma.201605056.

(18) Zhao, Y.; Zhao, X.; Zang, Y.; Di, C. A.; Diao, Y.; Mei, J. Conjugation-Break Spacers in Semiconducting Polymers: Impact on Polymer Processability and Charge Transport Properties. *Macromolecules* **2015**, *48* (7), 2048–2053. https://doi.org/10.1021/acs.macromol.5b00194.

(19) Savagatrup, S.; Zhao, X.; Chan, E.; Mei, J.; Lipomi, D. J. Effect of Broken Conjugation on the Stretchability of Semiconducting Polymers. *Macromol. Rapid Commun.* **2016**, *37* (19), 1623–1628. https://doi.org/10.1002/marc.201600377.

(20) Zhu, X.; Shao, B.; Vanden Bout, D. A.; Plunkett, K. N. Directing the Conformation of Oligo(Phenylenevinylene) Polychromophores with Rigid, Nonconjugatable Morphons. *Macromolecules* **2016**, *49* (10), 3838–3844. https://doi.org/10.1021/acs.macromol.6b00067.

(21) Hailes, R. L. N.; Oliver, A. M.; Gwyther, J.; Whittell, G. R.; Manners, I. Polyferrocenylsilanes: Synthesis, Properties, and Applications. *Chem. Soc. Rev.* **2016**, *45* (19), 5358–5407. https://doi.org/10.1039/c6cs00155f.

(22) Bellas, V.; Rehahn, M. Polyferrocenylsilane-Based Polymer Systems. *Angew. Chemie - Int. Ed.* **2007**, *46* (27), 5082–5104. https://doi.org/10.1002/anie.200604420.

(23) Kulbaba, K.; Macdonald, P. M.; Manners, I. Molecular Motions in Poly(Ferrocenes): Solid-State Deuterium NMR Studies of Poly(Ferrocenylsilanes) near Their Glass Transition Temperature. *Macromolecules* **1999**, *32* (4), 1321–1324. https://doi.org/10.1021/ma9816867.

(24) Smith, C. W.; Tan, K. H.; Evans, K. E.; Resendes, R.; Bartole-Scott, A.; Manners, I.

Mechanical Properties of the Novel Organometallic Polymer Poly(Ferrocenyldimethylsilane). *J. Polym. Sci. Part B Polym. Phys.* **2005**, *43* (17), 2280–2288. https://doi.org/10.1002/polb.20495.

(25) Manners, I. Poly (Ferrocenylsilanes): Novel Organometallic Plastics. *Chem. Commun.* **1999**, 857–865. https://doi.org/10.1039/A810043H.

(26) Foucher, D. A.; Tang, B. Z.; Manners, I. Ring-Opening Polymerization of Strained, Ring-Tilted Ferrocenophanes: A Route to High-Molecular-Weight Poly(Ferrocenylsilanes). *J. Am. Chem. Soc.* **1992**, *114* (15), 6246–6248. https://doi.org/10.1021/ja00041a053.

(27) Deffner, B.; Jimaja, S.; Kroeger, A.; Schlüter, A. D. Tensile Behavior of a Substituted Poly(m-,p-Phenylene) versus Its Parent Counterpart and Synthesis of Related Polyarylenes. *Macromol. Chem. Phys.* **2017**, *218* (5), 1–7. https://doi.org/10.1002/macp.201600561.

(28) Kandre, R.; Feldman, K.; Meijer, H. E. H.; Smith, P.; Schlüter, A. D. Suzuki Polycondensation Put to Work: A Tough Poly(Meta-Phenylene) with a High Glass-Transition Temperature. *Angew. Chemie - Int. Ed.* **2007**, *46* (26), 4956–4959. https://doi.org/10.1002/anie.200700966.

(29) Mathew, S. M.; Engle, J. T.; Ziegler, C. J.; Hartley, C. S. The Role of Arene-Arene Interactions in the Folding of Ortho-Phenylenes. *J. Am. Chem. Soc.* **2013**, *135* (17), 6714–6722. https://doi.org/10.1021/ja4026006.

(30) Mathew, S.; Crandall, L. A.; Ziegler, C. J.; Hartley, C. S. Enhanced Helical Folding of Ortho-Phenylenes through the Control of Aromatic Stacking Interactions. *J. Am. Chem. Soc.* **2014**, *136* (47), 16666–16675. https://doi.org/10.1021/ja509902m.

(31) Wang, T.; Golder, M. R. Advancing Macromolecular Hoop Construction: Recent Developments in Synthetic Cyclic Polymer Chemistry. *Polym. Chem.* **2021**, *12*, 958–969. https://doi.org/10.1039/d0py01655a.

(32) Haque, F. M.; Grayson, S. M. The Synthesis, Properties and Potential Applications of Cyclic Polymers. *Nat. Chem.* **2020**, *12*, 433–444. https://doi.org/10.1038/s41557-020-0440-5.

(33) Yamamoto, T. Synthesis of Cyclic Polymers and Topology Effects on Their Diffusion and Thermal Properties. *Polym. J.* **2013**, *45* (7), 711–717. https://doi.org/10.1038/pj.2012.213.

(34) Ochs, J.; Pagnacco, C. A.; Barroso-Bujans, F. Macrocyclic Polymers: Synthesis, Purification, Properties and Applications. *Prog. Polym. Sci.* **2022**, *134*, 101606. https://doi.org/https://doi.org/10.1016/j.progpolymsci.2022.101606.

(35) Dodgson, K.; Sympson, D.; Semlyen, J. A. Studies of Cyclic and Linear Poly(Dimethyl Siloxanes): 2. Preparative Gel Permeation Chromatography. *Polymer (Guildf).* **1978**, *19* (11), 1285–1289. https://doi.org/10.1016/0032-3861(78)90306-3.

(36) Honda, S.; Yamamoto, T.; Tezuka, Y. Topology-Directed Control on Thermal Stability: Micelles Formed from Linear and Cyclized Amphiphilic Block Copolymers. *J. Am. Chem. Soc.* **2010**, *132* (30), 10251–10253. https://doi.org/10.1021/ja104691j.

(37) Pal, D.; Garrison, J. B.; Miao, Z.; Diodati, L. E.; Veige, A. S.; Sumerlin, B. S. Nanobowls from Amphiphilic Core-Shell Cyclic Bottlebrush Polymers. *Macromolecules* **2022**, *55* (17), 7446–7453. https://doi.org/10.1021/acs.macromol.2c01232.

(38) Xiao, L.; Qu, L.; Zhu, W.; Wu, Y.; Liu, Z.; Zhang, K. Donut-Shaped Nanoparticles Templated by Cyclic Bottlebrush Polymers. *Macromolecules* **2017**, *50* (17), 6762–6770. https://doi.org/10.1021/acs.macromol.7b01512.

(39) Pal, D.; Miao, Z.; Garrison, J. B.; Veige, A. S.; Sumerlin, B. S. Ultra-High-Molecular-Weight Macrocyclic Bottlebrushes via Post-Polymerization Modification of a Cyclic

Polymer. *Macromolecules* **2020**, *53* (22), 9717–9724. https://doi.org/10.1021/acs.macromol.0c01797.
(40) Liu, Z.; Huang, Y.; Zhang, X.; Tu, X.; Wang, M.; Ma, L.; Wang, B.; He, J.; Ni, P.; Wei, H. Fabrication of Cyclic Brush Copolymers with Heterogeneous Amphiphilic Polymer Brushes for Controlled Drug Release. *Macromolecules* **2018**, *51* (19), 7672–7679. https://doi.org/10.1021/acs.macromol.8b00950.
(41) Yang, J.; Wang, R.; Xie, D. Aqueous Self-Assembly of Amphiphilic Cyclic Brush Block Copolymers as Asymmetry-Tunable Building Blocks. *Macromolecules* **2019**, *52* (18), 7042–7051. https://doi.org/10.1021/acs.macromol.9b01393.
(42) Lecommandoux, S.; Borsali, R.; Schappacher, M.; Deffieux, A.; Narayanan, T.; Rochas, C. Microphase Separation of Linear and Cyclic Block Copolymers Poly(Styrene-b-Isoprene): SAXS Experiments. *Macromolecules* **2004**, *37* (5), 1843–1848. https://doi.org/10.1021/ma035627r.
(43) Minatti, E.; Viville, P.; Borsali, R.; Schappacher, M.; Deffieux, A.; Lazzaroni, R. Micellar Morphological Changes Promoted by Cyclization of PS-b-PI Copolymer: DLS and AFM Experiments. *Macromolecules* **2003**, *36* (11), 4125–4133. https://doi.org/10.1021/ma020927e.
(44) Tu, X. Y.; Liu, M. Z.; Wei, H. Recent Progress on Cyclic Polymers: Synthesis, Bioproperties, and Biomedical Applications. *J. Polym. Sci. Part A Polym. Chem.* **2016**, *54* (11), 1447–1458. https://doi.org/10.1002/pola.28051.
(45) Golba, B.; Benetti, E. M.; De Geest, B. G. Biomaterials Applications of Cyclic Polymers. *Biomaterials* **2021**, *267* (June 2020), 120468. https://doi.org/10.1016/j.biomaterials.2020.120468.
(46) Miao, Z.; Esper, A. M.; Nadif, S. S.; Gonsales, S. A.; Sumerlin, B. S.; Veige, A. S. Semi-Conducting Cyclic Copolymers of Acetylene and Propyne. *React. Funct. Polym.* **2021**, *169* (August), 105088. https://doi.org/10.1016/j.reactfunctpolym.2021.105088.
(47) Ree, B. J.; Satoh, Y.; Isono, T.; Satoh, T. Influence of Topological Confinement on Nanoscale Film Morphologies of Tricyclic Block Copolymers. *Macromolecules* **2021**, *54* (9), 4120–4127. https://doi.org/10.1021/acs.macromol.1c00214.
(48) Laurent, B. A.; Grayson, S. M. An Efficient Route to Well-Defined Macrocyclic Polymers via "Click" Cyclization. *J. Am. Chem. Soc.* **2006**, *128* (13), 4238–4239. https://doi.org/10.1021/ja0585836.
(49) Kricheldorf, H. R.; Weidner, S. M. High Molar Mass Cyclic Poly(L-Lactide) via Ring-Expansion Polymerization with Cyclic Dibutyltin Bisphenoxides. *Eur. Polym. J.* **2018**, *105*, 158–166. https://doi.org/10.1016/j.eurpolymj.2018.05.036.
(50) Bielawski, C. W.; Benitez, D.; Grubbs, R. H. An "Endless" Route to Cyclic Polymers. *Science* **2002**, *297* (5589), 2041–2044. https://doi.org/10.1126/science.1075401.
(51) Xia, Y.; Boydston, A. J.; Yao, Y.; Kornfield, J. A.; Gorodetskaya, I. A.; Spiess, H. W.; Grubbs, R. H. Ring-Expansion Metathesis Polymerization: Catalyst-Dependent Polymerization Profiles. *J. Am. Chem. Soc.* **2009**, *131* (7), 2670–2677. https://doi.org/10.1021/ja808296a.
(52) Song, A.; Parker, K. A.; Sampson, N. S. Cyclic Alternating Ring-Opening Metathesis Polymerization (CAROMP). Rapid Access to Functionalized Cyclic Polymers. *Org. Lett.* **2010**, *12* (17), 3729–3731. https://doi.org/10.1021/ol101432m.
(53) Blencowe, A.; Qiao, G. G. Ring-Opening Metathesis Polymerization with the Second Generation Hoveyda-Grubbs Catalyst: An Efficient Approach toward High-Purity

Functionalized Macrocyclic Oligo(Cyclooctene)S. *J. Am. Chem. Soc.* **2013**, *135* (15), 5717–5725. https://doi.org/10.1021/ja312418z.

(54) Wang, T.-W.; Huang, P.-R.; Chow, J. L.; Kaminsky, W.; Golder, M. R. A Cyclic Ruthenium Benzylidene Initiator Platform Enhances Reactivity for Ring-Expansion Metathesis Polymerization. *J. Am. Chem. Soc.* **2021**, *143* (19), 7314–7319. https://doi.org/10.1021/jacs.1c03491.

(55) Levenson, A. M.; Morrison, C. M.; Huang, P.-R.; Wang, T.-W.; Carter-Schwendler, Z.; Golder, M. R. Ancillary Ligand Lability Improves Control in Cyclic Ruthenium Benzylidene Initiated Ring-Expansion Metathesis Polymerizations. *ACS Macro Lett.* **2023**, 1286–1292. https://doi.org/10.1021/acsmacrolett.3c00520.

(56) Von Kugelgen, S.; Bellone, D. E.; Cloke, R. R.; Perkins, W. S.; Fischer, F. R. Initiator Control of Conjugated Polymer Topology in Ring-Opening Alkyne Metathesis Polymerization. *J. Am. Chem. Soc.* **2016**, *138* (19), 6234–6239. https://doi.org/10.1021/jacs.6b02422.

(57) Roland, C. D.; Li, H.; Abboud, K. A.; Wagener, K. B.; Veige, A. S. Cyclic Polymers from Alkynes. *Nat. Chem.* **2016**, *8*, 791–796. https://doi.org/10.1038/nchem.2516.

(58) Jakhar, V.; Pal, D.; Ghiviriga, I.; Abboud, K. A.; Lester, D. W.; Sumerlin, B. S.; Veige, A. S. Tethered Tungsten-Alkylidenes for the Synthesis of Cyclic Polynorbornene via Ring Expansion Metathesis: Unprecedented Stereoselectivity and Trapping of Key Catalytic Intermediates. *J. Am. Chem. Soc.* **2021**, *143* (2), 1235–1246. https://doi.org/10.1021/jacs.0c12248.

(59) Nadif, S. S.; Kubo, T.; Gonsales, S. A.; VenkatRamani, S.; Ghiviriga, I.; Sumerlin, B. S.; Veige, A. S. Introducing "Ynene" Metathesis: Ring-Expansion Metathesis Polymerization Leads to Highly Cis and Syndiotactic Cyclic Polymers of Norbornene. *J. Am. Chem. Soc.* **2016**, *138* (20), 6408–6411. https://doi.org/10.1021/jacs.6b03247.

(60) Miao, Z.; Gonsales, S. A.; Ehm, C.; Mentink-Vigier, F.; Bowers, C. R.; Sumerlin, B. S.; Veige, A. S. Cyclic Polyacetylene. *Nat. Chem.* **2021**, *13* (8), 792–799. https://doi.org/10.1038/s41557-021-00713-2.

(61) Niu, W.; Gonsales, S. A.; Kubo, T.; Bentz, K. C.; Pal, D.; Savin, D. A.; Sumerlin, B. S.; Veige, A. S. Polypropylene: Now Available without Chain Ends. *Chem* **2019**, *5* (1), 237–244. https://doi.org/10.1016/j.chempr.2018.12.005.

(62) Miao, Z.; Gonsales, S. A.; Ehm, C.; Mentink-Vigier, F.; Bowers, C. R.; Sumerlin, B. S.; Veige, A. S. Cyclic Polyacetylene. *Nat. Chem.* **2021**, *13* (8), 792–799. https://doi.org/10.1038/s41557-021-00713-2.

Chapter 2: Shape shifting polymers from bullvalene

2.1 Background

2.1.1 The bullvalene story

Bullvalene is a "shape-shifting" hydrocarbon cage that undergoes Hardy-Cope rearrangements at room temperature to access over one million degenerate isomers (Figure 2.1A). The existence of bullvalene was first hypothesized by Doering and Roth in 1963 when studying the activation energies of different Hardy-Cope rearrangements.[1] Using deuterium doped analogs, it was observed that the Hardy-Cope rearrangement proceeded with an activation energy of about 35 kcal/mol. However, if the single bond is part of a cyclopropane ring, the activation energy is substantially lowered; the activation energy for the Hardy-Cope rearrangement of divinylcyclopropane was calculated to be 21 kcal/mol. However, this rearrangement only took place at 190 °C, which is higher than expected for this low activation energy. It was hypothesized that isomerization from cis- to trans-divinylcyclopropane increased the activation energy of this process. Doering and Roth then synthesized homotropilidene, a divinylcylopropane compound where the alkenes are locked in the *cis* position (Figure 2.1). Remarkably, ^{1}H NMR at room temperature showed only broad featureless peaks, while at –50 °C sharp multiplets were present. These observations demonstrate that the Hardy-Cope rearrangement of homotropilidene is so fast at room temperature that it is undetectable on the ^{1}H NMR timescale, while at –50 °C it slows down such that individual isomers can by distinguished by ^{1}H NMR.

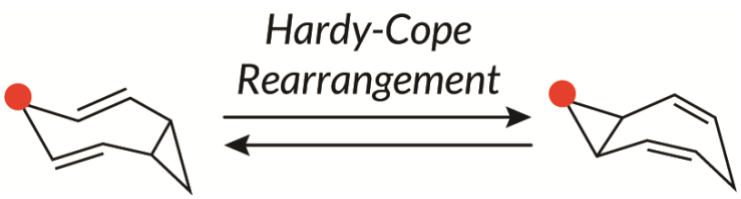

Figure 2.1. Hardy-Cope rearrangement of homotropilidene

It was hypothesized that this rearrangement occurs through a boat-like transition state; if a third ethylene bridge was added to this structure, the alkenes would be locked into the Hardy-Cope rearrangement transition state, further lowering the activation energy for this process. This molecular cage is known as bullvalene; a molecule that can rearrange to form over one million degenerate isomers and thus have no permanent structure (Figure 2.2). Bullvalene was first synthesized by Schröder in 1963 through a thermal dimerization of cyclooctatetraene followed by a photochemical rearrangement. Its fluxionality was confirmed by one broad ^{1}H-NMR peak at room temperature which sharpened into a singlet as the temperature increased.[2] After its initial discovery, bullvalene research have slowed due to tedious syntheses, however there has been a recent resurgence due to the development of more streamlined synthetic methods. In 2010, a gold catalyzed oxidative cyclization was employed to make substituted barbaralones which were used to access bullvalene and other fluxional molecules.[3] Bode developed a synthesis of static oligosubstituted dihydrobullvalenes whose fluxionality could be induced under basic conditions.[4]

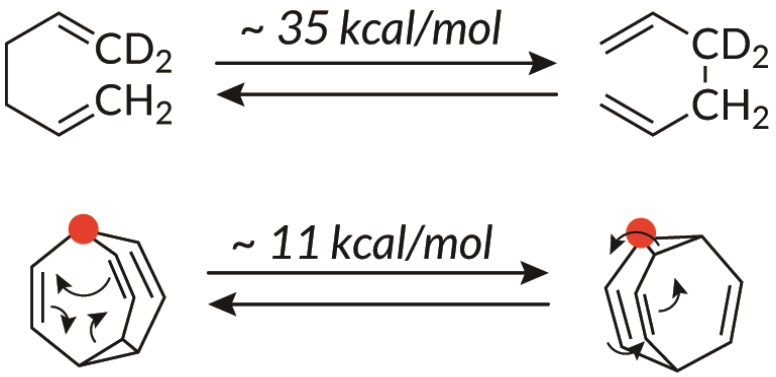

Figure 2.2. Comparing activation energies of the Hardy-Cope rearrangements of 1,5-hexadiene and bullvalene

2.1.2 Supramolecular bullvalene applications

With these updated synthetic routes, the structural properties of bullvalene have been investigated on the supramolecular scale (Figure 2.3). Bode made ^{13}C labeled bullvalenes to be used as supramolecular sensors that could selectively bind to fullerenes[5] or polyols,[6] creating a new isomer distribution with unique ^{13}C-NMR barcodes. Similarly, McGonigal explored shape-selective crystallization in barbaralane, a fluxional bullvalene derivative.[7] The most recent method to access bullvalenes was developed by Fallon in 2019 and involves a cobalt mediated [6+2] cycloaddition followed by a photosensitized di-pi-methane rearrangement.[8] This method is compatible with a variety of functional groups including boronate esters, which opens up the possibility for further functionalization.[9] Fallon uses this method to access *bis*-3-pyridyl bullvalenes that can self-assemble into fluxional coordination cages in the presence of a metal cation.[10] Subsequently, Fallon demonstrated further utility of bullvalene in the biomedical field by using it as a linker in vanomycin dimers; these fluxional antibiotics significantly outperformed control vanomycin

dimers in eradicating gram-positive bacteria without causing drug resistance. These examples from Bode, McGonigal, and Fallon demonstrate how the pericyclic rearrangement can be harnessed to access architectures that aren't reliant on the inherent conformational freedom of a system. We hypothesized that these design principles could be applied to access π-rich polymers with decreased rigidity; bullvalene would provide an isomeric ensemble of linkers to kink seemingly stiff macromolecular chains (Figure 2.4).

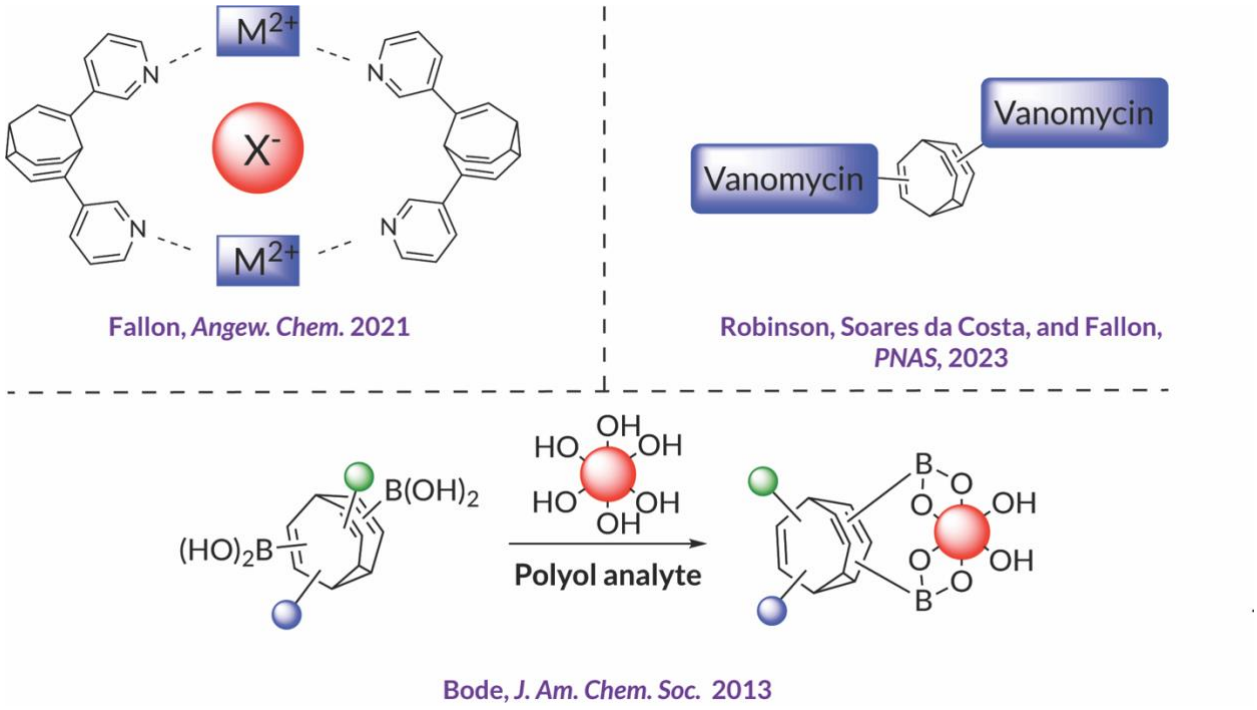

Figure 2.3. Fluxional molecules sampling an ensemble of isomers provides a platform for supramolecular applications

2.1.3 Proposed work and summary of results

Herein, we explore this paradigm by linking bullvalene co-monomers (10–50 mol %) alongside rigid *p*-phenylenes to access poly(bullvalene-*co*-phenylene)s (**PB$_x$P$_y$**) (*x*=% bullvalene; *y*=% phenylene). Through gel permeation chromatography (GPC) and differential scanning calorimetry (DSC), we demonstrate that the resulting π-rich **PB$_x$P$_y$** backbones are less rigid than analogous poly(*p*-phenylene)s (**PB$_0$P$_{100}$**) and have tuneable thermal properties dependent on bullvalene density. **PB$_{50}$P$_{50}$**s remain dynamic in solution, as assessed by variable temperature NMR (VT NMR) spectroscopy, so these materials may also find future utility in stimuli-responsive applications.

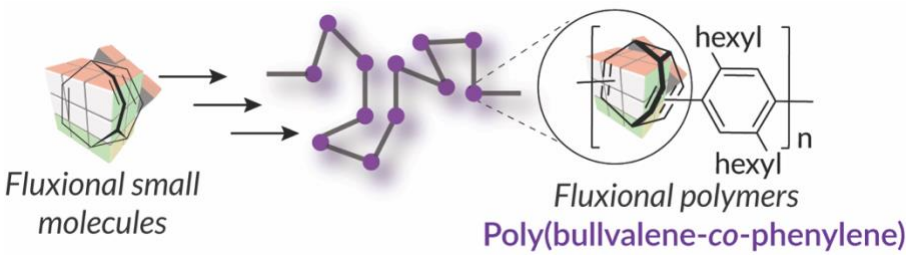

Figure 2.4. Our proposed work to incorporate bullvalene into the polymer backbone

2.2 Synthesis and solution-state characterization of poly(bullvalene-*co*-phenylenes)

To realize our target bullvalene co-polymers, bis-boronate ester bullvalene was envisioned as the ideal building block for subsequent polymerization with 2,5-di-hexyl-1,4-dibromobenzene under Suzuki-Miyuara polycondensation (SPC) conditions. Recent reports from Fallon demonstrate the construction of substituted bullvalenes through a facile two-step process. First, a Co-catalyzed formal [6+2] cycloaddition of cyclooctatetraene (**COT**) and 1,2-bis(boronic acid pinacol ester)ethyne yields the corresponding disubstituted bicyclo[4.2.2]-deca-2,4,7,9-tetraene in 72 % yield. Subsequent Zimmerman (di-π-methane) rearrangement of

cycloadduct under photosensitized conditions (365 nm, thioxanthone) afforded the necessary bullvalene monomer in 60 % yield.

With this key monomer in hand, we screened a variety of SPC reaction conditions with bromotoluene to access the envisioned co-polymers. Using the most successful conditions from these reactions, XPhos Pd G3, potassium phosphate, toluene, 60 °C), we were able to obtain $PB_{50}P_{50}$s with number-average molar masses (M_n) of 1.5 kDa ($PB_{50}P_{50}$-1.5 k)—21 kDa ($PB_{50}P_{50}$-21 k) and dispersities (Đ) of 1.2–1.6, as assessed by gel permeation chromatography coupled with a multi-angle light scattering detector (GPC-MALS) (Table 2.1), following purification with preparative GPC. To assess the structural role of bullvalene within π-rich polymers, we synthesized an analogous rigid alkyl-substituted poly(p-phenylene) (PB_0P_{100}-5.0 k) (Mn=5.0 kDa, Đ=1.2) as well as several randomly doped samples ($PB_{34}P_{66}$-3.4 k, $PB_{22}P_{78}$-3.9 k, $PB_{10}P_{90}$-3.0 k. Solubility is limited only for PB_0P_{100}-5 k; only lower molar mass PB_0P_{100}-5.0 k (Mn=5.0 kDa) was soluble for GPC analysis (33 mass % of total sample).

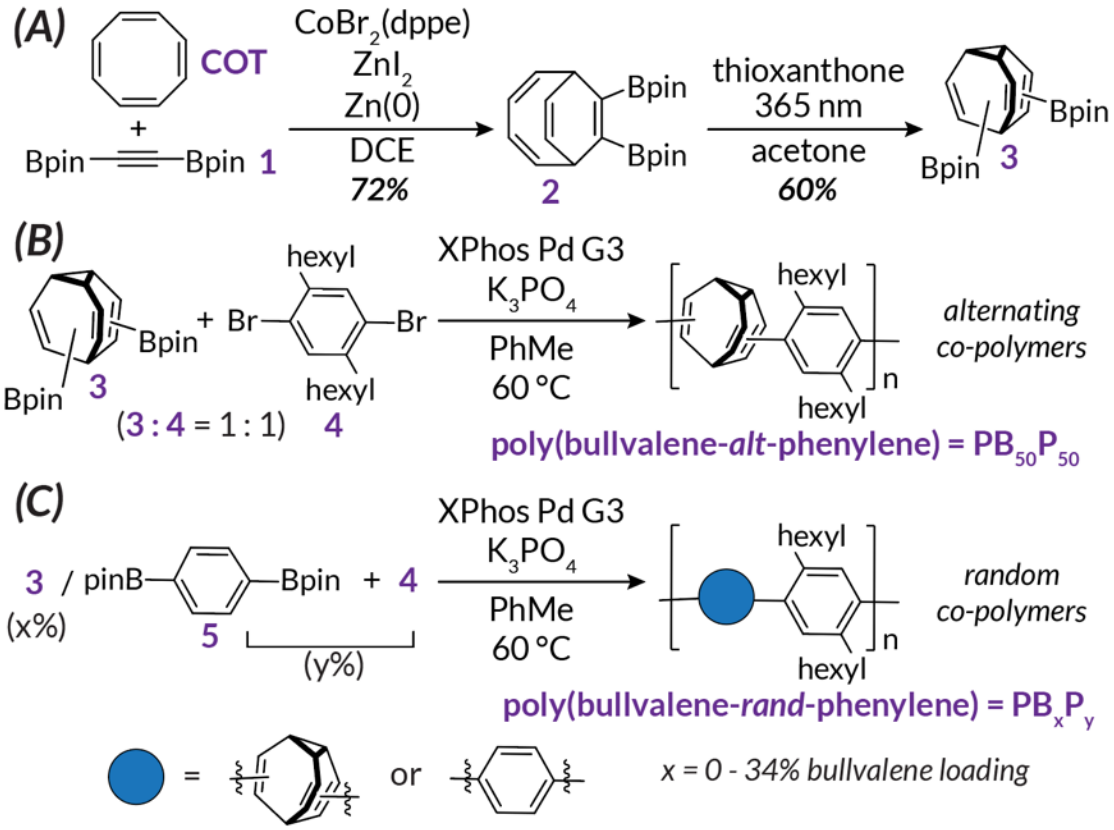

Scheme 2.1. (A) Synthesis of bullvalene monomer; (B) Synthesis of alternating bullvalene-*alt*-phenylene polymers (**PB$_{50}$P$_{50}$**); (C) Synthesis of random bullvalene-*rand*-phenylene polymers (i.e., bullvalene-doped polyphenylenes, **PB$_x$P$_y$**).

Sample	M_n (kDa)	Đ	$[\eta]_w$ (mL/g)	R_h (nm)
$PB_{50}P_{50}$-1.5k	1.5	1.2	2.0	0.96
$PB_{50}P_{50}$-5.8k	5.8	1.2	4.0	1.9
$PB_{50}P_{50}$-11k	11	1.4	4.0	3.1
$PB_{50}P_{50}$-21k	21	1.6	6.0	4.1
$PB_{34}P_{66}$-3.4k	3.4	1.2	6.4	1.8
$PB_{22}P_{78}$-3.9k	3.9	1.1	6.9	1.9
$PB_{10}P_{90}$-3.0k	3.0	1.1	4.7	1.3
PB_0P_{100}-5.0k	5.0	1.1	12.2	9.1

Table 2.1. Solution-state data measured by GPC-MALS-IV-RI after purification by preparative GPC.

Compared to similarly sized **PB_0P_{100}-5.0 k**, **$PB_{50}P_{50}$-5.8 k** has a smaller hydrodynamic radius (R_h=1.9 nm vs. 9.1 nm), indicating a short persistence length compared to conventional π-rich polymers. Similar conclusions can also be made using a Mark-Houwink-Sakurada (MHS) analysis from MALS and intrinsic viscosity (IV) data (Figure 2.2) that relates the IV of a sample, [η], with chain conformation (α) as a function of molar mass ($[\eta]=KM^{\alpha}$). **PB_0P_{100}-5.0 k** has an MHS exponential term of α=1.3 suggesting an extended backbone approaching that of a rigid rod, while **$PB_{50}P_{50}$** samples have MHS exponential terms of α=ca. 0.3–0.6 suggesting a much denser conformation. Related phenomena are commonly seen in single-chain nanoparticles. Randomly doped polymers (e.g., **$PB_{22}P_{78}$-3.9 k**) approximate a random-coil (α=0.82–0.86), suggesting that even just 10–20 % of stochastic bullvalene kinks drastically impact π-rich polymer backbone conformations.

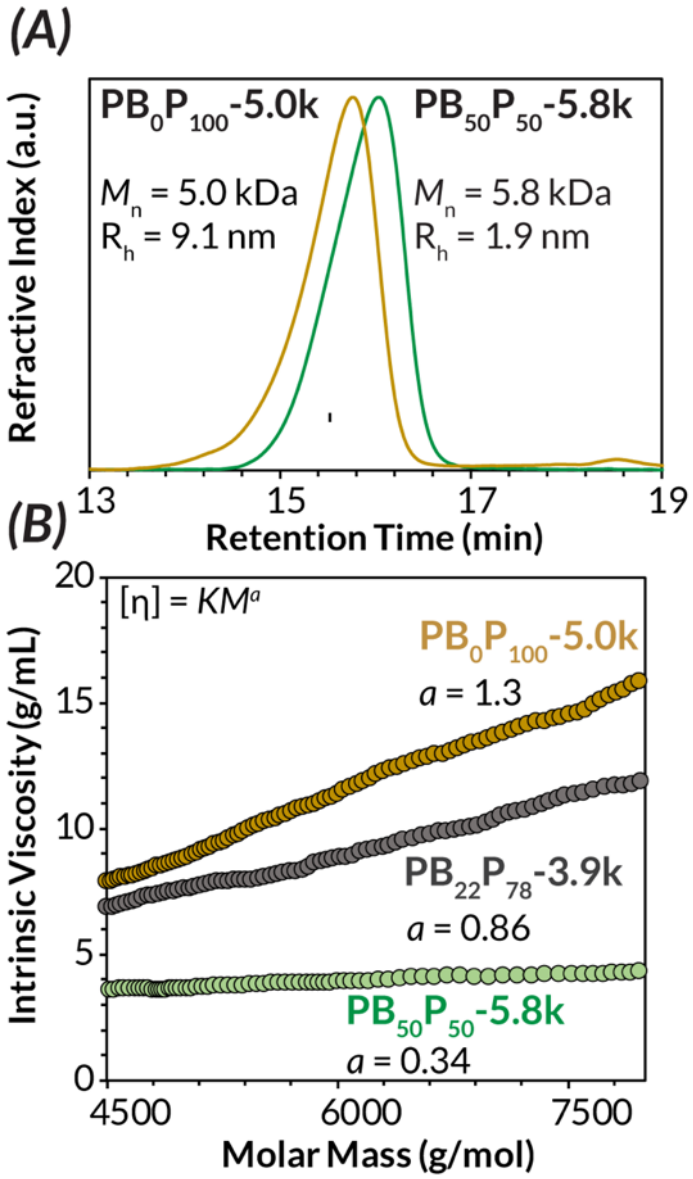

Figure 2.5. (A) GPC traces of similarly sized **PB_0P_{100}-5.0k** and **$PB_{50}P_{50}$-5.8k** demonstrating stark differences in backbone geometry; (B) Conformational analyses of bullvalene-*co*-phenylenes using Mark-Houwink-Sakurada plots

2.3 Thermal characterization of poly(bullvalene-*co*-phenylenes)

Thermal data also supports our claim that stochastic bullvalene kinks decrease rigidity in π-rich polymers. Alternating $PB_{50}P_{50}$s are amorphous with low T_gs (21–44 °C) as measured via differential scanning calorimetry (DSC) (Figure 2.6). These thermal transitions are much lower than those of crystalline PB_0P_{100}-2.6 k (Tcc=77 °C, Tm=128 °C), (Figure 2.3 and 2.5) and indicate differences in interchain interactions between each class of polymers despite potential side-chain plasticization effects. Despite their low T_g values, $PB_{50}P_{50}$s are relatively thermally stable ($T_{10\%}$=243 °C) relative to PB_0P_{100} ($T_{10\%}$=364 °C) as measured by thermal gravimetric analysis (TGA) (Figure 2.4). Interestingly, randomly doped PB_xP_y samples (Figure 2.6) reveal a continuum of thermal transitions ranging from low-Tg materials ($PB_{34}P_{66}$-3.4 k, Tg=13 °C) to multiphase amorphous ($PB_{22}P_{78}$-3.9 k, Tg=37 °C and 99 °C) to crystalline materials ($PB_{10}P_{90}$-3.0 k, T_m=129 °C). Overall, by simply varying bullvalene density and sequence, this privileged building block can modulate the thermal properties of π-rich polymers relative to PB_0P_{100}. Importantly, thermal properties are tuned without introducing significant crystalline domains as is observed with alkyl conjugation-break spacers (e.g., poly(p-phenylene octylene)).

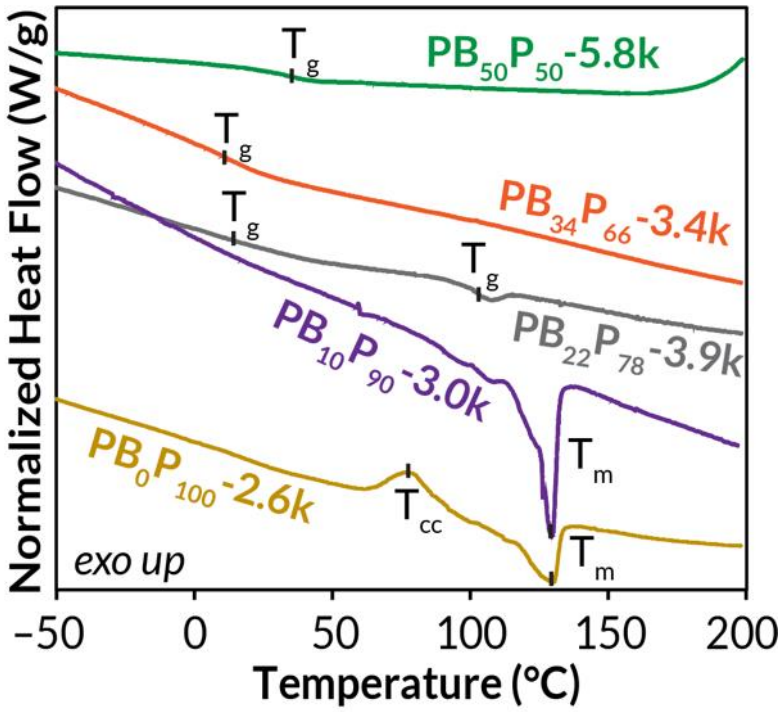

Figure 2.6. DSC traces of bullvalene-*co*-phenylenes demonstrating differences in thermal properties as a function of bullvalene doping and architecture (**PB$_x$P$_y$**, x = 0 – 34%).

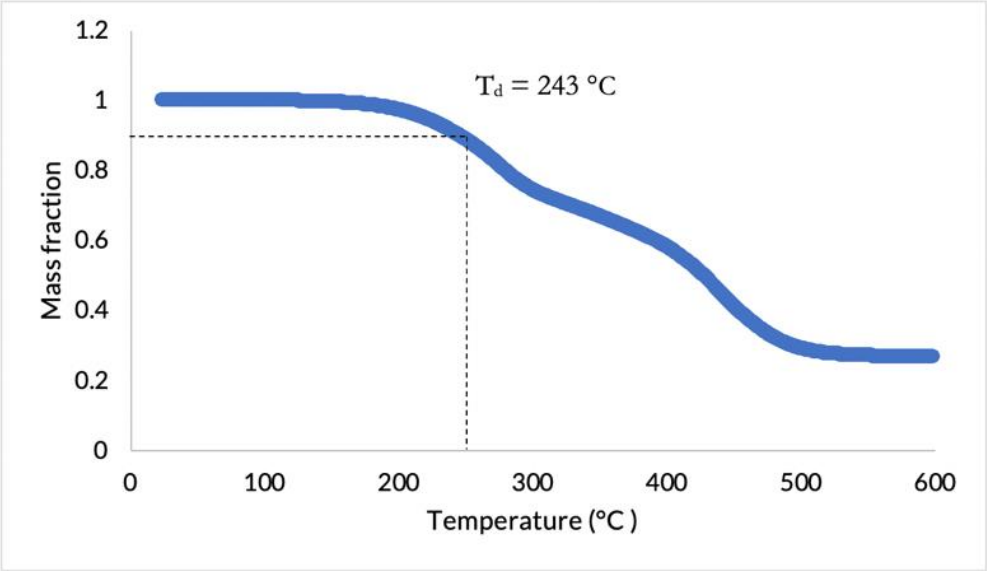

Figure 2.7. TGA curve of **PB$_{50}$P$_{50}$-5.8k** showing a $T_{10\%}$ (10% mass loss) of 243 °C.

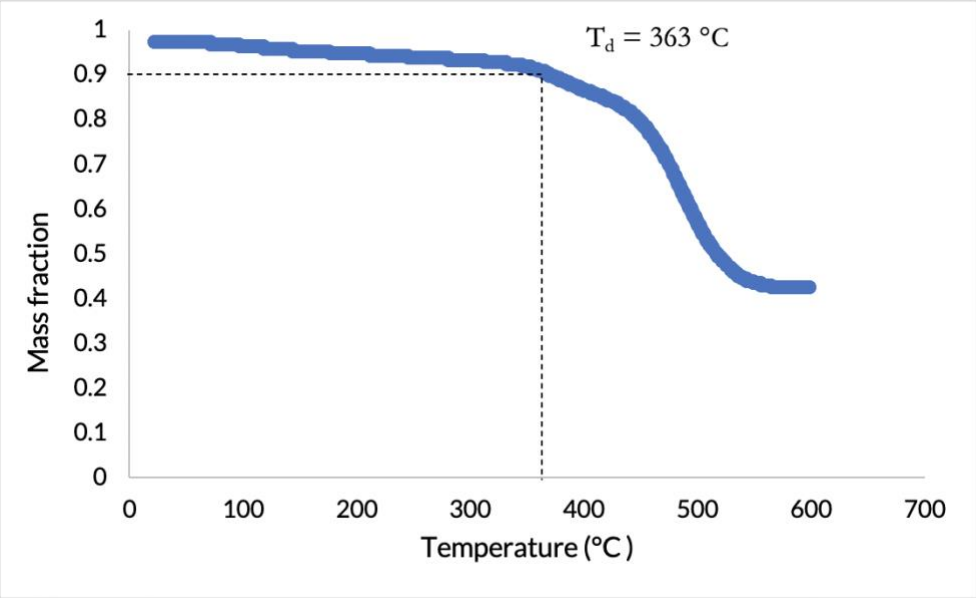

Figure 2.8. TGA curve of **PB_0P_{100}-5.0k** showing a $T_{10\%}$ (10% mass loss) of 363 °C.

It is both convenient and synthetically efficient to use a single monomer (i.e., bullvalene) that functions as a self-contained library of myriad isomers to introduce structural kinks into π-rich macromolecules. We surmise that bullvalene's ensemble of isomers within **PB_xP_y**s provides the necessary *non-uniform* kinks to modulate chain architecture and subsequent thermal properties. Although it would be difficult to determine bullvalene isomer population in our polymeric samples, solution-state analysis of model diphenylbullvalene by Fallon suggests that three major isomers are favored in solution, each with a unique and non-linear geometry. Hence, we expect a distribution of at least three distinct monomer geometries along the backbones of **PB_xP_y** samples. Bullvalene *always* provides structural kinks because substituent co-linearity is impossible to achieve with any valence isomer. Attempts to synthesize *p*-phenylene co-polymer analogs with other rigid spacers (e.g., adamantane, cyclohexene, norbornadiene) were futile (see Experimental for details). Even if accessible, we anticipate that such polymers would exhibit non-tunable thermal properties since the *uniform* kinks within poly(*m*-phenylene)s and poly(1,3-

adamantane)s afford only high T_g materials. For example, kinked poly(*m*-phenylene) has T_g=149 °C (M_w=27 kDa) and kinked butyl-substituted poly(1,3-adamantane) has T_g=123 °C–205 °C (M_n=1.5–6.0 kDa). These data demonstrate that structural backbone kinks, if uniform in nature, do not significantly depress the material's thermal transition. In other words, bullvalene is unique because resulting chain architectures approximate those of alkyl-bridged polymers (i.e., seemingly flexible) while still maintaining a rigid structure only possible through inclusion of and aromatic and/or cage-like linker. Tensile testing was attempted on these polymers through a collaboration with Prof. Xiaodan Gu at University of Mississippi, however $\mathbf{PB_xP_y}$ samples were below the entanglement molecular weight of these materials and therefore were too brittle to obtain any information of their mechanical properties (Figure 2.9).

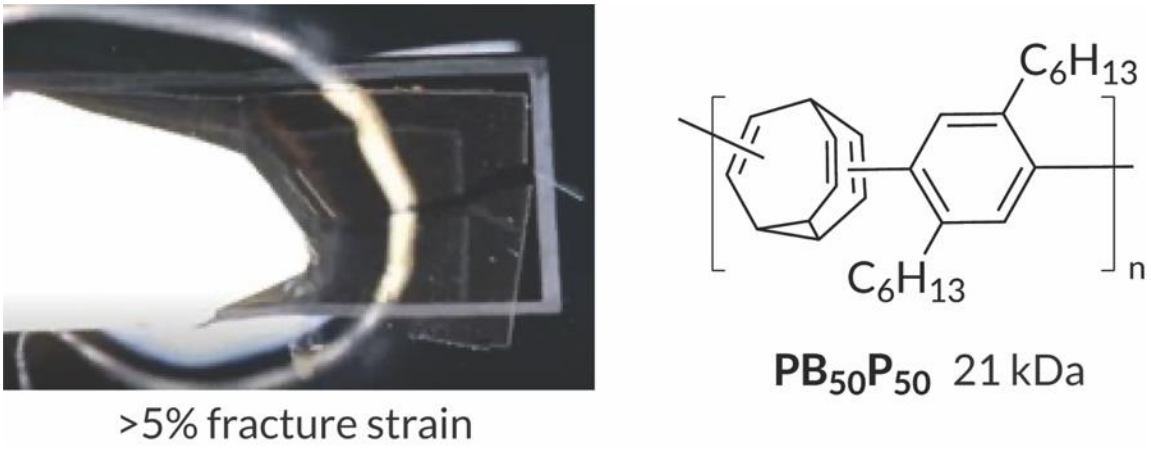

Figure 2.9 Attempted mechanical testing of a 21 kDa $\mathbf{PB_{50}P_{50}}$

2.4 Assessing the fluxionality of poly(bullvalene-co-phenylene)

Bullvalene is further unique because it presents opportunities for stimuli-responsive "shape-shifting" behavior within π-rich macromolecules. Such behavior would require a dynamic backbone where bullvalene could still undergo Hardy-Cope rearrangements despite bearing polymeric substituents. To assess whether bullvalene remains fluxional within polymer backbones,

we analyzed **PB$_{50}$P$_{50}$** chain dynamics by solution-state variable temperature (VT) ^{1}H NMR spectroscopy (Figure 2.10, 2.11, and 2.12).

These experiments confirm that both bis-Bpin bullvalene monomer and bullvalene units within **PB$_{50}$P$_{50}$**s remain dynamic in solution. At low temperatures (ca. −40 °C), the rate of the Hardy-Cope rearrangement slows and distinct bullvalene isomers in **PB$_{50}$P$_{50}$-5.8 k** can begin to be distinguished on the ^{1}H NMR timescale through analysis of the olefinic peaks (ca. δ 6.0 ppm). As the temperature increases to 25 °C and above, these distinct olefinic peaks broaden as the rate of the Hardy-Cope rearrangement increases. Similar temperature dependent olefinic peak (ca. 6 ppm) broadening is observed for small molecule model di-tolyl bullvalene (Figure 2.11). These observations demonstrate that bullvalene does not get "locked" in a **PB$_{50}$P$_{50}$** polymer chain, but instead retains a similar fluxionality barrier as small molecule analog **S2-Me**. Importantly, the steric bulk of polymeric substituents has little influence over chain dynamics because species interconvert via a *chemical process* rather than a *physical process* (i.e. bond rotations).

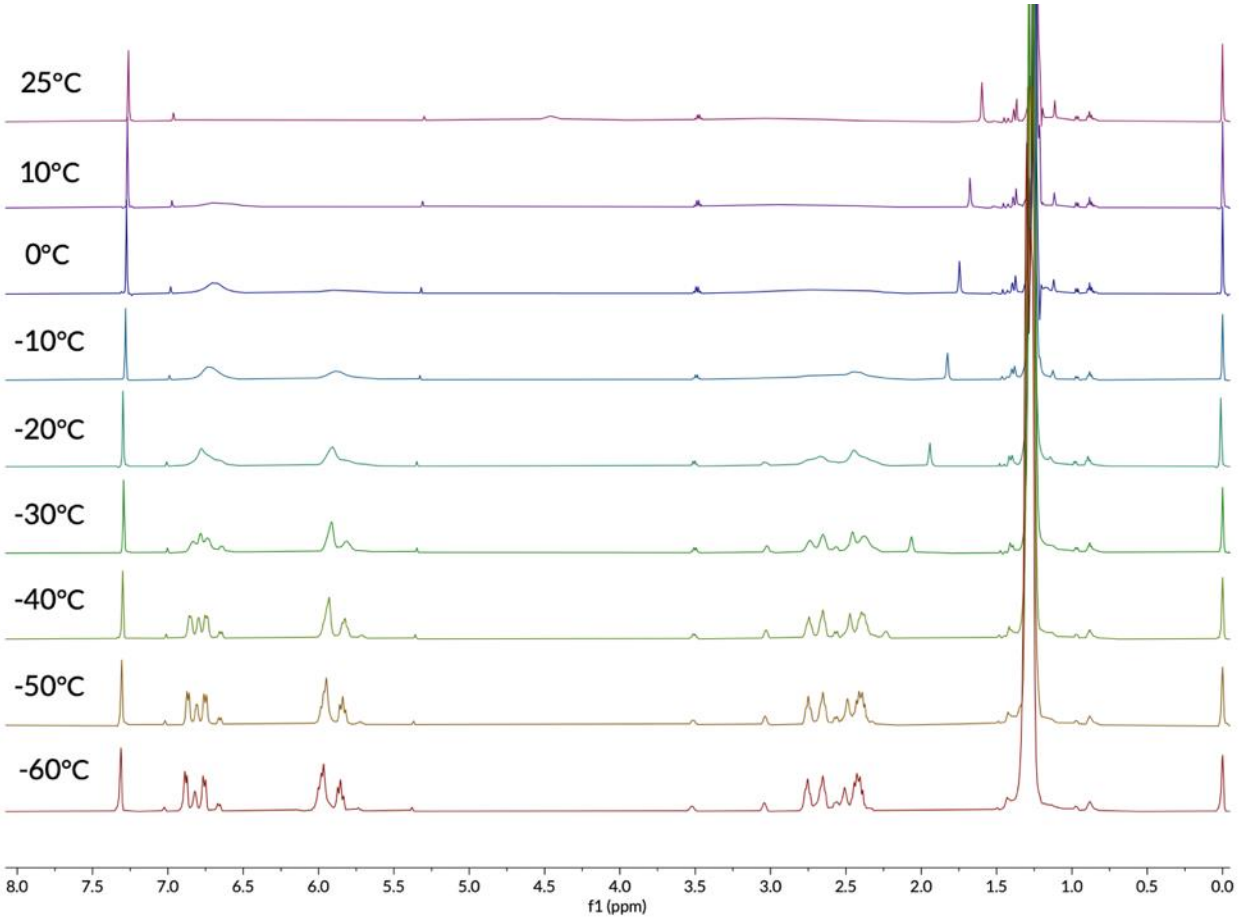

Figure 2.10. Variable-temperature ^{1}H NMR (500 MHz, $CDCl_3$) stacked spectra of bis-Bpin bullvalene **3** from –60 °C to 25 °C in 10 °C intervals.

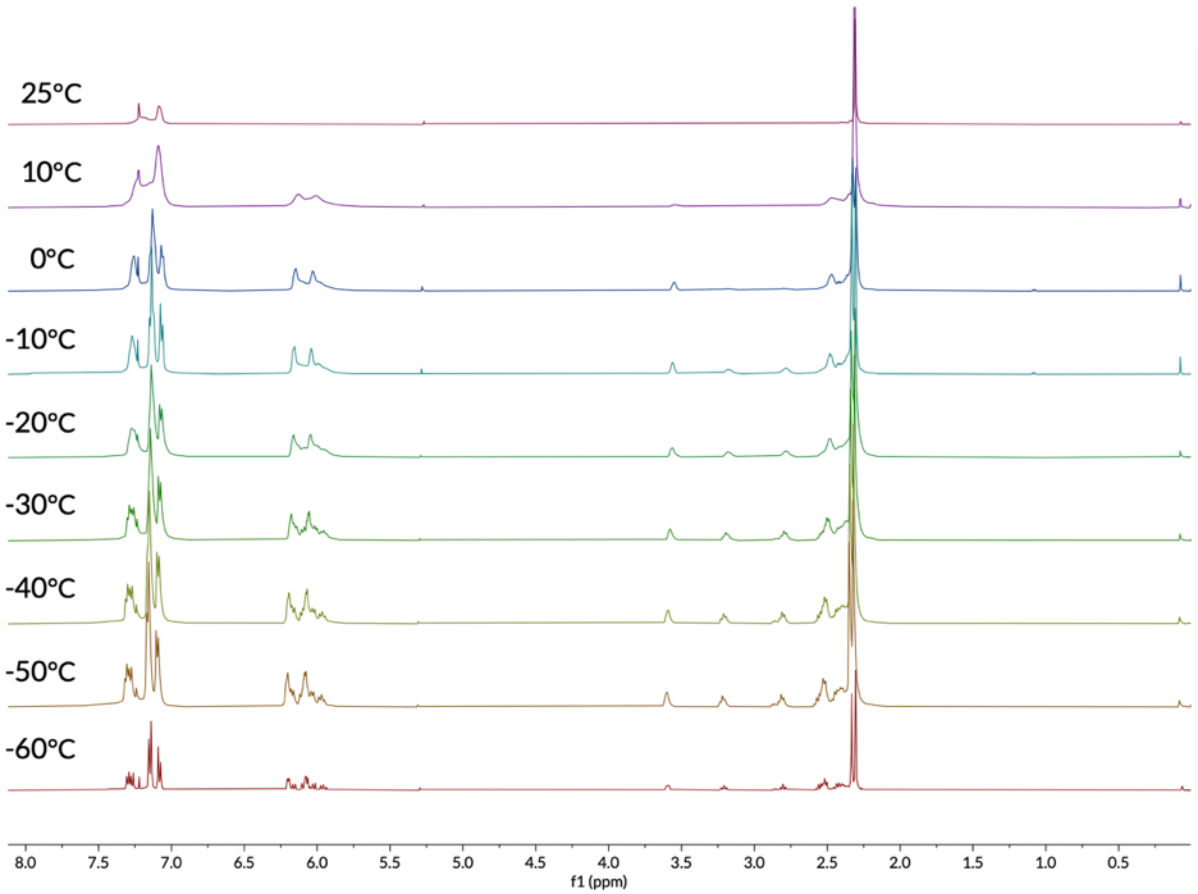

Figure 2.11 Variable-temperature ^{1}H NMR (500 MHz, $CDCl_3$) stacked spectra of bis-tolyl bullvalene from –60 °C to 25 °C in 10 °C intervals.

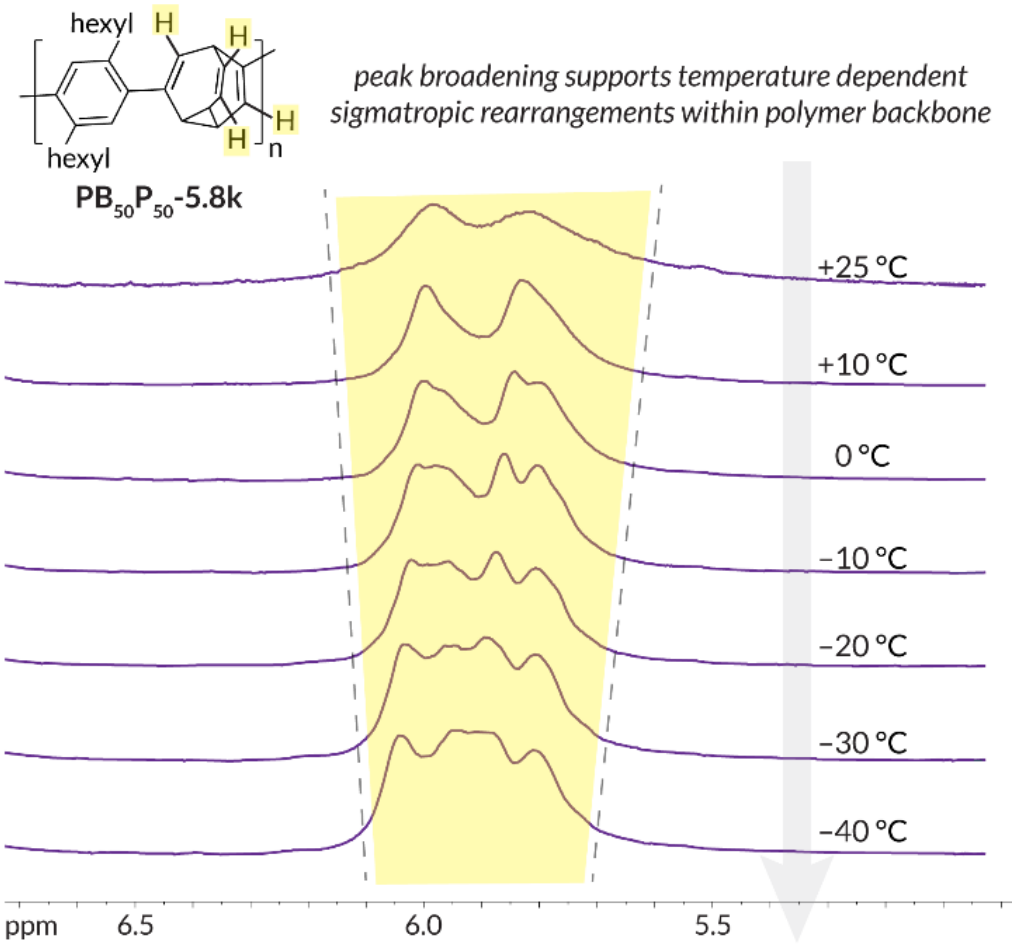

Figure 2.12. Solution-state VT ^{1}H NMR spectrum of **PB$_{50}$P$_{50}$-5.8k** from –40 °C to +25 °C in $CDCl_3$.

Similarly, significant broadening is observed in the **PB$_{50}$P$_{50}$-5.8 k** ^{13}C NMR spectrum compared to that of **PB$_{0}$P$_{100}$-5.0 k**, further distinguishing the unique chain dynamics in our system compared to those of more traditional π-rich macromolecules (see Supporting Information for details). The solution-state dynamics of **PB$_{50}$P$_{50}$**s provide discrete evidence that despite potential steric constraints within a polymer chain, bullvalene can still undergo temperature-dependent Hardy-Cope rearrangements with higher molecular weight substituents. It is therefore feasible that observed backbone kinks in **PB$_{x}$P$_{y}$**s arise during chain propagation and/or polymer chain

reorganization via solution-state Hardy-Cope rearrangements. While there is extensive evidence supporting bulk fluxionality in crystalline small molecule bullvalenes, experiments probing the dynamics of **PB$_{50}$P$_{50}$s** in the bulk via solid-state cross-polarization magic angle spinning (CPMAS) ^{13}C NMR spectroscopy were inconclusive and warrant further investigation.

2.5 Dihydrobullvalene comparison polymers

The working hypothesis discussed so far attributes tunable polymer architectures (i.e., backbone kinks) and thermal properties to the self-contained isomeric library provided by a single bullvalene building block. Although it is unclear if bulk fluxionality in **PB$_{50}$P$_{50}$s** is operative, quelling the Hardy-Cope rearrangement through olefin reduction would provide insight to a second scenario where active bullvalene fluxionality (i.e., dynamics) also impacts physical properties. Such a reduction is not straightforward on **PB$_{50}$P$_{50}$s**, however; reduction of unsubstituted bullvalene using H_2 and Pd/C yields a 2 : 3 ratio of cyclopropane ring-opened bullvalene to hexahydrobullvalene. To avoid cyclopropane cleavage that also lead to undesired structural changes, we turned to diimide reduction conditions. While we could achieve full olefin reduction of unsubstituted bullvalene under these conditions (30 % yield), we were unable to achieve full reduction of model diarylbullvalene **S2-H** as assessed by ^{1}H NMR spectroscopy (Figure 2.14). In the case of **S2-H** reduction, we surmise that only the unsubstituted alkene is reduced; this claim is supported by the presence of approximately two olefinic protons in the ^{1}H NMR specta after addition of either 1 equivalent or an excess (8 equivalents) of diimide reagent. The resulting dihydrobullvalene structure resembles semibullvalene and bullvalone; importantly, this fluxional motif does *not* permit geometric changes.

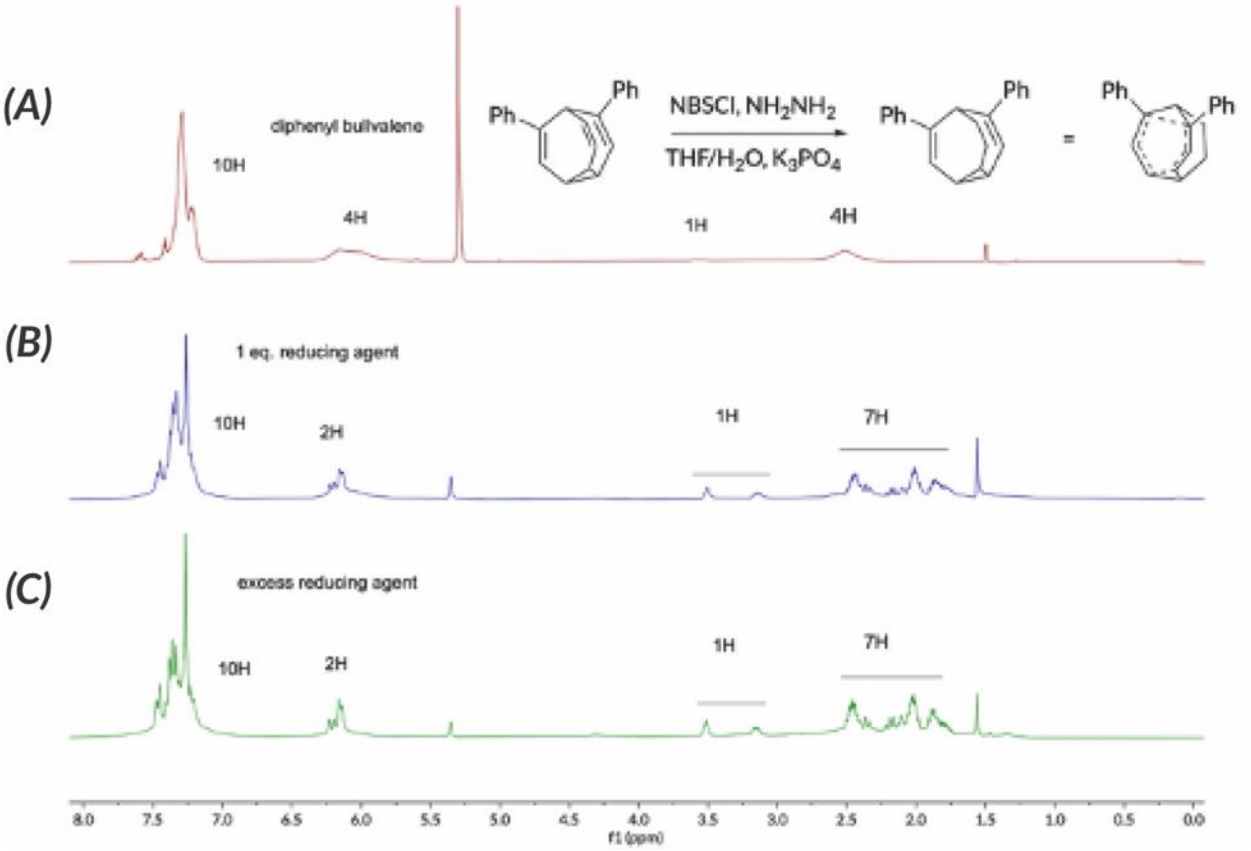

Figure 2.14. A) ^{1}H NMR spectrum (CD_2Cl_2) of diphenyl bullvalene (**S2-H**). B) ^{1}H NMR spectrum (CD_2Cl_2) of **S2-H** reduced with 1 eq. of diimide reducting agent. C) ^{1}H NMR spectrum (CD_2Cl_2) of **S2-H** reduced with excess (8 eq.) of diimide reducing agent.

Following diimide reduction, semi-hydrogenated ***red*-PB$_{50}$P$_{50}$** could not be reduced further, even with extended reaction times or alternative reductants (e.g., Pt/C catalyzed hydrogenation). Hence, diimide reduction methodology is an ideal method to quell the Hardy-Cope rearrangement in polymeric samples with minimal impact on molecular architecture (i.e., kinks). The diimide reduction of **PB$_{50}$P$_{50}$-5.8 k** (NsCl, N_2H_4, K_3PO_4) led to no significant change in GPC retention time or intrinsic viscosity, confirming that **PB$_{50}$P$_{50}$-5.8 k** and ***red*-PB$_{50}$P$_{50}$** have similar solution-state conformations. These combined results support the direct impact of stochastic backbone kinks, rather than bullvalene fluxional dynamics, in dictating physical properties.

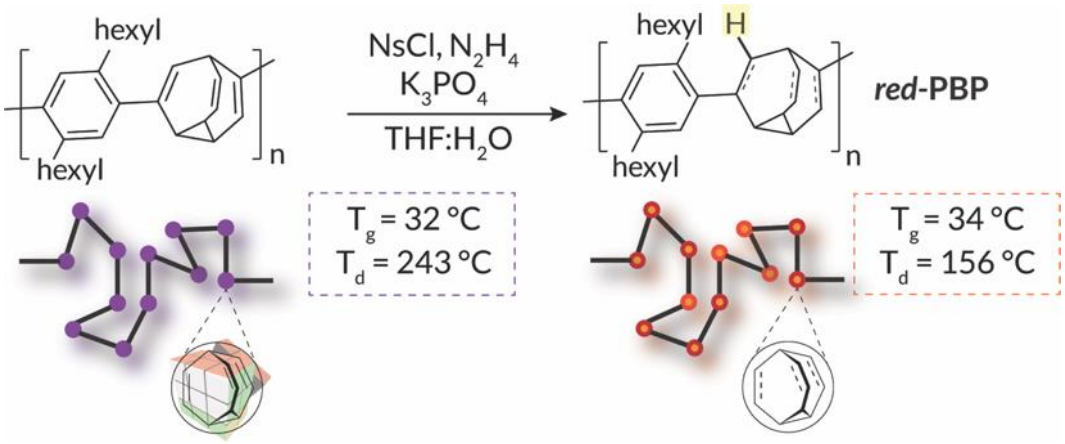

Figure 2.14. Diimide reduction of **PB$_{50}$P$_{50}$-5.8k** to **redPB$_{50}$P$_{50}$**

Solution-state ^{1}H NMR spectroscopy of ***red*-PB$_{50}$P$_{50}$** shows significantly less temperature dependence on residual olefin peak shape relative to olefins in a **PB$_{50}$P$_{50}$-5.8 k** ^{1}H NMR spectrum, confirming that ***red*-PB$_{50}$P$_{50}$** contains minimal active fluxional bullvalenes in solution (Figure 2.12). In the bulk, there is no significant change in T_g from **PB$_{50}$P$_{50}$-5.8 k** to ***red*-PB$_{50}$P$_{50}$** (Figure 2.11, T_g=32–34 °C), demonstrating that stochastic kinks arising from the ensemble of incorporated bullvalene isomers, rather than chain dynamics, drive the low observed T_g values. Once bullvalenes are mostly reduced in ***red*-PB$_{50}$P$_{50}$**, solution-state and bulk properties remain constant. The generation of ***red*-PB$_{50}$P$_{50}$** strongly supports bullvalene fluxionality as most influential in *accessing* a given architecture (i.e., structural argument) rather than *modulating* large fluctuations in polymer shape or radius (i.e., dynamics argument). In other words, bullvalene isomers are responsible for metastable kinks, the driving force behind the observed thermal properties in **PB$_{50}$P$_{50}$-5.8 k** and ***red*-PB$_{50}$P$_{50}$** on the DSC timescale. These conclusions are consistent with our previous observations that physical properties are intimately related to the density of bullvalene in the polymer backbone. Analysis of ***red*-PB$_{50}$P$_{50}$** confirms that stochastic

structural kinks drive differences in thermal properties, independent of whether kinks arise from actively fluxional bullvalenes.

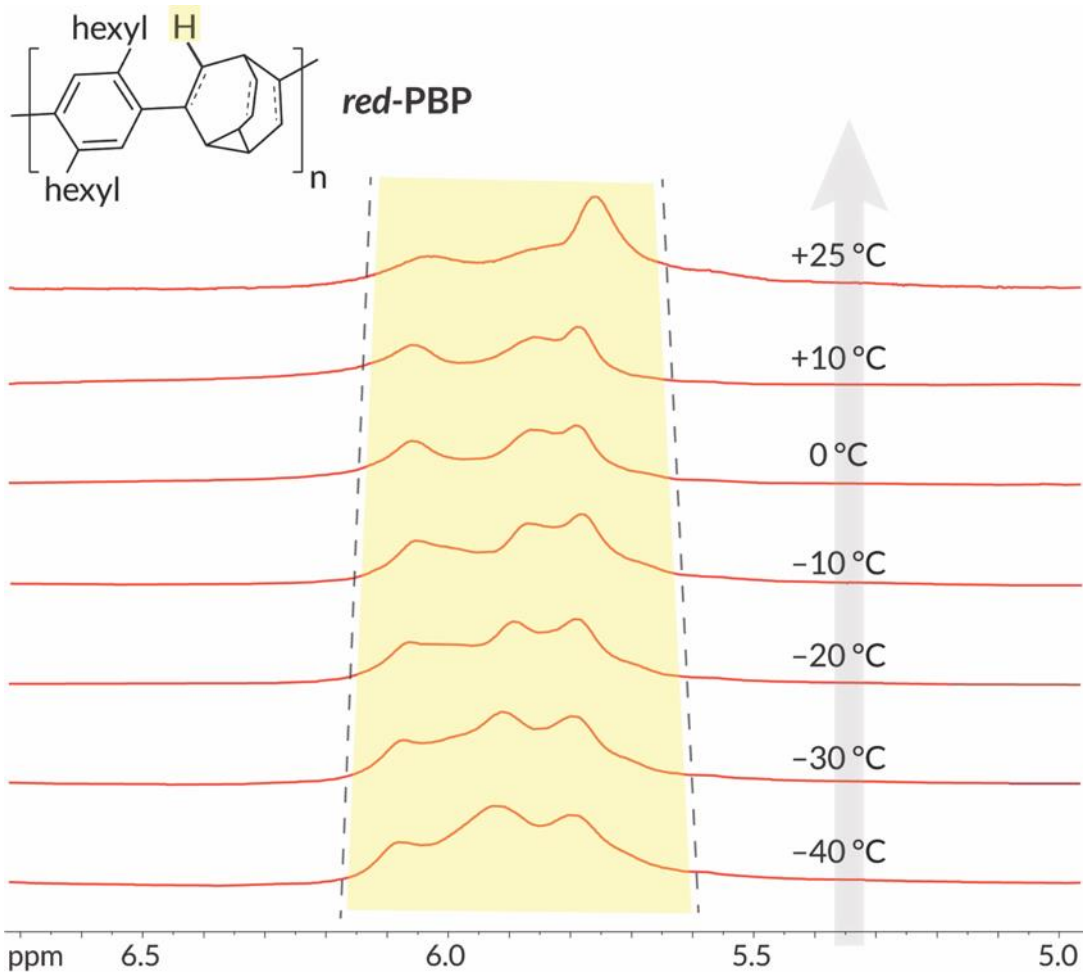

Figure 2.15. ^{1}H NMR spectra of residual olefin signals in red-$PB_{50}P_{50}$ following reduction from –40°C to +25°C in $CDCl_3$.

2.6 The thermal stability of bullvalene

Interestingly, ***red*-PB$_{50}$P$_{50}$** had a much lower thermal decomposition temperature ($T_{d,\ 10\%}$ = 156°C) suggesting that the presence of bullvalene monomer units may play a role in augmenting the thermal stability of these polymers (Figure 2.13). The structure of these polymers is also almost identical, except for the presence of an additional alkene in PB$_{50}$P$_{50}$. However, the presence of an additional alkene should not have such a profound effect on the decomposition temperature. For example, polyethylene has a higher decomposition temperature than polybutadiene ($T_{d,\ 10\%}$ = 430°C vs $T_{d,\ 10\%}$ = 386°C). We hypothesize that the thermal stability of PB$_{50}$P$_{50}$ originates from the fluxionality of the bullvalene monomer units; the constant pericyclic rearrangements of bullvalene relieve cyclopropane ring strain and therefore imparting additional thermal stability.

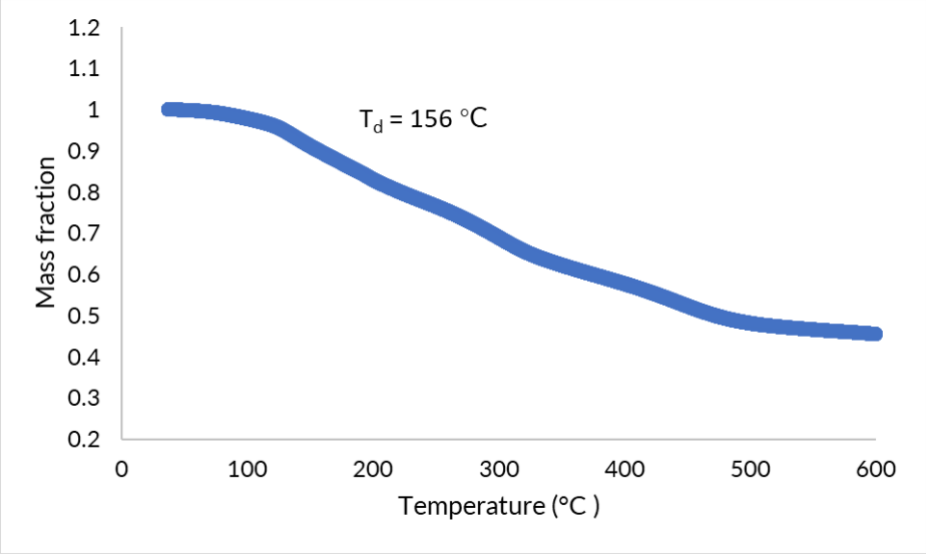

Figure 2.16. TGA curve of red-**PB$_{50}$P$_{50}$-5.0k** showing a $T_{10\%}$ (10% mass loss) of 156 °C.

To test this hypothesis, we synthesized model small-molecule bullvalenes with varying levels of fluxionality and studied their thermal decomposition profiles using TGA. We chose mono- and di-tolyl substituted bullvalenes as fluxional model compounds due to their structural similarity to our polymers. These compounds were synthesized using a Suzuki-Miyaura cross-

coupling of bis-Bpin bullvalene with *o*-bromotoluene. Because we were able to control the level of reduction of these compounds through number of substituents, we were able to synthesize a library of model bullvalenes with varying degrees of fluxionality. Reduction of the resulting tolyl substituted bullvalenes under diimide conditions resulted in a semi-fluxional di-tolyl bullvalene and a completely static mono-tolyl bullvalene (Figure 2.14A and 2.14B). Gratifyingly, we observed that for both tolyl substituted bullvalenes, the thermal stability decreased upon reduction (Figure 2.14C). This change was more significant for the mono-tolyl bullvalene ($T_{d,\,10\%}$ = 171.77°C for fluxional compound vs $T_{d,\,10\%}$ = 156.06°C for the reduced compound) than it was for the di-tolyl bullvalene ($T_{d,\,10\%}$=196.93°C for the fluxional compound vs $T_{d,\,10\%}$=187.08°C for the reduced compound). These observations support our hypothesis that the pericyclic rearrangements of bullvalene impart added thermal stability in polymer chains, presenting another advantage of using bullvalene as a monomer unit. To expand on these studies, we plan on investigating the decomposition pathways of fluxional and reduced bullvalene cages. To accomplish this, we will use TGA-MS (thermal gravimetric analysis-mass spectroscopy) to identify the decomposition products of these compounds. From there, we will propose possible decomposition reactions; if our hypothesis is correct, the decomposition pathway of the reduced bullvalene will be initiated by breaking of the strained cyclopropane.

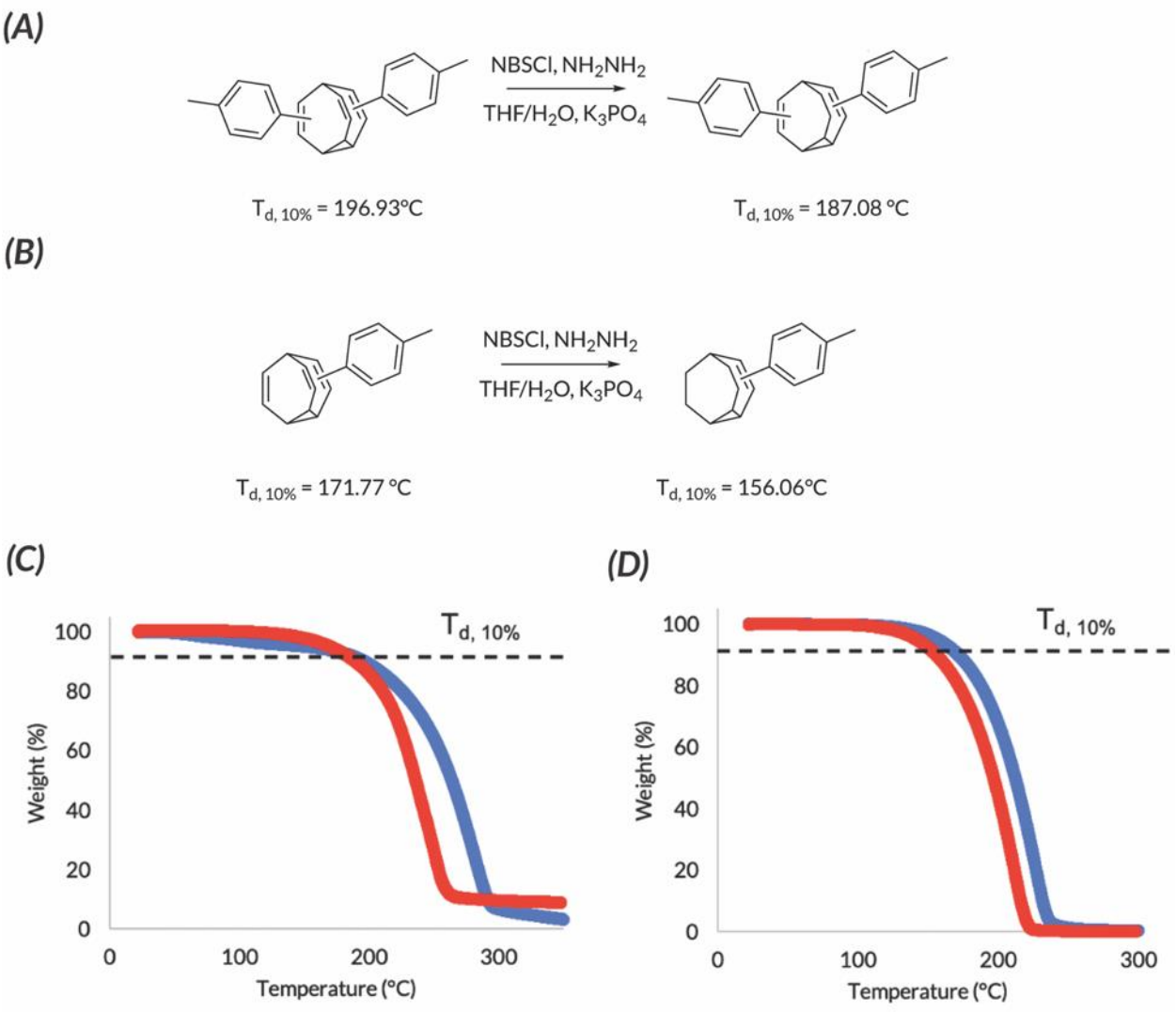

Figure 2.17. (A) Diimide reduction of di-tolyl bullvalene to access a semi-fluxional bullvalene analog; (B) Diimide reduction of mono-tolyl bullvalene to access a static bullvalene analog; (C) Comparison of decomposition profiles of fluxional (blue) and reduced (red) di-tolyl bullvalenes using TGA; (D) Comparison of decomposition profiles of fluxional (blue) and reduced (red) mono-tolyl bullvalenes using TGA

2.7 Attempts at making poly(bullvalene)

2.7.1 Motivation

Inspired by the unusual physical properties of $\mathbf{PB_xP_y}$ polymers, we sought to expand the scope of polymers that can be made using bullvalene building blocks. We have shown that with just 22% bullvalene incorporation, the physical properties are altered drastically, turning pi-rich rigid polymers into amorphous materials with near room temperature glass transitions. Based on these results, we wondered what the physical properties of a fully fluxional poly(bullvalene) would be. With this goal in mind, we investigated methods of directly coupling substituted bullvalenes. One method that was particularly appealing was a mild oxidative homocoupling of aryl boronic esters because we could readily access bis-Bpin bullvalene monomers (Figure 2.15).[11]

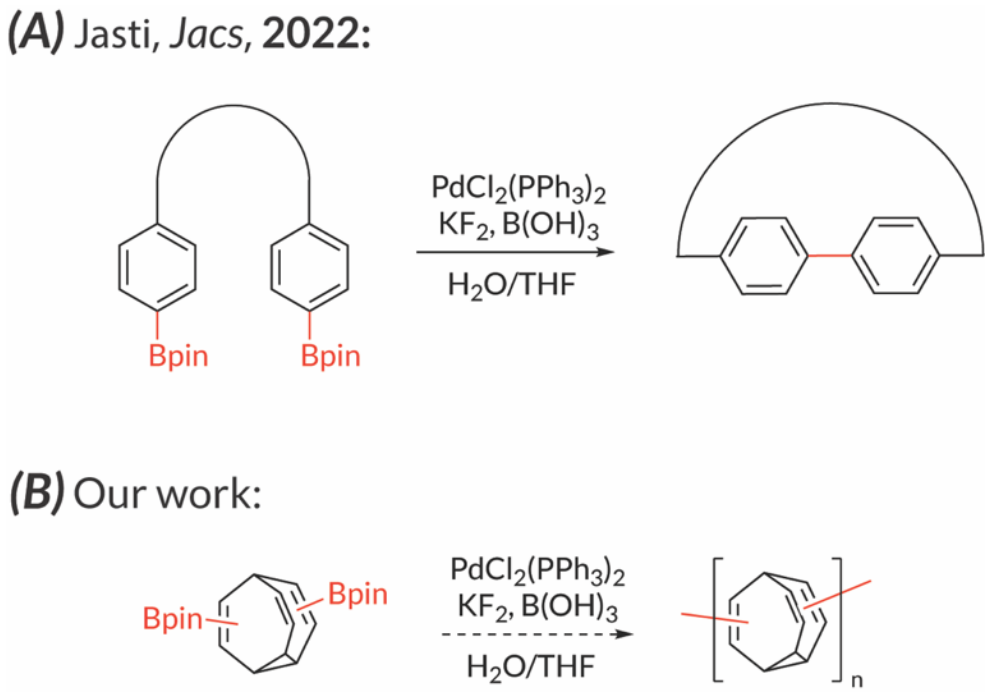

Figure 2.18. A) Mild intramolecular oxidative homocoupling conditions used to generate strained macrocycles; B) Using oxidative homocoupling conditions to attempt to synthesize poly(bullvalene) from *bis*-Bpin bullvalene.

2.7.2 Attempts at making poly(bullvalene)

We screened a variety of concentrations and temperatures to homopolymerize bis-Bpin bullvalene using this Pd catalyzed oxidative homocoupling approach, and encouragingly, observed polymeric species in each reaction (Table 2.2). Ultimately, the most promising conditions produced a 4.8 kDa polymer and were run at 60°C at 1.0 M. Inspired by ball mill Suzuki couplings, these polymerizations were also attempted in the solid state unsuccessfully; no reaction was observed.

Type of reaction	**Concentration (M)**	**Temperature (°C)**	**Polymer?**	**Approx. size (kDa)***
Solution	0.1	rt	Yes	1.1
Solution	0.5	rt	Yes	1.5
Solution	0.5	60	Yes	2.9
Solution	1.0	60	Yes	4.8
Ball mill	30 uL solvent	rt	No	x
Ball mill	No solvent	rt	No	x

Table 2.2. Conditions for oxidative homocoupling polymerizations of *bis*-Bpin bullvalene; size measured by GPC-MALS.

Unfortunately, the resulting polymeric species from these reactions were very difficult to characterize. Due to the rapid pericyclic rearrangements, these polymers could have no permanent structure and therefore no characteristic NMR peaks. However, ^{1}H NMR peaks were quite broad at room temperature which was promising for the presence of bullvalene in the polymeric species. In an attempt to further characterize these polymers, we looked at temperature dependence on peak broadness using ^{1}H NMR. Surprisingly, we did not see the characteristic peak sharpening at low temperatures that is usually observed in bullvalene containing compounds (Figure 2.16).

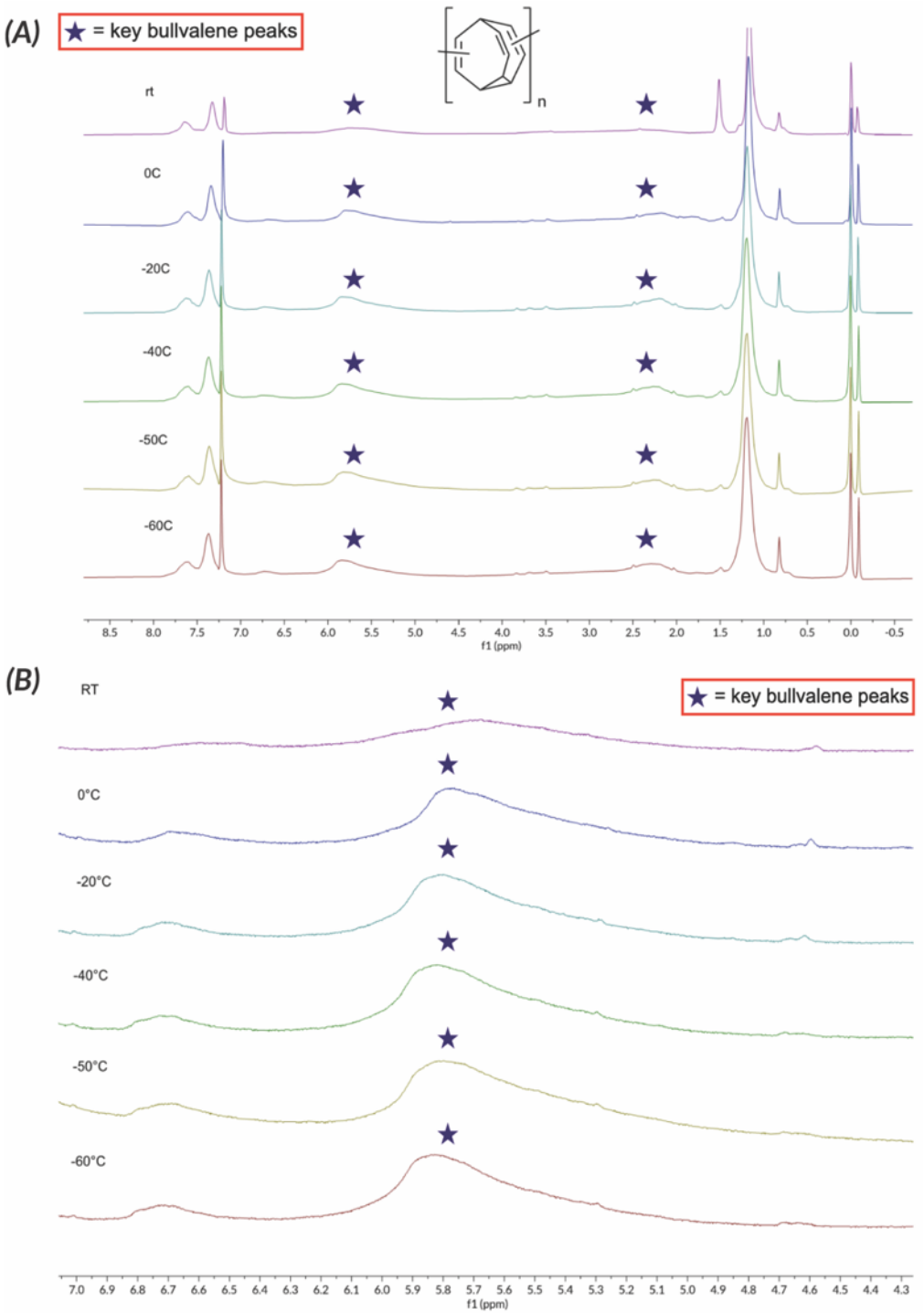

Figure 2.19. A) VT ^{1}H NMR of polymeric species obtained by oxidative homocoupling polymerization of *bis*-Bpin bullvalene; B) Zoom on the alkene region of the above spectrum

To explain these observations, we speculated that bullvalene was either decomposing over the course of the reaction, or that directly linked bullvalenes could undergo a rearrangement with one another separate from the typical bullvalene Hardy-Cope rearrangement. To rule out the first hypothesis, we subjected a TMS substituted bullvalene to the reaction conditions and did not observe any decomposition, indicating that the bullvalene cage can withstand oxidative homocoupling conditions. Because bullvalene substituents are most likely to be in the alkene position, we hypothesized that poly(bullvalenes) would also be linked in the alkene position. This could be problematic because Fallon demonstrated that divinyl bullvalenes could undergo an alternate pericyclic rearrangement (Figure 2.17).[12] This rearrangement could be possible for our polymers, and could propagate across the entire polymer chain.

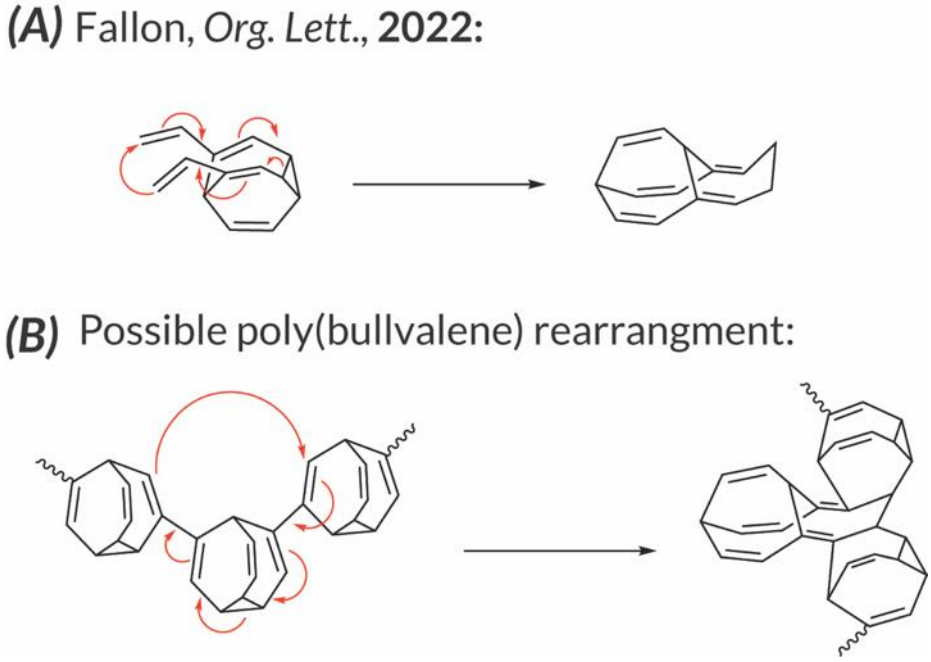

Figure 2.20. A) Divinyl bullvalene pericyclic rearrangement; B) Possible pericyclic rearrangement in poly(bullvalene).

2.7.3 Ongoing work

To gain more insight the composition of our polymers, future efforts will include synthesizing model small molecule bullvalene dimers and trimers from boronate ester bullvalenes. With small molecules, we will be able to more easily elucidate the structure and fluxionality to determine if they are going through similar rearrangements to divinyl bullvalenes. Once it is determined that we have poly(bullvalene) in hand, we will optimize polymerization conditions to access higher molecular weights on larger scales to assess the thermal and possibly mechanical properties of these fully fluxional polymers.

2.8 Attempts at incorporating bullvalene into commodity polymers

2.8.1 Motivation

In an effort to further expand the scope of bullvalene containing polymers and assess their industrial utility, we aim to incorporate bullvalene into commodity polymers such as polyurethanes. Polyurethanes are a class of polymers characterized by a carbamate linkage between monomer units, comprising myriad consumer materials including both thermoplastics and networks.[13] These polymers are typically comprised of rigid and flexible subunits; the ratios of rigid and flexible monomers can be adjusted to tailor the physical properties leading to a broad range of applications, including adhesives, coatings, building materials, and insulation.[14] The most common method to synthesize polyurethanes is through an addition reaction of diisocyanate and diol monomer units.[15] We hypothesize that by using bullvalene as a chemically flexible unit in polyurethanes, we can further tailor these materials to achieve properties and architecture that are not possible using traditional *physically* flexible monomer units (Figure 2.18). Additionally, we hypothesized that polyurethanes would be a good material to test the mechanical properties of bullvalene containing polymers. Because the addition reaction to make polyurethanes is more

efficient that the Suzuki couplings used to make **PB$_x$P$_y$**, we hypothesized we could more easily access polymers above the entaglement molecular weight for these materials.

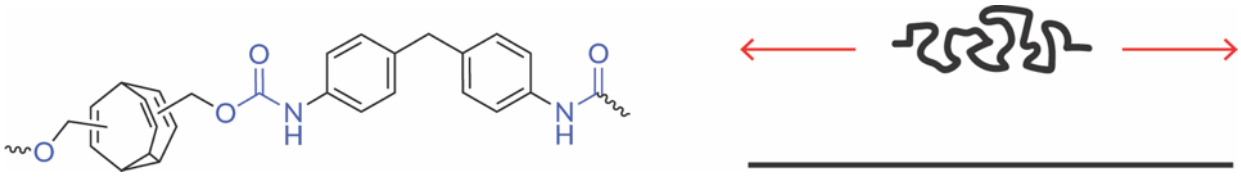

Figure 2.21. Target bullvalene polyurethane and envisioned tensile testing

2.8.2 Attempted synthesis of bullvalene containing polyurethanes

To achieve the desired polyurethane, we envisioned dimethanol bullvalene as the flexible monomer unit to couple with an aryl diisocyanate using a Lewis acid catalyst. We attempted to synthesize the dimethanol bullvalene using the previously reported cobalt mediated [6+2] cycloaddition of 1,4-butyne diol and cyclooctatetraene followed by a photosensitized di-pi methane rearrangement. Unfortunately, yields for this method were low (~5% yield across two steps) due to the formation of lumibullvalene byproduct during the photochemical rearrangement (Figure 2.19).[16] Because we were attempting to make large amounts of polymer with high molecular weights for mechanical testing, we investigated alternate methods to achieve higher yields of the bullvalene monomer.

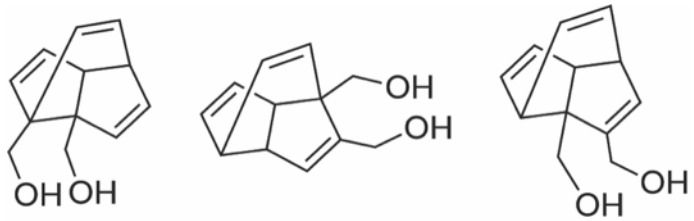

Figure 2.22. Lumibullvalene byproducts observed in the photochemical rearrangement of the dimethanol cycloadduct

First, we speculated that that the proximity of the alcohol to the bullvalene cage in the photochemistry was driving the formation of lumibullvalene. To overcome this, we decided to

target diethanol bullvalene with the intention that a two-carbon spacer would improve yield. Unfortunately, we observed no conversion of starting material to cycloadduct in the cobalt mediated [6+2] cycloaddition. Before optimizing this step, we decided to test the photochemistry on a mono substituted ethanol substituted bullvalene to ensure that efforts towards the two-carbon spacer monomer was worthwhile. Regrettably, lumibullvalene formation was still favorable, even with the alcohol further away from the bullvalene cage. We also attempted a tetrahydropyran protected diol, but observed decomposition under the deprotection conditions (bullvalene appears to be unstable under acidic conditions. Acetoxy and acetal protecting groups were also attempted with little success; lumibullvalene was the major product during the photochemistry step. So far, the most promising method involves TBS protection of the diol at the alkyne stage of the synthesis.

However, this adds two steps with only a small improvement in yield, so future efforts will go towards continuing to investigate alternate methods of diol synthesis (Figure 2.20).

Nevertheless, we investigated conditions for addition polymerizations initially using dimethanol cyclohexane as a test compound with methylene diphenyl isocyante, but ran into solubility issues. Using hexamethylene diisocyanate catalyzed by dibutyltin dilaurate appeared successful; lots of insoluble material formed within 5 minutes of the reaction. Characterization of these compounds was difficult because they were minimally soluble in chloroform, however polymeric material was observed by GPC after partial

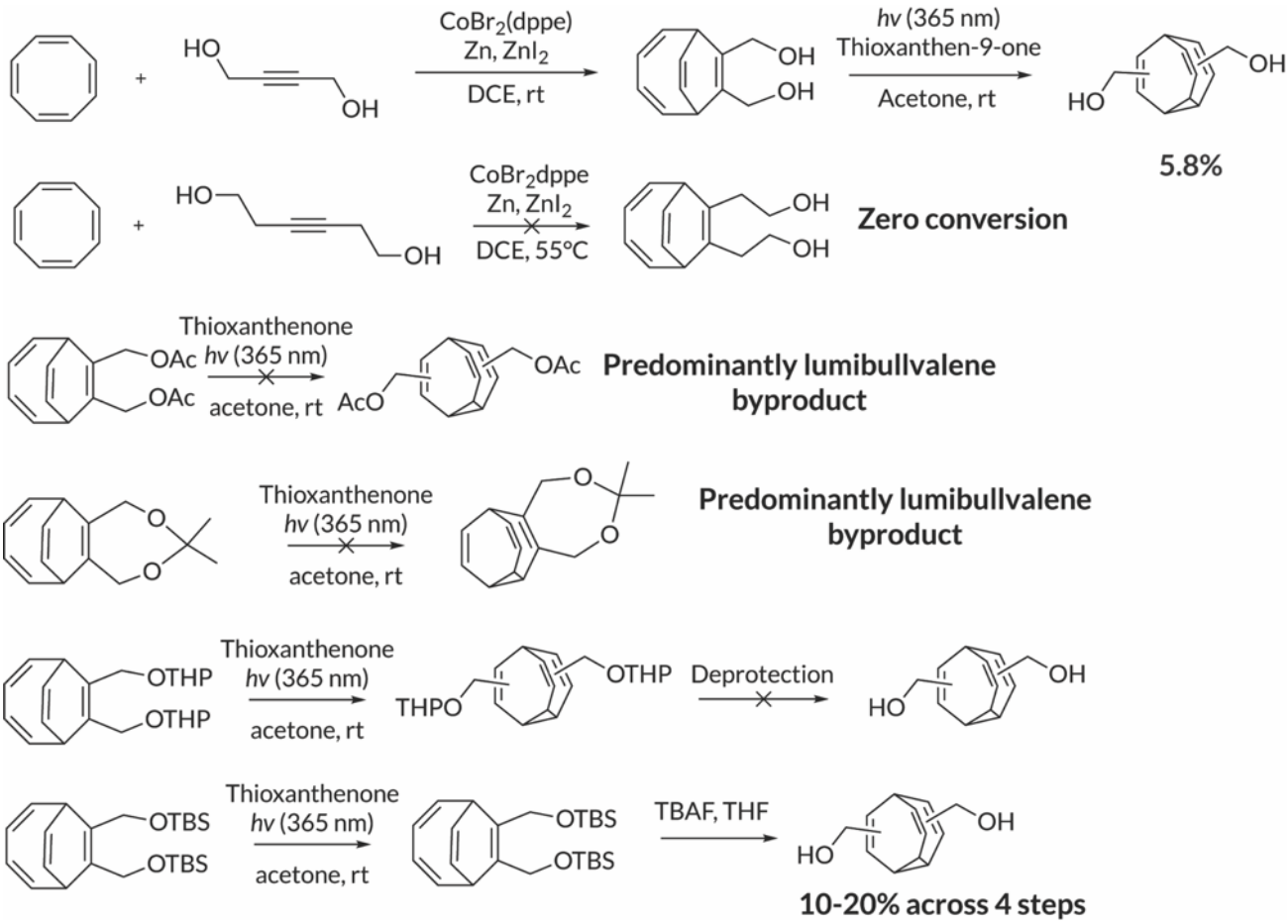

Figure 2.23. Efforts towards bullvalene diol monomer

solubilization in chloroform was achieved using sonication. Once bullvalene diol monomers can be reliably synthesized, these conditions will be employed to synthesize bullvalene containing polyurethanes. A variety of diisocyanate monomer units can be used, and solubility, thermal properties, and mechanical properties will be studied as a function of monomer rigidity.

2.8.3 Preliminary efforts towards bullvalene containing polycarbonates

Similar to polyurethanes, polycarbonates are another class of versatile commodity polymers with a variety of applications including plastics, construction materials, lenses, and electronics.[17] These tough, lightweight materials are characterized by a carbamate linkage and typically synthesized using either a diol monomer and phosgene, or through a transesterification polymerization.[18] We decided to target this class of polymers because we could use the same diol monomer unit as the polyurethanes and it presents the opportunity for incorporating bullvalene into commodity products such as BPA. During bullvalene monomer synthesis, we ran into the same issues that are illustrated in section 2.8.4. Ongoing efforts will go into optimizing monomer synthesis, however polymerization conditions were investigated to determine a potential route towards bullvalene polycarbonates.

Using dimethanol cyclohexane, polymerization with triphosgene in pyridine afforded polymeric product (observed by GPC) in less than ten minutes, highlighting the efficiency of this class of polymerization. However, subjecting the bullvalene monomer to these conditions resulted in no polymeric product by GPC and apparent decomposition of the bullvalene unit by ^{1}H NMR. Attempted polymerizations under milder conditions using dimethylcarbonate afforded no reaction. Future efforts will go towards investigating mild transesterification conditions to produce a

bullvalene polycarbonate, and eventual copolymerization with bisphenol A, to investigate how the properties of a commodity polymer can be tuned using chemical flexibility (Figure 2.21).

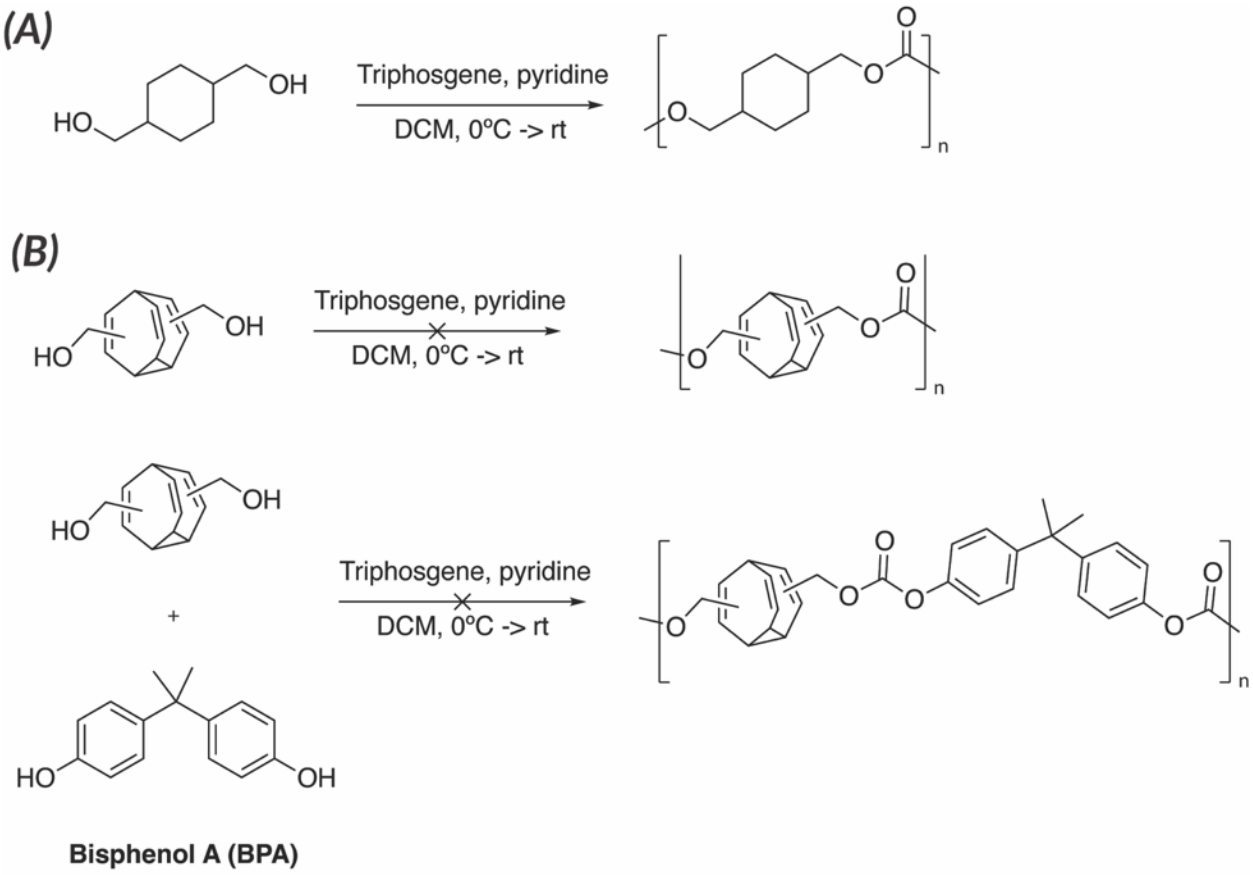

Figure 2.24. A) Test polycarbonate polymerization; B) Efforts towards bullvalene polycarbonates

2.9 Summary

In summary, we synthesized a series of alternating (**$PB_{50}P_{50}$**) and randomly doped (**$PB_{50}P_{50}$**) poly(bullvalene-*co*-phenylene)s using a Suzuki-Miyuara polycondensation. These polymers exhibit good thermal stability ($T_{10\%}$=243 °C) and have tuneable thermal properties relative to traditional **PB_0P_{100}-5.0 k**. **$PB_{50}P_{50}$**s have low glass transition temperatures of 21–44 °C caused by randomly kinked bullvalene building blocks. We can further tune the solution-state and thermal

properties of π-rich materials by randomly doping poly(*p*-phenylene)s (**PB**$_x$**P**$_y$) with varying bullvalene densities (x=0–34 %). We demonstrate that alternative rigid conjugation break spacers (e.g., cyclohexene, norbornadiene, adamantane) that could potentially perturb materials properties are not only difficult to introduce within poly(*p*-phenylene) backbones compared to bullvalene, but are also incapable of yielding the *non-uniform* kinks necessary to modulate backbone architecture. Bullvalene incorporation represents a fundamentally new approach to control chain rigidity because stochastic backbone kinks originate from a single rigid molecular cage. We anticipate that bullvalene can act as an internal plasticizer to modulate properties within other classes of π-rich polymers. Furthermore, solution-state fluxionality will allow bullvalene-containing polymers to serve as a motif from which to construct a wide array of responsive and dynamic soft materials in the near future.

Ongoing work includes investigating the origin of the thermal stability of bullvalene. In small molecule model compounds, bullvalene's thermal stability decreases upon reduction, suggesting that its fluxionality may play a role in this process. Further experiments using TGA/MS should provide further insight on bullvalene's decomposition pathway and products formed. Further investigation will go into synthesizing and characterizing poly(bullvalene) and incorporating bullvalene into commodity polymers such as polyurethanes and polycarbonates.

2.10 Experimental

2.10.1 General considerations

All reagents were purchased from commercial suppliers and used as received unless otherwise noted. Bis-Bpin alkyne was purchased from Tokyo Chemical Industry (TCI) or prepared using the procedure detailed below. Glassware was flame dried or dried in an oven overnight at 120 °C before use. Degassed and anhydrous tetrahydrofuran (THF), dichloromethane (DCM), toluene, and diethyl ether (Et_2O) were obtained from a JC Meyer solvent purification system. 1,2 dichloroethane (DCE) was dried over 3Å molecular sieves for at least 3 days before use. All moisture and air-sensitive reactions were performed under inert atmosphere (nitrogen) using standard Schlenk technique. SiliaFlash F60 (40-63 μm, 230-400 mesh) silica gel was used for column chromatography. Automated flash chromatography was performed using a Yamazen Smart Flash AKROS system. Preparative gel permeation chromatography (prep-GPC) was performed using a Japan Analytical Industries LaboACE recycling preparative HPLC system equipped with JAIGEL-2.5HR and JAIGEL-3HR columns in series using chloroform (stabilized with 0.5% - 1.0% ethanol) as the mobile phase. Photochemistry was performed using an EvoluChem PhotoRedOx Box (HepatoChem) with 365 nm LEDs.

^{1}H nuclear magnetic resonance (^{1}H NMR) and ^{13}C nuclear magnetic resonance (^{13}C NMR) spectra were obtained on a Bruker AVANCE-300, Bruker AVANCE-500, or Bruker DRX-500 NMR spectrometer. Variable temperature VT-^{1}H NMR spectra were taken on a Bruker AVANCE-500 NMR spectrometer. ^{1}H NMR spectra were taken in chloroform-*d* ($CDCl_3$, referenced to TMS, δ 0.00 ppm), benzene-*d6* (C_6D_6, referenced to residual C_6H_6, δ 7.16 ppm), or dichloromethane-*d2* (CD_2Cl_2, referenced to residual CH_2Cl_2, δ 5.32 ppm). Small molecule ^{13}C NMR spectra were taken in chloroform-*d* (referenced to chloroform, δ 77.16 ppm).

Polymer ^{13}C solution-state 1D spectra were recorded on a 800 MHz Bruker Avance III spectrometer equipped with a TCI-HCN cryoprobe with Z-gradient. An acquisition time of 255 ms was employed with a recycle delay of 2 s. GARP broadband decoupling and NOE enhancement irradiation was used to get sensitivity-enhanced ^{1}H decoupled ^{13}C spectra. A total of 2048 scans were used to obtain the $\mathbf{PB_0P_{100}}$ spectrum and 4096 scans were used for the $\mathbf{PB_{50}P_{50}}$ spectrum. The spectral width was set to 160 ppm, centered at 75 ppm. A 90 degree tip angle was used for all the scans.

Solid-state NMR experiments were conducted on a Bruker AVANCE III 300 NMR with ^{13}C and ^{1}H resonance frequencies of 75.5 and 300.1 MHz, respectively. The samples were packed in 4 mm diameter rotors. The magic-angle spinning (MAS) frequency was set to 12,000 ± 5 Hz. In ^{13}C cross polarization (CP)MAS NMR experiments, ramp CP with a maximum rf field strength for ^{1}H of 50 kHz and ^{13}C fixed rf field strength of 62 kHz were used. ^{1}H 90° pulse length, CP contact time, and recycle delay were set to 3.3 μs, 2 ms, and 2 s, respectively. The ^{13}C chemical shift was calibrated externally based on the methine peak of adamantane at 29.46 ppm.

NMR spectra were analyzed on MestreNova software. Chemical shifts are represented in parts per million (ppm); splitting patterns are assigned as s (singlet), d (doublet), t (triplet), q (quartet), p (quintet), m (multiplet), and br (broad); coupling constants, *J*, are reported in hertz (Hz).

Gel permeation chromatography (GPC) data were collected on Agilent 1260 HPLC equipped with a Wyatt 8-angle DAWN NEON light-scattering detector, ViscoStar NEON viscometer, and Optilab NEON refractive index detector. GPC samples were analyzed at a flow rate of 1 mL/min in chloroform stabilized with 0.5% - 1.0% ethanol through two Agilent PLgel MIXED-C columns

at 35 ºC. dn/dc values were determined by the 100% mass recovery method using Wyatt Astra 7.3 software.

Thermogravimetric analysis (TGA) data was collected using a TA Discovery Q5000 thermogravimetric analyzer. Samples were heated in hermetically sealed aluminum Tzero pans a rate of 10 °C per minute from 25 °C to 600 °C under an N_2 atmosphere. Differential scanning calorimetry (DSC) data was collected using a TA Discovery DSC 2500. Samples were freeze dried from benzene to remove residual solvents before measurement. Samples were heated from room temperature to 200 °C (heating rate = 5 °C per minute) followed by cooling to between 0 °C and –75 °C (cooling rate = 5 °C per minute) to clear the thermal history. Samples were then re-heated 200 °C (heating rate = 5 °C per minute) for data collection ("second heat").

2.10.2 Preparation of monomers

Synthesis of bis-Bpin-acetylene (1,2-bis(4',4',5',5'-tetramethyl-1,3,2-dioxaborolan-2-yl)ethyne) (1)

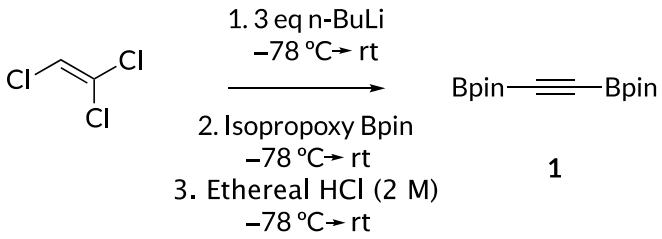

1

A solution of trichloroethylene (4.49 mL, 49.9 mmol, 1.00 eq.) in 320 mL dry THF was prepared in a dry 1 L flask and cooled to -78°C. A 2.09 M solution of *n*-BuLi in hexanes (71.8 mL, 150 mmol, 3.00 eq.) was added dropwise to the trichloroethylene solution over 15 minutes using a cannula. The reaction mixture was warmed to room temperature and stirred for 18 hours under nitrogen. The reaction mixture was then cooled to -78°C and 2-isopropoxy-4,4,5,5-tetramethyl-

1,3,2-dioxaborolane (20.4 mL, 99.8 mmol, 2.00 eq.) was added dropwise over 15 minutes using a cannula. The solution warmed to room temperature and stirred under nitrogen. After 4 hours, the reaction was quenched by adding 2.0 M ethereal HCl (50 mL, 100 mmol, 2.00 eq.) dropwise over 20 minutes using a syringe. The mixture warmed to room temperature over 30 minutes, then was filtered through celite and evaporated to dryness. The white solid was washed with cold hexanes (3 x 20 mL) and decanted. The remaining solid was then extracted with room temperature hexanes (6 x 500 mL) and filtered through celite. The filtrate was evaporated to dryness yielding bis-Bpin acetylene **1** as a white powder (8.10 g, 58%). ^{1}H-NMR (300 MHz, $CDCl_3$) δ = 1.25 (s, 24H); ^{13}C-NMR (300 MHz, $CDCl_3$) δ = 84.6 (C-C), 24.5 (CH_3), (C-B not observed). Characterization data agreed with the literature.[9]

Synthesis of $CoBr_2$(dppe)

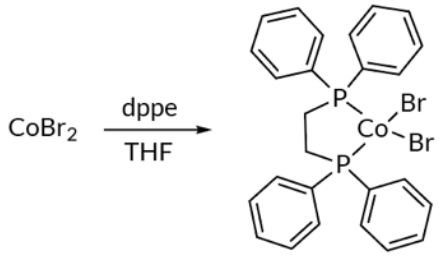

Diphenylphosphinoethane (dppe, 3.33 g, 8.37 mmol, 1.00 eq.) was added to a 250 mL flame dried flask. The flask was then evacuated and refilled with nitrogen three times. Dry THF (50 mL) was added to the reaction flask and stirred until dppe was completely dissolved. Then, $CoBr_2$ (1.83 g, 8.37 mmol, 1.00 eq.) was added and the reaction stirred at room temperature under nitrogen. The reaction mixture was filtered under vacuum and the precipitate (catalyst) was dried under vacuum (ca. 100 mTorr) for 6 hours yielding the catalyst as a green powder (5.12 g, 99%).[19]

Synthesis of bis-Bpin bicyclo[4.2.2]deca-2,4,7,9-tetraene (2)

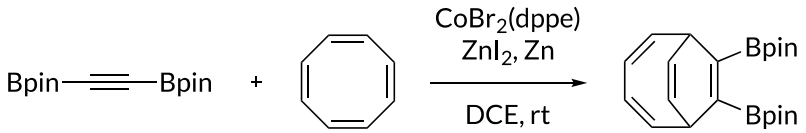

1 2

$CoBr_2$(dppe) (555 mg, 0.899 mmol, 0.100 eq.), ZnI_2 (574 mg, 1.80 mmol, 0.200 eq.), and Zn (176 mg, 2.70 mmol, 0.300 eq.) were added to a flame dried flask with a magnetic stir bar. The flask containing solids was evacuated and refilled 3 times. Then, 10 mL dry, degassed DCE (sparged with nitrogen for 20 minutes) was added and the mixture stirred for 15 minutes under nitrogen. Cyclooctatetraene (1.01 mL, 8.99 mmol, 1.00 eq.) and bis-Bpin alkyne **1** (2.50 g, 3.60 mmol, 1.00 eq.) were added to the reaction mixture and the reaction stirred for 6 hours at room temperature under nitrogen. Once the reaction was complete, diethyl ether (10 mL) was added to precipitate the catalyst and the mixture was filtered through neutral alumina. The filtrate was evaporated to dryness. The resulting brown oil was purified via column chromatography using 40% dichloromethane in hexanes (R_f = 0.35) yielding the target cycloadduct **2** as a yellow/colorless oil (2.5 g 72%). ^{1}H-NMR (300 MHz, $CDCl_3$) δ = 6.17-6.11 (tt, 2H), 5.73-5.68 (m, 4H), 3.42-3.38 (m, 2H), 1.27 (s, 24H). Characterization data agrees with the literature.[9]

Synthesis of bis-Bpin bullvalene (3)

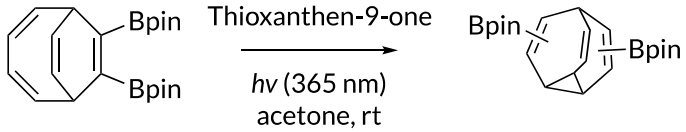

2 3

Thioxanthen-9-one (78.0 mg, 0.370 mmol, 0.250 eq.) and the bis-Bpin cycloadduct **2** (3.00 g, 1.46 mmol, 1.00 eq.) were dissolved in acetone (1 mL) in an 8 mL vial and capped under air. The reaction mixture was placed in the EvoluChem PhotoRedOx box, irradiated with UV light (λ =

365 nm), and stirred at room temperature for 18 hours. Then, the reaction mixture was evaporated to dryness. The resulting yellow solid was purified via prep-GPC (retention time = 27.4 minutes) followed by recrystallization in diethyl ether (1 mL ether per 100 mg crude product at 35°C). The resulting white crystals were washed with hexanes (1 x 3 mL). The crystals were then dried under vacuum yielding bis-Bpin bullvalene **3** (1.80 g, 60%). ^{1}H-NMR (300 MHz, $CDCl_3$, –60 °C) δ = 6.89 (m, 1H), 6.82 (s, 0.5H), 6.77 (m, 1H), 6.67 (s, 0.2H), 5.97 (m, 2H), 5.85 (m, 1H), 5.75 (s, 0.12H), 3.04 (s, 0.2H), 2.75 (m, 1H), 2.67 (m, 1H), 2.51-2.43 (m, 3H), 1.31 (s, 36H). Characterization data agrees with literature.[9]

Synthesis of 1,4-dihexyl benzene (4)

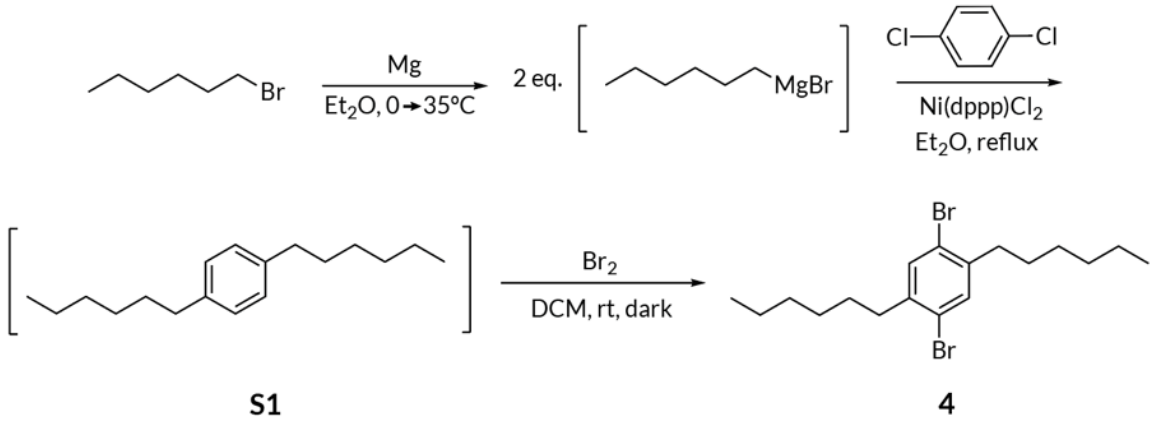

S1 **4**

A solution of bromohexane (2.55 mL, 18.2 mmol, 1.00 eq.) in diethyl ether (20.0 mL) was prepared in a flame dried 100 mL flask. Magnesium (486 mg, 20.0 mmol, 1.10 eq.) was added to a separate flame dried 100 mL flask, suspended in dry diethyl ether (2 mL), and cooled to 0 °C. The bromohexane solution was slowly added to the flask containing Mg over 20 minutes using a cannula. As the bromehexane was added, the reaction mixture turned black and opaque and the

Mg pieces disappeared as the reaction progressed. The reaction was heated to reflux and stirred for 3 hours under nitrogen.

1,4-dichlorobenzene (1.00 g, 6.80 mmol, 1.00 eq.) and Ni(dppp)Cl_2 (42.0 mg, 0.0760 mmol, 0.0113 eq.) were added to a separate flame dried 100 mL flask fitted with a condenser. The flask and condenser were evacuated and refilled with nitrogen 3 times. Then, the solids were dissolved in dry diethyl ether (5 mL) and cooled in an ice bath. After stirring for 15 minutes, the previously generated hexyl magnesium bromide (0.90 M, 15.0 mL, 2.20 eq.) was added dropwise to the reaction mixture. As the Grignard reagent was added, the reaction mixture turned from red to dark brown/black. After 24 hours, the reaction mixture was cooled to 0 °C, and water (0.500 mL) was added dropwise followed by 2.0 M aq. HCl (5.00 mL). Once the reaction was quenched, the ice bath was removed and the reaction mixture warmed up to room temperature. The reaction mixture was transferred to a separatory funnel and the organic layer was collected. The aqueous layer was washed with diethyl ether (2 x 5 mL). The combined organic layers were washed with water (2 x 5 mL) and dried over magnesium sulfate, decanted, and evaporated to dryness. The crude black/brown oil was distilled at 100 °C under vacuum (ca. 100 mTorr). The resulting colorless oil, 1,4-dihexyl benzene **S1**, was used in the next reaction without further purification.

1,4-dihexyl benzene **S1** (1.43 g, 5.78 mmol, 1.00 eq.) and iodine (7.20 mg, 0.0280 mmol, 0.010 eq.) were added neat to a 25 mL flask with a stir bar. The reaction vessel was covered in foil to exclude light. The reaction stirred at 0 °C for 20 minutes. Then, bromine (0.610 mL, 12.0 mmol, 2.05 eq.) was added dropwise to the reaction mixture. The reaction stirred at room temperature open to air for 1 day. After 18 hours, a 20% aq. KOH solution (2.70 mL) was added to the reaction mixture. The reaction mixture was warmed to 35 °C and stirred until the color changed from dark red to yellow/orange. Then, the reaction mixture cooled to room temperature and transferred to a

separatory funnel and 5 mL DCM was added. The organic (DCM) layer was collected and the aq. layer was extracted with DCM (3 x 5 mL). The organic layers were combined, dried over sodium sulfate, and evaporated to dryness. The resulting white/yellow crystals were recrystallized in warm ethanol (2.5 mL ethanol per 1 g crude product at 60 °C. The resulting white crystals were filtered and dried under vacuum to afford **4** (1.10 g, 77%). ^{1}H-NMR (300 MHz, $CDCl_3$) δ = 7.35 (s, 2H), 2.63 (br t, *J* = 8.0 Hz, 4H), 1.65-1.56 (m, 4H), 1.36-1.31 (overlap, 12H), 0.89 (t, *J* = 7.0 Hz, 6H). Characterization data agrees with the literature.

2.10.3 Preparation of polymers (PB_xP_y)

Suzuki cross coupling of bis-Bpin bullvalene and aryl bromide

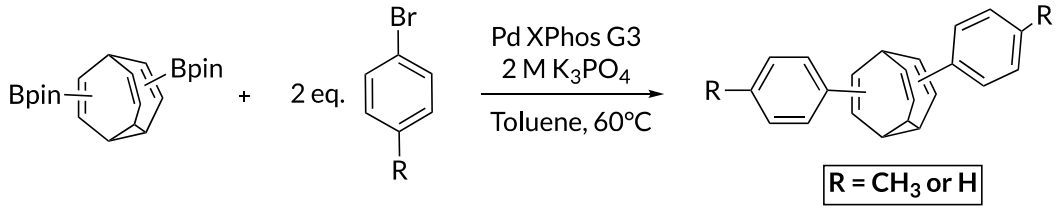

Isomer distribution at –60°C for **R = H**:

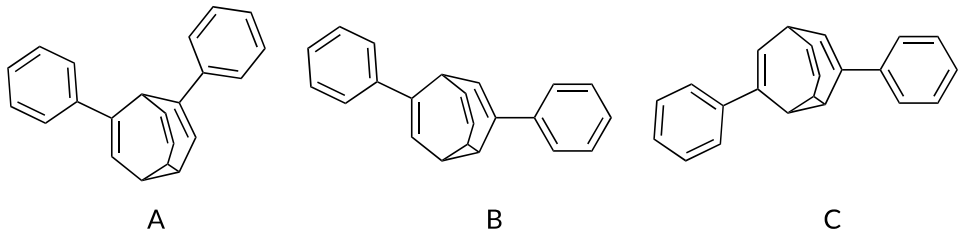

A:B:C = 51:39:10

S2-H: Bis-Bpin bullvalene **3** (200 mg, 0.523 mmol 1.00 eq.), bromobenzene (164 mg, 1.05 mmol, 2.00 eq.), and Pd XPhos G3 (48.0 mg, 0.0523 mmol, 0.100 eq.) were added to a 50 mL Schlenk flask with a stir bar and the flask was evacuated and refilled with nitrogen 3 times. Degassed

(sparged for 30 minutes) toluene (12 mL) and 2M aq. potassium phosphate (2 mL) were added to the reaction mixture. The reaction was stirred under nitrogen at 60 °C. After 24 hours, the reaction mixture was diluted with 10 mL diethyl ether, filtered through a short silica plug. The filtrate was dried over sodium sulfate and evaporated to dryness. The reaction mixture was further purified via column chromatography using 40% DCM in hexanes (R_f = 0.4) yielding **S2-H** as a white solid (160 mg, 95%). ^{1}H-NMR (300 MHz, $CDCl_3$, 25°C) δ = 7.48-7.05 (overlap, 10H), 6.51-5.52 (br, 4H), 3.76-3.30 (br, 1H), 2.77-2.14 (br, 3H).

S2-Me: Bis-Bpin bullvalene **3** (280 mg, 0.730 mmol 1.00 eq.), *p*-bromotoluene (269 mg, 0.670 mmol, 2.00 eq.), and Pd XPhos G3 (122 mg, 0.13 mmol, 0.200 eq.) were added to a 50 mL Schlenk flask with a stir bar and the flask was evacuated and refilled with nitrogen 3 times. Degassed (sparged for 30 minutes) toluene (10 mL) and 2M aq. potassium phosphate (3 mL) were added to the reaction mixture. The reaction was stirred under nitrogen at 60 °C. After 24 hours, the reaction mixture was transferred to a separatory funnel and diluted with additional toluene (2 mL) and water (2 mL). The organic layer was washed with water (2 x 1 mL), dried over sodium sulfate, and decanted into a new 25 mL flask. To the solution, SiliCycle MetS triamine Pd scavenger (100 mg, 2:1 product/resin mass ratio) was added and stirred for 6 hours. The solution was filtered through neutral alumina and the filtrate was evaporated to dryness. The reaction mixture was further purified using preparative GPC (retention time = 27 min) yielding bis-tolyl bullvalene **S2-Me** as a white solid (192 mg, 85%). ^{1}H-NMR (300 MHz, $CDCl_3$, 25°C) δ = 7.09-7.22 (br, 8H), 6.22-6.01 (br, 4H), 2.43-2.31 (br, 10H).

Suzuki polycondensation of bis-Bpin bullvalene and 2,5-dibromo-1,4-dihexyl benzene (representative procedure for alternative co-polymer $PB_{50}P_{50}$ synthesis)

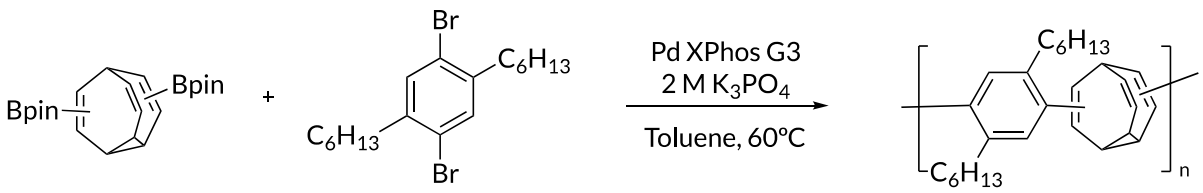

3 **4** **$PB_{50}P_{50}$**

Bis-Bpin bullvalene **3** (100 mg, 0.26 mmol, 1.20 eq.), 2,5-dibromo-1,4-dihexyl benzene **4** (88 mg, 0.22 mmol (1.00 eq.) and Pd XPhos G3 (40.0 mg, 0.044 mmol, 0.200 eq.) were added to a flask with a stir bar and the flask was evacuated and refilled 3 times. After sparging with N_2 for 30 minutes, 6 mL dry toluene and 1 mL degassed 2 M potassium phosphate were added to the reaction mixture. The reaction stirred under nitrogen at 60 °C. After 48 hours, the reaction mixture was transferred to a separatory funnel and diluted with an additional 2 mL toluene and 2 mL water. The organic layer was washed with 2 x 1 mL water and dried over sodium sulfate. The solution was then transferred to a new flask and SiliCycle MetS triamine Pd Scavenger (100 mg, 2:1 product/resin mass ratio) was added and stirred for 6 hours. The solution was filtered through neutral alumina and the filtrate was evaporated to dryness. The polymer was further purified using preparative GPC (retention time = 18 - 24 minutes for a 10 kDa polymer). The purified product was freeze dried by dissolving in 2 mL benzene, freezing in liquid N_2, and drying overnight under vacuum (ca. 100 mTorr) yielding a yellow solid (50 mg, dn/dc = 0.1114 mL/g). ^{1}H-NMR (300 MHz, $CDCl_3$, 25°C) δ = 6.90 (s, 2H), 5.98-5.81 (br, 3.5H), 2.59 (br, 7H), 1.54 (s, 5H), 1.27 (s, 14H), 0.85 (s, 6H).

Suzuki polycondensation of bis-Bpin bullvalene 3 and/or 1,4-benzenedibornic acid bis(pinacol) ester 5 with 2,5-dibromo-1,4-dihexyl benzene (representative procedure for random co-polymer $PB_{34}P_{66}$ synthesis)

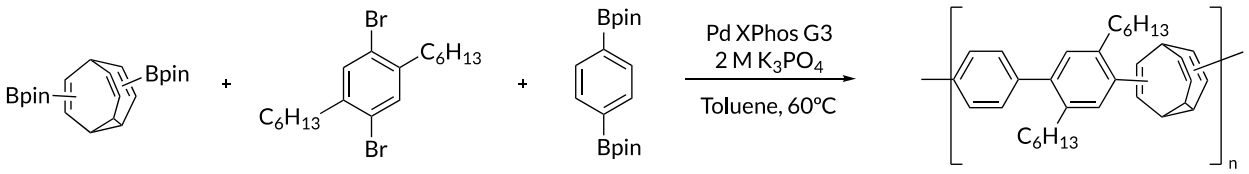

3 4 5

2,5-Dibromo-1,4-dihexyl benzene **4** (100 mg, 0.247 mmol 1.00 eq.), 1,4-benzenediboronic acid bis(pinacol) ester **5** (40.8 mg, 124 mmol, 0.500 eq.), bis-Bpin bullvalene **3** (47.3 mg, 124 mmol, 0.500 eq.) and Pd XPhos G3 (45.4 mg, 0.0495 mmol, 0.200 eq.) were added to a flask with a stir bar and the flask was evacuated and refilled 3 times. After sparging with N_2 for 30 minutes, 6 mL dry toluene and 1 mL degassed 2 M potassium phosphate were added to the reaction mixture. The reaction stirred under nitrogen at 60 °C. After 48 hours, the reaction mixture was transferred to a separatory funnel and diluted with an additional 2 mL toluene and 2 mL water. The organic layer was washed with 2 x 1 mL water and dried over sodium sulfate. The solution was then transferred to a new flask and SiliCycle MetS triamine Pd Scavenger (100 mg, 2:1 product/resin mass ratio) was added and stirred for 6 hours. The solution was filtered through neutral alumina and the filtrate was evaporated to dryness. The polymer was further purified using preparative GPC. The purified product was freeze dried by dissolving in 2 mL benzene, freezing in liquid N_2, and drying overnight under vacuum (ca. 100 mTorr) yielding a yellow solid with a 34% bullvalene incorporation determined using peak integration on ^{1}H-NMR. ^{1}H-NMR (300 MHz, $CDCl_3$, 25°C) δ = 7.37-7.32 (m, 3.1H), 7.01-6.86 (br, 1.5H), 6.30-5.50 (br, 1.5H), 2.75-2.25 (br, 5.5H), 1.54 (s, 4H), 1.27 (s, 15H), 0.85 (s, 7H).

Suzuki polycondensation of 2,5-dibromo-1,4-dihexyl benzene (4) and 1,4-benzenediboronic acid bis(pinacol) ester (synthesis of PB_0P_{100})

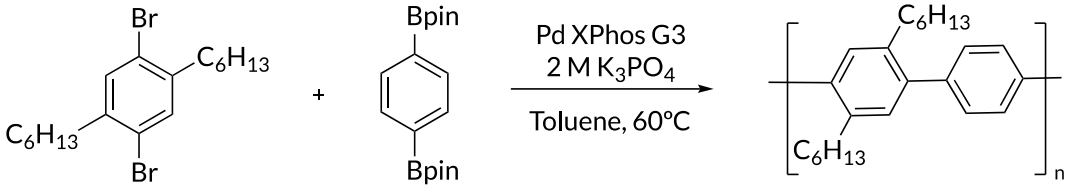

4 5 PB_0P_{100}

1,4-Benzenediboronic acid bis(pinacol) ester (330 mg, 0.606 mmol, 1.00 eq.), 2,5-dibromo-1,4-dihexyl benzene **4** (404 mg, 0.606 mmol, 1.00 eq.) and Pd XPhos G3 (111 mg, 0.121 mmol, 0.200 eq.) were added to a flask with a stir bar and the flask was evacuated and refilled 3 times. After sparging with N_2 for 30 minutes, 6 mL dry THF and 1 mL degassed 2 M potassium phosphate were added to the reaction mixture. The reaction stirred under nitrogen at 60 °C. After 48 hours, the reaction mixture was transferred to a separatory funnel and diluted with an additional 2 mL toluene and 2 mL water. The mixture was extracted with 3 x 5 mL toluene. The organic layer was washed with 2 x 1 mL water and dried over sodium sulfate. The solution was then transferred to a new flask and SiliCycle MetS triamine Pd Scavenger (100 mg, 2:1 product/resin mass ratio) was added and stirred for 6 hours. The solution was filtered through neutral alumina and the filtrate was evaporated to dryness. Only 60 mg of the 180 total mg (33% by mass) of the polymer was soluble in chloroform. This soluble material was further purified using preparative GPC to separate unreacted monomer (retention time = 18 - 24 minutes for a 5.5 kDa polymer). The purified product was freeze dried by dissolving in 2 mL benzene, freezing in liquid N_2, and drying overnight under vacuum (ca. 100 mTorr) yielding poly(phenylene) **PB_0P_{100}** as a yellow solid (50 mg, dn/dc = 0.1325 mL/g). ^{1}H-NMR (300 MHz, $CDCl_3$, 25 °C) δ = 7.81, (s, 1H), 7.69 (br, 1H), 7.46-7.31 (br, 4H), 2.67-2.52 (br, 4H), 1.56-1.41 (br, 9H), 1.26-1.08 (br, 9H), 0.82-0.73 (br, 6H).

2.10.4 Bullvalene reduction studies

Synthesis of Bicyclo[4.2.2]deca-2,4,7,9-tetraene (S3)

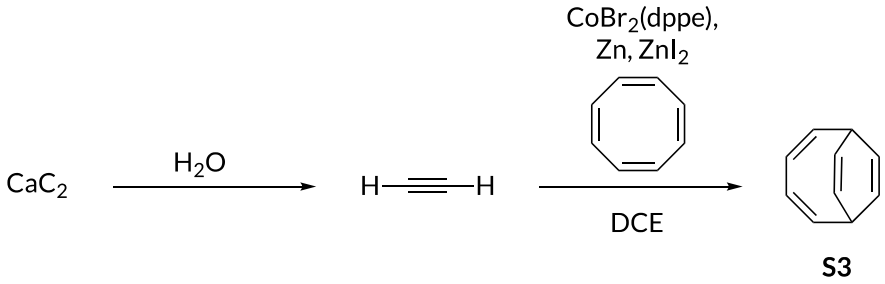

$CoBr_2$(dppe) (296 mg, 0.480 mmol, 0.100 eq.), ZnI_2 (306 mg, 0.960 mmol, 0.200 eq.), and Zn (94.1 mg, 1.44 mmol, 0.100 eq.) were added to a flame dried flask with a magnetic stir bar. The flask containing solids was evacuated and refilled with nitrogen 3 times. Then, dry, degassed DCE (6.00 mL) was added and the mixture stirred for 15 minutes under nitrogen. Cyclooctatetraene (0.540 mL, 4.80 mmol, 1.00 eq.) were added to the reaction mixture. C_2H_2 were generated *in situ* by suspending CaC_2 (12.3 g, 192 mmol, 80.0 eq.) in $CHCl_3$ (20 mL) in a 3-necked flask. The 3-necked flask was connected to the reaction mixture through a tube filled with Drierite. The reaction mixture was left to stir for 16 hours. Once the reaction was complete, DCM (10 mL) was added to precipitate the catalyst and the mixture was filtered through neutral alumina. The filtrate was evaporated to dryness. The resulting brown oil was purified through column chromatography using hexane in hexanes (R_f = 0.4) yielding the target cycloadduct as a white solid (0.270 g, 43%). ^{1}H-NMR (500 MHz, $CDCl_3$) δ 6.24-6.20 (td, J = 8.72, 3.50 Hz, 2H), 5.85-5.81 (m, 2H), 5.64-5.62 (dd, J = 3.86, 2.54 Hz, 4H), 3.27-3.23 (dddd, J = 8.80, 6.43, 4.00, 2.47 Hz, 2H). Characterization data agrees with the literature.[8]

Synthesis of Bullvalene (S4)

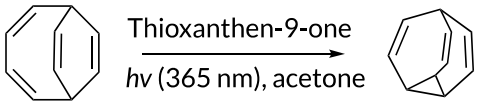

S3 S4

Thioxanthen-9-one (110 mg, 0.520 mmol, 0.250 eq.) and bicyclo[4.2.2]deca-2,4,7,9-tetraene **S3** (0.270 g, 2.10 mmol, 1.00 eq.) were dissolved in acetone (3.00 mL) in a vial and capped under air. The reaction mixture was placed in a the EvoluChem PhotoRedOx box and irradiated with UV light (λ = 365 nm) and stirred at room temperature for 18 hours. Then, the reaction mixture was evaporated to dryness. The resulting crude product was then purified through column chromatography using 20% DCM in hexanes (R_f = 0.35) to afford white solid **S4** (92 mg, 34%). ^{1}H-NMR (500 MHz, $CDCl_3$) δ 6.72-4.35 (br), 1.75-3.45 (br). Characterization data agrees with the literature.[8]

H_2 and Pd/C hydrogenation of bullvalene

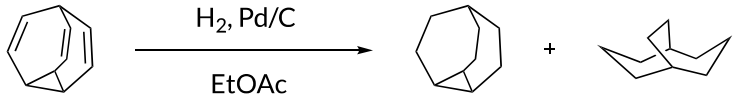

Bullvalene S5 S6

Bullvalene (30 mg, 0.230 mmol, 1.00 eq.) was dissolved in ethyl acetate (2.50 mL) and transferred to a 25 mL round bottom flask with a stir bar. Pd/C (5 mol%, 7.20 mg, 0.0346 mmol, 0.150 eq.) was added to the reaction, and the flask was fitted with a 3-way adapter attached to the vacuum line and a hydrogen balloon. The flask was evacuated and refilled 7 times with hydrogen and the reaction stirred overnight at room temperature under H_2 atmosphere (1 atm). The reaction mixture was filtered through Celite and evaporated to dryness yielding a 2:3 ratio of ring-opened reduced

bullvalene **S5** to hexahydrobullvalene **S6** as a volatile white solid (30% combined ^{1}H NMR yield). Analytically pure samples for characterization were isolated by prep-GPC. **5**: ^{1}H-NMR (500 MHz, $CDCl_3$) δ 2.19 (br, 2H), 1.73-1.45 (overlap, 16H). ^{13}C-NMR (500 MHz, CDCl3) δ 33.71, 32.88, 30.40, 22.80. MS (EI) *m/z* calcd for $C_{10}H_{18}$ [M^+] 138.1, found 138.1. **6**: ^{1}H-NMR (500 MHz, $CDCl_3$) δ 2.17-2.11 (m, 7H), 1.66-1.60 (m, 6H), 0.79-0.75 (m, 3H). ^{13}C-NMR (500 MHz, CDCl3) δ 29.36, 27.33, 22.19, 17.12. MS (EI) *m/z* calcd for $C_{10}H_{16}$ [M^+] 136.1, found 136.2. Characterization data agrees with the literature.[20]

H_2 and Pd/C hydrogenation of $PB_{50}P_{50}$

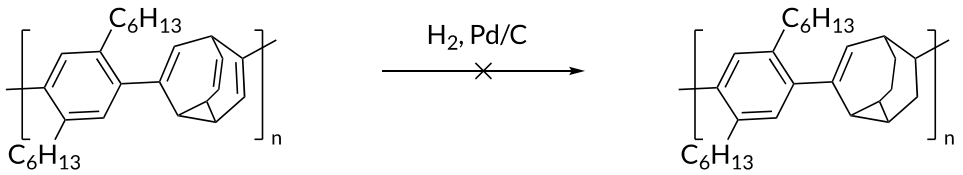

$PB_{50}P_{50}$ **Partially reduced $PB_{50}P_{50}$**

$PB_{50}P_{50}$ (20.0 mg, 0.000741 mmol, 1.00 eq) was dissolved in ethyl acetate (2.00 mL) and transferred to a 25 mL round bottom flask with a stir bar. Pd/C (5 mol%, 0.82 mg, 0.008 mmol, 10.8 eq.) was added to the reaction and the flask was fitted with a 3-way adapter attached to the vacuum line and a hydrogen balloon. The flask was evacuated and refilled 7 times with hydrogen and the reaction stirred for 18 hours at room temperature under H_2 atmosphere (1 atm). The reaction mixture was filtered through celite and evaporated to dryness. ^{1}H NMR spectrum only showed partial reduction of the polymer, so the reaction mixture was resubjected to the same conditions two additional times. Even after resubjection, alkene signals still remained in the ^{1}H NMR spectrum.

Diimide reduction of Bullvalene

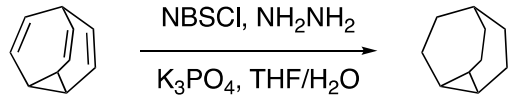

Bullvalene **S5**

Bullvalene (56.0 mg, 0.430 mmol, 1.00 eq.), 2-NsCl (571 mg, 2.58 mmol, 6.00 eq.) and K_3PO_4 (297 mg, 1.29 mmol, 3.00 eq.) was dissolved in THF (8.00 mL) in a 20 mL vial equipped with a stir bar and cooled in an ice bath. Hydrazine hydrate (0.250 mL, 5.16 mmol, 12.0 eq.) was transferred to the reaction vial in less than 1 minute. Deionized water (1 mL) was transferred to the reaction mixture. The reaction mixture was warmed up to room temperature and stirred for 16 hours. THF was then removed under reduced pressure. The crude ^{1}H-NMR still had trace alkene resonances, showing that we were not able to achieve full reduction even with increased equivalencies of diimide and extended reaction time. The mixture was then dissolved in 15 mL hexanes and 15 mL water and transferred into a separatory funnel. The product was then extracted with hexane (3 x 30 mL) then washed with water (2 x 30 mL) and brine (30 mL). The combined organic layers were then evaporated to dryness under reduced pressure. The product was then purified via column chromatography (SiO_2) using 100% hexane (R_f = 0.9) yielding a low boiling white solid, **S5** (21 mg, 36%). ^{1}H-NMR (500 MHz, $CDCl_3$) δ 2.17-2.11 (m, 7H), 1.66-1.60 (m, 6H), 0.75-0.79 (m, 3H). ^{13}C-NMR (500 MHz, $CDCl_3$) δ 29.32, 27.26, 22.14, 17.13. Characterization data agrees with literature.[21]

Diimide reduction of diphenyl bullvalene

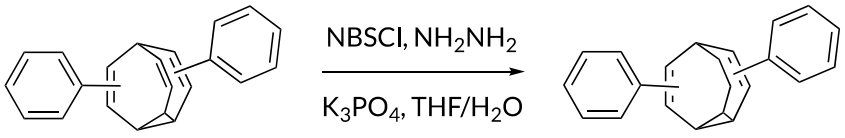

Diphenyl bullvalene **S2-H** (48.6 mg, 0.172 mmol, 1.00 eq.), 2-NsCl (306 mg, 1.38 mmol, **8.00 eq.** or 38.2 mg, 0.172 mmol, **1.00 eq.**) and K_3PO_4 (159 mg, 0.689 mmol, **4.00 eq.** or 19.8 mg, 0.0862 mmol, **0.500 eq.**) was dissolved in THF (0.5 mL) in an 8 mL vial equipped with a stir bar and cooled in an ice bath. Hydrazine hydrate (0.134 mL, 2.76 mmol, **16.0 eq.** or 0.0168 mL, 0.345 mmol, **2.00 eq.**) was transferred to the reaction vial in less than 1 minute. *These two reactions represent diimide reduction conditions with either* ***„excess diimide reagent“*** *or* ***„1 equivalent of diimide reagent“****, respectively.* Deionized water (0.5 mL) was transferred to the reaction mixture. The reaction mixture was warmed up to room temperature and stirred for 16 hours. THF was then removed under reduced pressure. The reaction mixture was evaporated to dryness and re-dissolved in dichloromethane (5 mL) and sodium bicarbonate (5 mL). The aqueous layer was extracted with DCM (5 x 5 mL). The organic layers were combined, dried over sodium sulfate, decanted, and evaporated to dryness. The product was purified using prep-GPC (RT = 28 min) yielding a colorless oil.

As evidenced by the ^{1}H NMR spectra following removal of reagent-derived byproducts by prep-GPC, there is no difference in reaction outcome for diimide reduction of **S2-H** with 1 equivalent of diimide reagent versus an excess (8 equivalents) of diimide reagent.

Diimide reduction of bullvalene-*alt*-phenylene (representative procedure; equivalencies vary based on M_n of $PB_{50}P_{50}$)

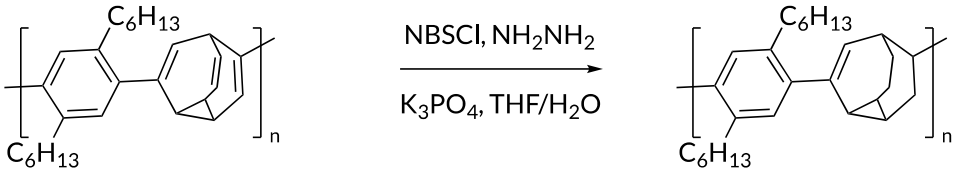

$PB_{50}P_{50}$ *red*-$PB_{50}P_{50}$

Bullvalene-*alt*-phenylene (**$PB_{50}P_{50}$-5.8k**, M_n = 5.8 kDa, 30.0 mg, 0.0052 mmol, 1.00 eq.) and NsCl (310 mg, 1.40 mmol, 270 eq.) were dissolved in THF (1.20 mL) in an 8 mL vial with a stir bar. Then, 2 mM aq. potassium phosphate (0.600 mL, 0.00130 mmol, 135 eq.) were added to the reaction mixture and stirred vigorously. 80% hydrazine hydrate (0.160 mL, 2.79 mmol, 540 eq.) was added dropwise to the reaction mixture and the reaction changed color from light yellow to orange. The reaction stirred at room temperature for 18 hours. The reaction mixture was evaporated to dryness and re-dissolved in dichloromethane (5 mL) and sodium bicarbonate (5 mL). The organic layer was washed with sodium bicarbonate (5 x 5 mL). The organic layer was dried over sodium sulfate, decanted, and evaporated to dryness. The reduced polymer, ***red*-$PB_{50}P_{50}$**, was further purified using prep-GPC (RT = 18-24 minutes). The purified product was freeze dried by dissolving in 2 mL benzene, freezing in liquid N_2, and drying overnight under vacuum (ca. 100 mTorr) yielding a light yellow solid (20 mg, dn/dc = 0.1110 mL/g). ^{1}H-NMR (300 MHz, $CDCl_3$, 25°C) δ = 6.85 (br, 2H), 5.59 (br, 2H), 2.54-2.37 (br, 6H), 1.48 (br, 5H), 1.22 (s, 16H), 0.79 (s, 6H).

2.10.5 Attempts towards other poly(phenylenes) with cyclic spacers

Unsuccessful attempts to access structurally similar hydrocarbon polymers to **$PB_{50}P_{50}$** are detailed in this section. Ultimately, comparisons in the manuscript are made against poly(*p*-phenylene) (**PB_0P_{100}**), and random bullvalene-doped co-polymers (**PB_xP_y**). We attempted to synthesize poly(*p*-phenylenes) with alternative "cyclic spacers" (in order of appearance below: cyclohexadiene, norbornadiene, and adamantane) but were unsuccessful in doing so. During these efforts, we concluded that **bullvalene** incorporation is actually one of the most efficient ways to introduce random "kinks" into π-rich materials.

Suzuki-Miyaura-like Polycondensation (Cyclohexadiene Spacer)

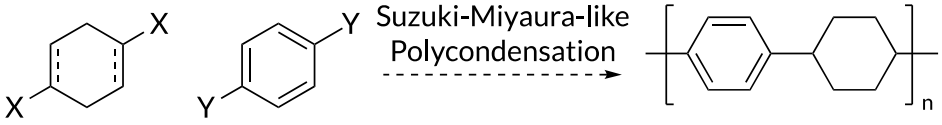

Attempted synthesis of cyclohexadiene ditriflate monomer

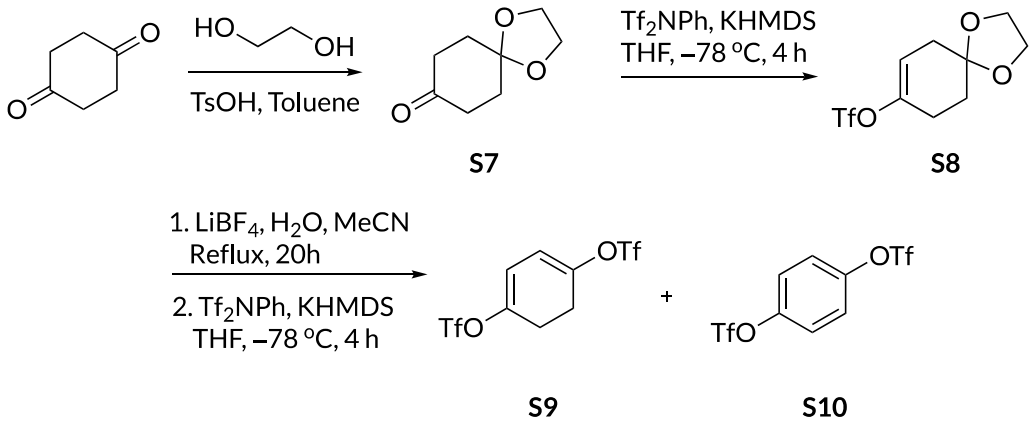

1,4-cyclohexanedione (5.00 g, 45.6 mmol, 1.00 eq.), *p*-toluenesulfonic acid (0.848 g, 4.56 mmol, 0.10 eq.), and ethylene glycol (3.32 g, 53.5 mmol, 1.2 eq.) were dissolved in toluene (45.0 mL) then added to a round bottom flask equipped with a Dean-Stark apparatus and heated to 120 °C. After 1.2 mL of water was collected in the Dean-Stark apparatus, the reaction was quenched with saturated sodium bicarbonate solution. The aqueous layer was then extracted with ethyl acetate (2 x 30 mL). The combined organic layer was washed with saturated sodium bicarbonate solution (2 x 30 mL), water (2 x 30 mL) and brine (1 x 30 mL) then dried over sodium sulfate, decanted, and evaporated to dryness. The product was then purified on SiO_2 using 50% ethyl acetate in hexane (R_f = 0.5) to afford a white solid product **S7** (1.53 g, 22%). ^{1}H-NMR spectrum is consistent with literature.[22]

S7 (1.15 g, 7.36 mmol, 1.00 eq.), *N*-Phenyl-bis(trifluoromethanesulfonimide) (3.42 g, 9.57 mmol, 1.30 eq.) were transferred into a flame dried round bottom flask. The flask containing solids was evacuated and refilled with nitrogen 3 times. Dry THF (80.0 mL) was added and the mixture stirred for 30 minutes under nitrogen at –78 °C. Then, potassium bis(trimethylsilyl)amide (KHMDS) (1 M in THF, 9.06 mL, 9.57 mmol, 1.30 eq.) was added dropwise to the reaction flask. The reaction was stirred at –78 °C for 4 hours, then quenched with water and warmed to room temperature. The mixture was then extracted with ethyl acetate (3 x 30 mL), and washed with water (2 x 30 mL) and brine (1 x 30 mL) then dried over sodium sulfate, decanted, and evaporated to dryness. The product was then purified on SiO_2 using 20% ethyl acetate in hexane to afford a white solid product **S8** (1.64 g, 77%). ^{1}H-NMR spectrum is consistent with literature.[22]

In a flame dried round bottom flask equipped with a water condenser, $LiBF_4$ (1.07 g, 11.4 mmol, 2.00 eq.). The flask containing solids was evacuated and refilled with nitrogen 3 times. Then MeCN (40 mL) was added to dissolve the solids and stirred for 5 minutes. **S8** (1.64 g, 5.70 mmol,

1.00 eq.) were dissolved in MeCN (15 mL) along with 80 drops of water. This mixture was added to the reaction flask dropwise and heated to 90 °C for 16 hours. The reaction mixture was then taken up by ethyl acetate, and washed with brine (1 x 30 mL), water (5 x 30 mL) and brine again (1 x 30 mL) then dried over sodium sulfate, decanted, and evaporated to dryness in a flame dried round bottom flask. *N*-Phenyl-bis(trifluoromethanesulfonimide) (2.65 g, 7.41 mmol, 1.30 eq.) was transferred into the flask. The flask containing solids was evacuated and refilled with nitrogen 3 times. Dry THF (60.0 mL) was added and the mixture stirred for 30 minutes under nitrogen at -78 °C. Then, KHMDS (1 M in THF, 7.40 mL, 7.41 mmol, 1.3 eq.) was added dropwise to the reaction flask. The reaction was stirred at –78 °C for 2 hours, then quenched with water and warmed to room temperature. The mixture was then extracted with ethyl acetate (3 x 30 mL), and washed with water (2 x 30 mL) and brine (1 x 30 mL) then dried over sodium sulfate, decanted, and evaporated to dryness. The crude NMR spectrum shows formation of the desired diene product[7], however, significant aromatic impurities (**S10**) were shown to be formed in large quantity. Purification of the material was unsuccessful and clean diene **S9** could not be isolated for subsequent Suzuki-Miyaura polycondensation reactions.

Suzuki-Miyaura-like Polycondensation (Norbornadiene Spacer)

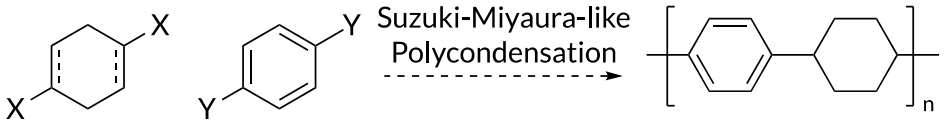

Synthesis of norbornadiene ditriflate monomer

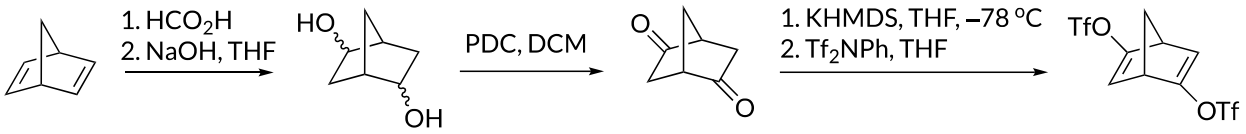

S11 **S12** **S13**

In a 100 mL round bottom flask, 2,5-norbornadiene (5.00 g, 54.3 mmol, 1.00 eq.) and formic acid (88% solution in water, 34.0, 325 mmol, 6.00 eq.) were added and heated to 120 °C for 20 hours. Then the excess formic acid was distilled off and the diformate was obtained by vacuum distillation (120 °C, 0.2 bar) as a clear liquid. The crude diformate was then transferred into a round bottom flask and dissolved in of THF (200 mL). The solution was cooled to 0 °C and a solution of NaOH (21.2 g, 325 mmol, 6.00 eq.) in water (30.0 mL) was added dropwise into the reaction flask. The reaction mixture was stirred for 16 hours before being taken up by ethyl acetate. Brine was added to the aqueous layer and extracted again with ethyl acetate then dried over sodium sulfate, decanted, and evaporated to dryness. A white solid **S11** (4.51 g, 65% over 2 steps) was obtained that was used without further purification.

2,5-norbornadiol **S11** (1.00 g, 7.80 mmol, 1.00 eq.) and crushed 4 Å molecular sieves (2 g) were suspended in DCM (50.0 mL) in a round bottom flask. Pyridinium dichromate (14.7 g, 39.0 mmol, 5.00 eq.) was added to the reaction then stirred for 16 hours. The mixture was then filtered through a pad of celite followed by a pad of SiO_2. A yellow oil **S14** (0.400 g, 42%) was collected. ^{1}H-NMR spectrum is consistent with literature.[23]

2,5-norbornadione **S12** (0.410 g, 3.30 mmol, 1.00 eq.) was dissolved in dry THF (25.0 mL) under nitrogen in a flame dried round bottom flask and stirred at –78 °C for 30 minutes. KHMDS (1 M in THF, 8.58 mL, 8.58 mmol, 2.60 eq.) was added to the flask dropwise and stirred for 1 hour at –78 °C. *N*-Phenyl-bis(trifluoromethanesulfonimide) (3.06 g, 8.58 mmol, 2.60 eq.) was dissolved in dry THF (10.0 mL) in a flame dried round bottom flask and added to the reaction mixture dropwise

and stirred for 3 hours then quenched with saturated aq. NH_4Cl solution and warmed to room temperature. The mixture was then extracted with pentane (3 x 50 mL), then washed with saturated aq. NH_4Cl solution (2 x 50 mL) then dried over sodium sulfate, decanted, and evaporated to dryness. The crude mixture was then purified on SiO_2 using pentane/toluene 99:1 to pentane/Et_2O 98:2 to pentane/Et_2O 80:20. The product collected was then further purified via prep-GPC to yield **S13** (0.720 g, 49%). ^{1}H-NMR spectrum is consistent with literature.[23]

Synthesis of bis-Bpin phenylene monomer

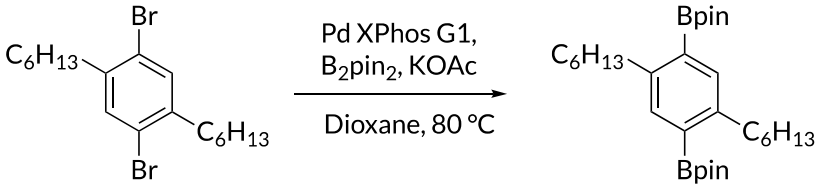

4 **S14**

In a flame dried round bottom flask, freshly ground B_2Pin_2 (3.76 g, 14.8 mmol, 6.00 eq.), freshly ground oven-dried KOAc (1.45 g, 14.8 mmol, 6.00 eq.), 2,5-dibromo-1,4-dihexylbenzene **4** (1.00 g, 2.47 mmol, 1.00 eq.), and Pd XPhos G1 (209 mg, 0.247 mmol, 0.1.00 eq.) were added. The flask containing solids was evacuated and refilled with nitrogen 7 times. Degassed dry 1,4-dioxane (25.0 mL) was transferred to the reaction flask under nitrogen. The mixture was heated to 80 °C and stirred for 48 hours. Then the mixture was cooled down to room temperature and filtered through a pad of Celite. Solvent was removed under reduced pressure and the crude product was recrystallized in MeOH. Then the product was transferred to a new flask and SiliCycle MetS triamine Pd Scavenger was added and stirred for 16 hours. The material was filtered then further

purified via prep-GPC to yield **S14** as a white solid (0.703 g, 57%). ^{1}H-NMR spectrum is consistent with literature.[24]

Attempted polycondensation reactions

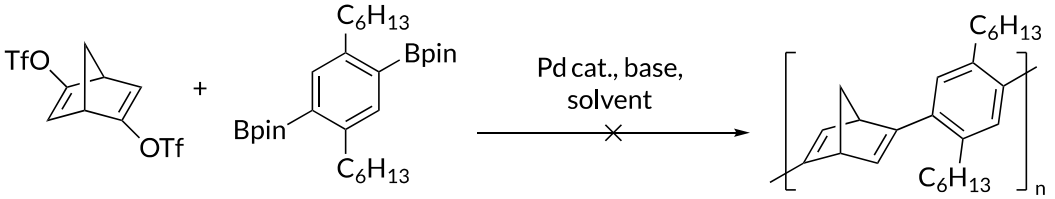

S13 **S14** **S15**

Representative Procedure Towards Polymeric S15: In a flame dried round bottom flask, 2,5-ditriflatenorbornadiene **S13** (1.00 eq.), 2,5-bisBpin-1,4-dihexylbenzene **S14** (1.00 eq.) and palladium catalyst were added. The flask containing solids was evacuated and refilled with nitrogen 5 times. After solvent (2.00 mL) was added, the reaction was heated to desired temperature. Then, 0.2 mL of 2 M aqueous base solution (0.200 mL) was added and the reaction mixture was stirred under nitrogen for 24 – 48 hours. After the mixture was cooled to room temperature, it was diluted with DCM, dried over sodium sulfate, and filtered through a pad of Celite followed by a pad of SiO_2. For all conditions, ^{1}H-NMR showed either minimal monomer consumption and/or an intractable mixture of products. Analytical GPC analysis did not show the formation of higher molecular weight oligomers/polymers.

Entry	Catalyst (eq.)	Solvent	Base	Temperature (°C)
1	Pd XPhos G3 (0.2)	Toluene	K_3PO_4	60
2	$Pd_2(dba)_3$, SPhos (0.2)	Toluene	K_3PO_4	60
3	P(*t*Bu)$_3$Pd G2 (0.25)	THF	KF	23
4	P(*t*Bu)$_3$Pd G2 (0.25)	THF	KF	50
5	P(*t*Bu)$_3$Pd G2 (0.4)	THF	KF	50
6	P(*t*Bu)$_3$Pd G2 (1)	THF	KF	50
7	P(*t*Bu)$_3$Pd G2 (0.4)	Toluene	KF	80
8	P(*t*Bu)$_3$Pd G2 (0.4)	Dioxane	KF	80

Table 2.3. Attempted cross-coupling conditions to make a poly(norbornadiene-*co*-phenylene) comparison polymer (**S15**).

Friedel-Craft Polymerization (Adamantane Spacer)

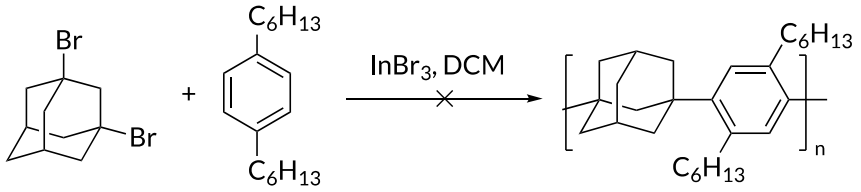

S1 **S16**

This attempted polymerization was inspired by past reports of adamantane Friedel-Crafts reactions.[25] $InBr_3$ (50.0 mg, 0.140 mmol, 0.400 eq.) were transferred into a flame dried round bottom flask covered with aluminum foil under nitrogen. The flask was then heated with a heat gun for 5 minutes under vacuum. 1,3-Dibromoadamantane (100 mg, 0.340 mmol, 1.00 eq.) and 1,4-dihexylbenzene **S1** (83.0 mg, 0.340 mmol, 1.00 eq.) were dissolved in dichloromethane (0.500 mL) in another flame dried round bottom flask and sparged with nitrogen for 30 minutes. Then, the solution was added to the $InBr_3$ dropwise. The reaction mixture was warmed to 35 °C and stirred for 16 hours. The organic layer was taken up by EtOAc and washed with water (5 x 10 mL) and brine (1 x 10 mL) then dried over sodium sulfate, decanted, and evaporated to dryness. The crude ^{1}H-NMR spectrum shows no formation of desired polymer **S16**. Analytical GPC analysis did not show the formation of higher molecular weight oligomers/polymers.

2.10.6 Suzuki polycondensation conditions

Eq. bullvalene monomer	Catalyst (mol %)	Solvent	M_n (kDa)	M_w (kDa)	Đ
1	$Pd(PPh_3)_4$ (2%)	Dioxane	0.48	0.65	1.4
1	Pd XPhos G3 (2%)	Dioxane	2.4	2.9	1.2
1	Pd XPhos G3 (2%)	Toluene	1.3	3.1	2.2
1	Pd XPhos G3 (10%)	Toluene	2.5	6.3	2.5
1	Pd XPhos G3 (20%)	Toluene	4.3	9.8	2.3
1.2	Pd SPhos G4 (20%)	Toluene	4.6	8.0	1.7
1.2*	Pd XPhos G3 (20%)*	Toluene*	21*	33*	1.6*

All reactions ran at 0.0433 M

*Conditions used to make $\mathbf{PB_{50}P_{50}}$ polymers for thermal analysis

Table 2.4. Screening conditions for Suzuki polycondensation

Target % bullvalene	Actual % bullvalene	Eq. 3	Eq. 4	Eq. 5	M_n (kDa)	M_w (kDa)	Đ
25	34	0.500	1.00	0.500	3.4	4.2	1.2
12	22	0.250	1.00	0.750	3.9	4.5	1.2
6	10	0.120	1.00	0.880	3.0	3.2	1.1

Table 2.5. Suzuki polycondensation conditions for bullvalene-doped co-polymers $\mathbf{PB_xP_y}$ and characterization by GPC-MALS-IV-RI

2.10.7 Analytical NMR Calculations of % Bullvalene in PB_xP_y Samples

The bullvalene percentage in each $\mathbf{PB_xP_y}$ sample was calculated using the ratio of aromatic peak integration to bullvalene alkene integration (Figure S2). First, the ratio of integration of the two peaks was observed on the ^{1}H-NMR spectrum. Then, each integration was divided by the number of protons per monomer unit. The normalized bullvalene alkene integration was then divided by

the total number of protons and multiplied by 100 to get the percentage of bullvalene monomer present in the sample.

25% bullvalene target as a representative example (**$PB_{34}P_{66}$-3.4k**):

4.6 H phenyl : 1.59 H bullvalene alkene

$$\frac{4.60\ \text{H}}{6\ H\ \text{per monomer unit}} = 0.767\ \text{H}\ \frac{1.59\ \text{H}}{4\ \text{H per monomer unit}} = 0.398$$

$$\frac{0.398\ \text{H}}{(0.767\ \text{H}+0.398\ \text{H})} * 100 = 34.2\%\ \text{bullvalene}$$

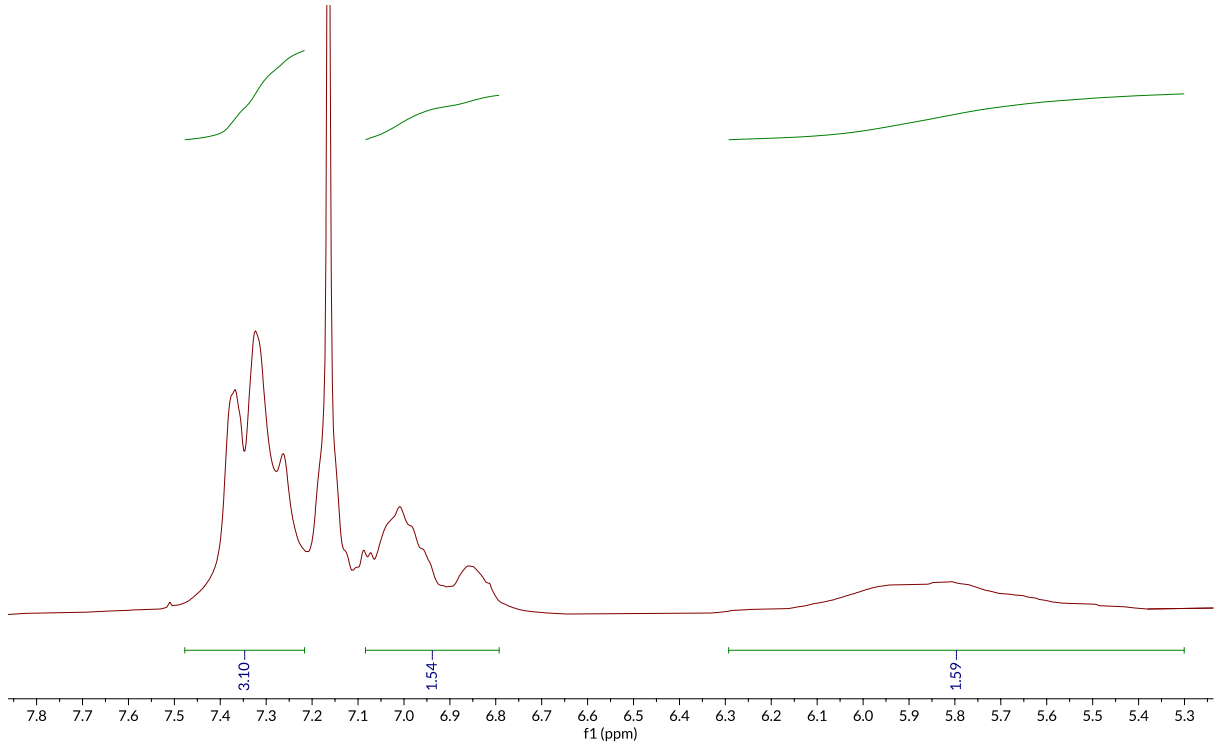

Figure 2.25. ^{1}H NMR spectrum (zoomed in) of **$PB_{34}P_{66}$-3.4k** depicting the regions of interest for calculating the amount of bullvalene incorporated into the co-polymer.

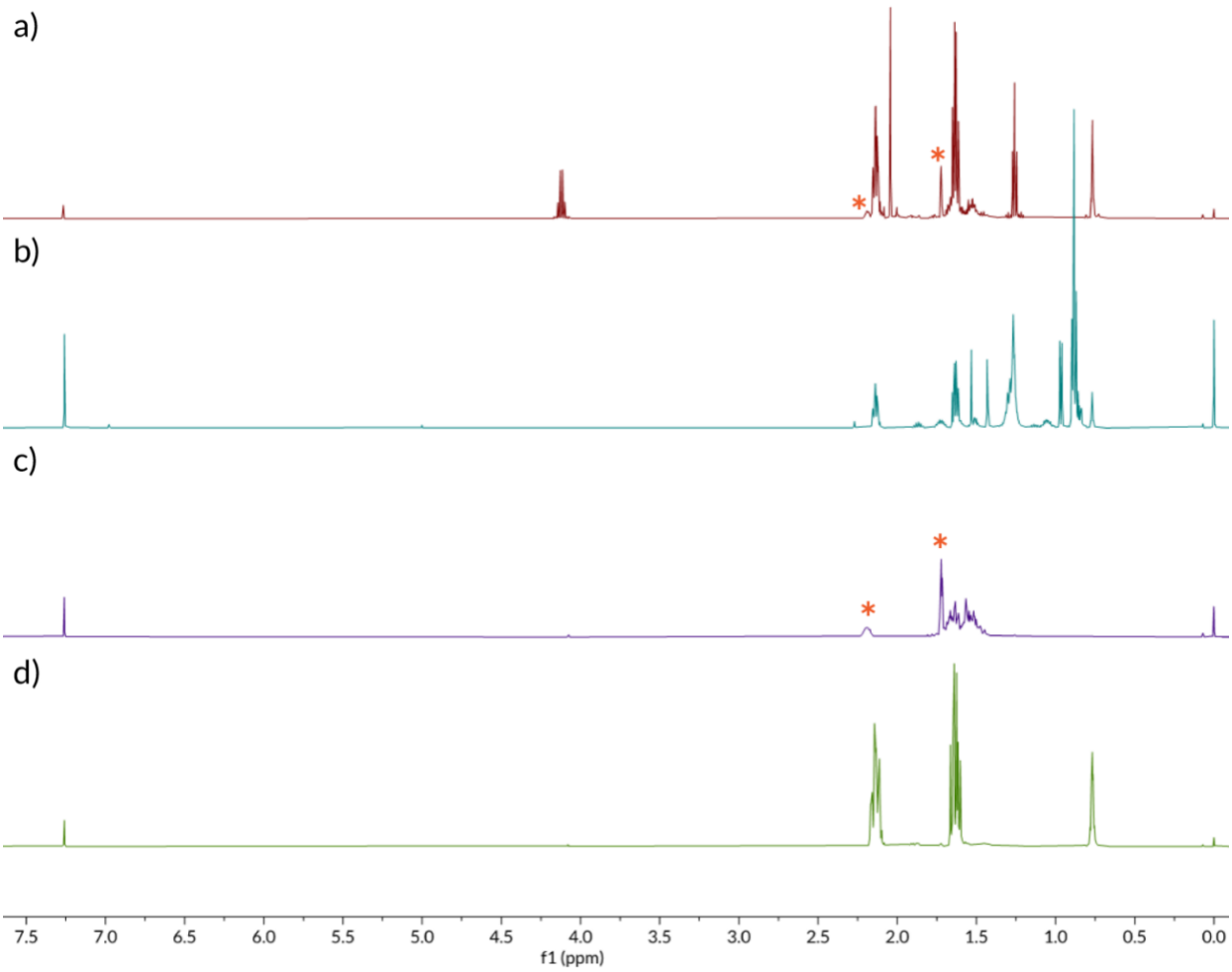

Figure 2.26. Comparison of **Bullvalene** reduction outcomes: Stacked ^{1}H NMR (500 MHz, $CDCl_3$) spectra of a) crude bullvalene H_2/Pd reduction product, b) crude diimide reduction product missing the broad resonance at 2.18 ppm and the peak at 1.72 ppm that would indicate ring opening (marked with *), c) purified ring opened bullvalene **5**, and d) purified hexahydrobullvalene **6**.

2.10.8 Synthesis of model compounds for testing thermal stability of bullvalene

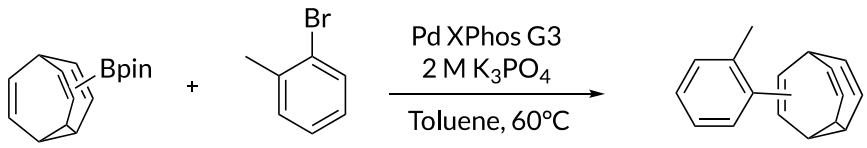

2M aq. potassium phosphate and 2-bromotoluene were sparged with nitrogen for 30 minutes. Pd XPhos G3 (110 mg, 0.12 mmol) and mono-Bpin bullvalene (300 mg, 1.2 mmol) were added to a vial with a stir bar and the vial was evacuated and refilled with nitrogen 4 times. After sparging, toluene (11 mL), 2-bromotoluene (0.14 mL, 1.2 mmol), and 2 M potassium phosphate (3 mL) were added to the reaction mixture. The reaction stirred under nitrogen at 60ºC overnight. The reaction mixture was cooled to room temperature and transferred to a separatory funnel. The mixture was washed with water (3 x 5 mL), then the organic layer was collected, dried over sodium sulfate, and filtered through neutral alumina. The filtrate was evaporated to dryness. The crude product was further purified through silica flash chromatography using 20-40% DCM in hexanes yielding the tolyl-bullvalene as a yellow solid (102 mg, 37%).

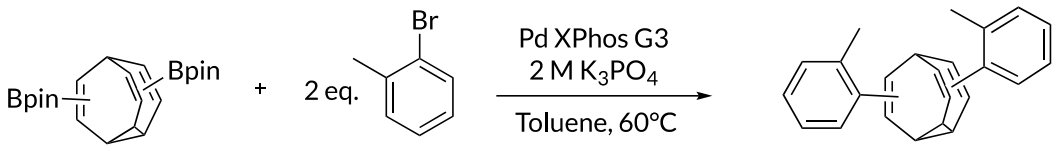

2M aq. potassium phosphate and 2-bromotoluene were sparged with nitrogen for 30 minutes. Pd XPhos G3 (28 mg, 0.031 mmol) and di-Bpin bullvalene (120 mg, 0.31 mmol) were added to a vial with a stir bar and the vial was evacuated and refilled with nitrogen 4 times. After sparging, toluene (11 mL), 2-bromotoluene (0.074 mL, 0.061 mmol), and 2 M potassium phosphate (3 mL) were added to the reaction mixture. The reaction stirred under nitrogen at 60ºC overnight. The reaction mixture was cooled to room temperature and transferred to a separatory funnel. The mixture was washed with water (2 x 5 mL), then the organic layer was collected, dried over sodium sulfate, and filtered through neutral alumina. The filtrate was evaporated to dryness. The crude product was

further purified through silica flash chromatography using 20-40% DCM in hexanes yielding the ditolyl-bullvalene as a yellow solid (62 mg, 67%).

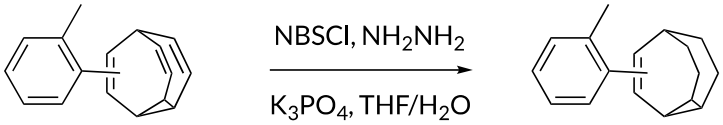

Monotolyl bullvalene (50 mg, 0.23 mmol), nosyl chloride (300 mg, 1.4 mmol), and potassium phosphate (160 mg, 0.68 mmol) were added to a 50 mL RBF. The reagents were dissolved in THF (2.3 mL) and water (2.3 mL), stirred vigorously, and cooled to 0°C. 80% hydrazine hydrate (0.14 mL, 2.3 mmol) was added to the reaction mixture allowed to gradually warm to room temperature, and stirred overnight. The reaction mixture was cooled to room temperature and transferred to a separatory funnel. The mixture was washed with DCM (2 x 10 mL), the organic layer was collected, dried over sodium sulfate, and evaporated to dryness. The product was further purified by flash chromatography using 10% DCM in hexanes (R_f = 0.85) yielding *red*-monotolyl bullvalene (30 mg, 50%).

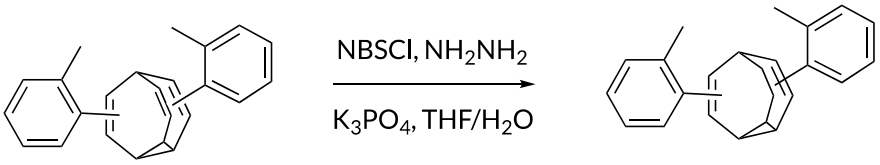

Ditolyl bullvalene (36 mg, 0.12 mmol), nosyl chloride (150 mg, 0.70 mmol), and potassium phosphate (80 mg, 0.35 mmol) were added to a 50 mL RBF. The reagents were dissolved in THF (2.3 mL) and water (2.3 mL), stirred vigorously, and cooled to 0°C. 80% hydrazine hydrate (0.056 mL, 1.2 mmol) was added to the reaction mixture allowed to gradually warm to room temperature, and stirred overnight. The reaction mixture was cooled to room temperature and transferred to a separatory funnel. The mixture was washed with DCM (2 x 10 mL), the organic layer was

collected, dried over sodium sulfate, and evaporated to dryness. The product was further purified by flash chromatography using 10% DCM in hexanes (R_f = 0.85) yielding *red*-ditolyl bullvalene (20 mg, 55%).

2.10.9 Efforts towards bullvalene diol monomers

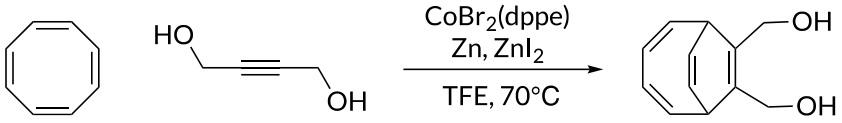

$CoBr_2$(dppe) (1.9 g, 1.2 mmol), ZnI_2 (1.2 g, 3.8 mmol), and Zn (380 mg, 5.8 mmol) were added to a flame dried flask with a magnetic stir bar. The flask containing solids was evacuated and refilled with nitrogen 3 times. Then, dry, degassed TFE (19 mL, sparged with nitrogen for 20 minutes) was added and the mixture stirred for 15 minutes under nitrogen and heated to 70°C. Cyclooctatetraene (2.2 mL, 19 mmol) and 1,4-butyne diol (3.3 g, 38 mmol) were added to the reaction mixture and the reaction stirred for 48 hours at room temperature under nitrogen. Once the reaction was complete, the mixture was cooled to room temperature and filtered through neutral alumina. The filtrate was evaporated to dryness. The resulting brown oil was purified via column chromatography using 5-50% EtOAc in DCM with 0.5% triethylamine yielding the target cycloadduct as a white solid (1.4 g, 40%).

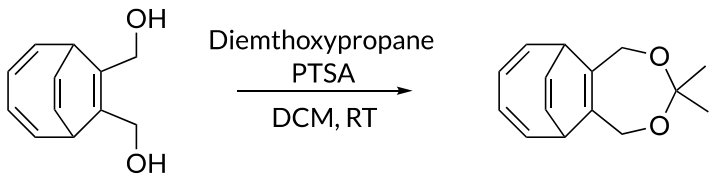

Dimethanol cycloadduct (170 mg, 0.74 mmol) and para-toluenesulfonic acid (7.0 mg, 0.037 mmol) were added to a flame-dried 25 mL Schlenk flask. The flask was evacuated and refilled with nitrogen three times, then dry degassed DCM (5.0 mL) was added. Dimethoxycyclopropane was sparged for 10 minutes then added to the reaction mixture (0.18 mL, 1.47 mmol). The reaction stirred for 16h under nitrogen at room temperature. The reaction mixture was quenched with sodium bicarbonate (5 mL) and transferred to a separatory funnel. The product was extracted with DCM (3 x 5 mL), then the combined DCM layers were washed with brine (7 mL), dried over sodium sulfate, and evaporated to dryness. The product was further dried at 45°C under vacuum to remove dimethoxycyclopropane (BP = 83°C), affording a white solid (135 mg, 80%).

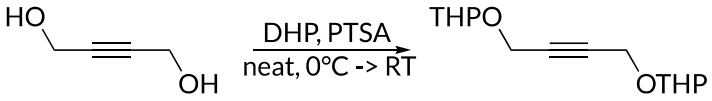

1,4-butyne diol (2.3 g, 23 mmol) and para-toluenesulfonic acid (44 mg, 0.23 mmol) were added to a flame dried 25 mL flask. The flask was evacuated and refilled with nitrogen three times. The flask was cooled to 0°C and 3,4-dihydro-2H-pyran (4.2 mL, 46 mmol) was added to the flask and stirred overnight under nitrogen. The reaction mixture was transferred to a separatory funnel and quenched with sodium bicarbonate (10 mL). The mixture was then extracted with ethyl acetate (3 x 10 mL). The organic layers were combined, dried over sodium sulfate, and evaporated to dryness. The rxn mixture was dried on high vac for 6h to obtain the THP protected alkyne (4.9 g, 83%).

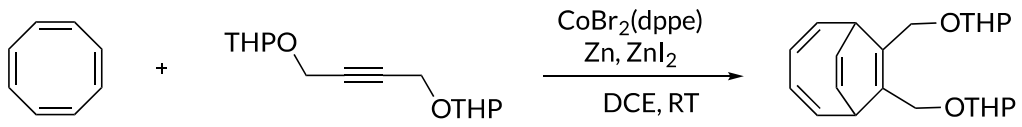

Co (1.9 g, 1.9 mmol), Zn (380 mg, 5.8 mmol), and ZnI_2 (1.2 g, 3.8 mmol) were added to a flame dried 50 mL Schlenk flask and the flask was evacuated and refilled with nitrogen three times. Alkyne and DCE were sparged with nitrogen separately for 30 minutes. DCE (20 mL) was added to the reaction mixture and stirred at room temperature for 15 minutes. COT (2.2 mL, 19 mmol) and alkyne (11 mL, 38 mmol) were then added to the reaction mixture and stirred for 16 hours under nitrogen. The reaction mixture was then filtered through alumina and evaporated to dryness. The product was purified using column chromatography with 30% EtOAc in hexanes (R_f = 0.5) to yield the product as a yellow oil (4.78 g, 69%).

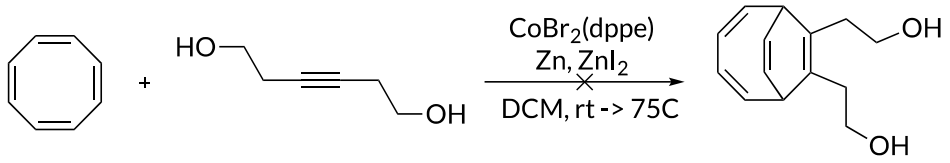

Co (110 mg, 0.18 mmol), Zn (34 mg, 0.53 mmol), and ZnI_2 (110 mg, 0.35 mmol) were added to a flame dried 50 mL Schlenk flask and the flask was evacuated and refilled with nitrogen three times. DCE was sparged with nitrogen separately for 30 minutes. DCE (2 mL) was added to the reaction mixture and stirred at room temperature for 15 minutes. COT (0.099 mL, 0.88 mmol) and alkyne (100 mg, 0.88 mmol) were then added to the reaction mixture and stirred for 16 hours under nitrogen. A 1 mL aliquot of the reaction was removed, filtered through neutral alumina and analyzed by ^{1}H NMR; only starting material was present. The reaction mixture was heated for an additional 2 days at 60°C and no reaction was observed.

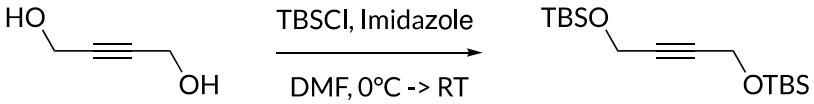

Imidazole (6.3 g, 93 mmol) and 1,4-butyne diol (2.0 g, 23 mmol) were added to a flame dried 100 mL flask and evacuated and refilled with nitrogen three times. The reaction mixture was dissolved

in dry DMF (20 mL). The diol solution was cooled to 0C and stirred for 20 minutes. Then, the TBSCl (10 g, 70 mmol) was added to the diol solution. Once addition was complete, the reaction mixture slowly warmed to rt and stirred overnight. The reaction mixture was quenched with sodium bicarbonate (50 mL). The rxn was transferred to a separatory funnel and extracted with EtOAc (3 x 100 mL). The EtOAc were combined then washed with LiCl (2 x 50 mL), water (2 x 50 mL), then brine (2 x 50 mL). The EtOAc was collected, dried over sodium sulfate, and evaporated to dryness. The crude product was used without further purification (10 g, 134%). ^{1}H-NMR (500 MHz, CDCl3) δ 4.34 (s, 4H), 0.91 (s, 18H), 0.12 (s, 12H).

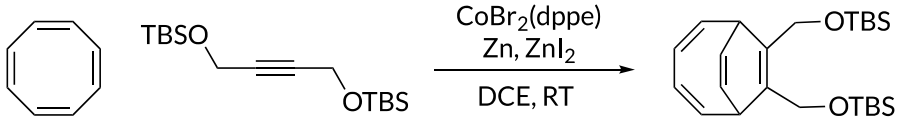

Co (590 mg, 0.95 mmol), Zn, (190 mg, 2.9 mmol) and ZnI_2 (610 mg, 1.9 mmol) were added to a flame dried 50 mL Schlenk flask and the flask was evacuated and refilled with nitrogen three times. Alkyne and DCE were sparged with nitrogen separately for 30 minutes. DCE (15 mL) was added to the reaction mixture and stirred at room temperature for 15 minutes. COT (1.1 mL, 9.5 mmol) and alkyne (3.0 g, 9.5 mmol) were then added to the reaction mixture and stirred for 16 hours under nitrogen. The reaction mixture was then filtered through alumina and evaporated to dryness. The product was purified using column chromatography with 30% DCM in hexanes (R_f = 0.25) to yield the product as a yellow oil (1.9 g, 47%). ^{1}H-NMR (300 MHz, $CDCl_3$) δ = 6.18 (m, 2H), 5.75-5.64 (m, 4H), 4.30-4.16 (m, 4H), 3.51 (m, 2H), 0.89 (s, 18H), 0.02 (s 12H).

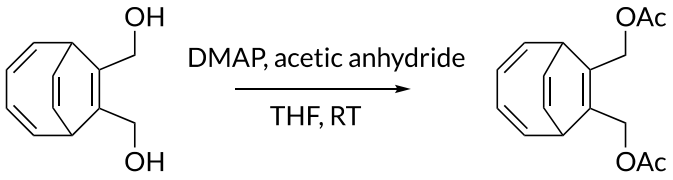

Dimethanol cycloadduct (100 mg, 0.521 mmol) was dissolved in dry DCM (3 mL) and transferred to a flame dried flask. Dimethylaminopyridine (3.4 mg, 0.052 mmol) and acetic anhydride (0.11 mL, 1.5 mmol) were then added, and the reaction mixture stirred at room temperature for four hours. The reaction mixture was quenched with water (1 mL) and transferred to a vial. The DCM layer was collected, dried over sodium sulfate, and evaporated to dryness (130 mg, 91%).

General procedure for photochemistry

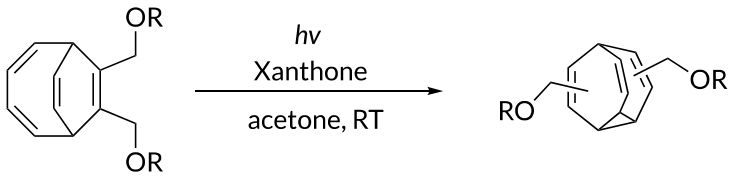

Xanthone (0.250 eq.) and cycloadduct (1.00 eq.) were dissolved in acetone (100 mg/mL) in an 8 mL vial and capped under air. The reaction mixture was placed in the EvoluChem PhotoRedOx box, irradiated with UV light (λ = 365 nm), and stirred at room temperature for 8 hours. Then, the reaction mixture was evaporated to dryness. The crude product was purified by column chromatography.

For R = H

Yield: 6 mg, 20%

For R = TBS

Yield: 5.71 g, 43%

For R = THP

Yield: 100 mg, 50%

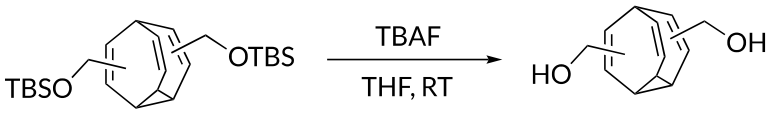

The TBS protected bullvalene (5.71 g, 13.6 mmol) was transferred to a flame dried Schlenk flask and evacuated and refilled with nitrogen three times. Then, dry THF (10 mL) was added followed by 1.0 M tetrabutylammonium fluoride in THF (41.0 mL, 41.0 mmol) and the rxn stirred at room temperature overnight. The THF was evaporated to dryness and the crude pdt was re-dissolved in water (30 mL) and ethyl acetate (30 mL). The water was extracted with ethyl acetate (3 x 30 mL). The organic layers were combined and washed with water (2 x 30 mL) and brine (30 mL).

The organic layer was dried over sodium sulfate and evaporated to dryness. The product was further purified using column chmoatography; a gradient of 50 to 100% EtOAc in hexanes was used to elute the product as a white solid (900 mg, 35%).

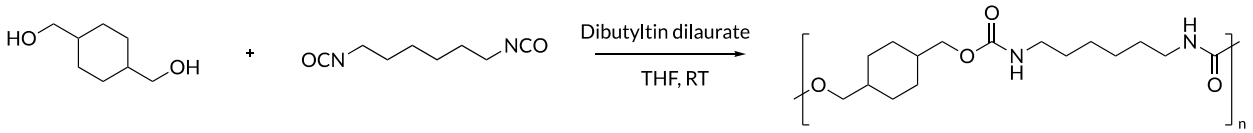

Dimethanol cyclohexane (50 mg, 0.35 mmol) was added to a flame dried 4 mL vial with a stir bar. The diol monomer was dissolved in dry THF (0.3 mL). Hexamethylene diisocyanate (0.055 mL, 0.35 mmol) followed by dibutyltin dilaurate (0.020 mL, (0.035 mmol) were added to each vial; white precipitate formed within 5 minutes. The reactions stirred overnight at room temperature

under nitrogen then evaporated to dryness, yielding 30 mg crude product (60% mass recovery). Samples were sonicated in chloroform for 2 hours to prepare for GPC analysis.

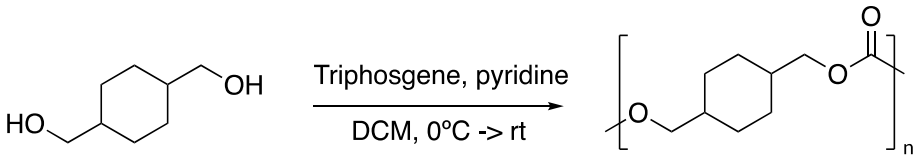

Dimethanol cyclohexane (50 mg, 0.35 mmol) was added to an oven dried 4 mL vial with a stir bar. Triphosegene (34 mg, 0.12 mmol) was added to the vial and dissolved in DCM (2 mL). Pyridine (0.14 mL, 1.7 mmol) was added and the reaction stirred under nitrogen for 1 hour. The reaction was allowed to gradually warm to room temperature. The reaction mixture was quenched with 1 mL sodium bicarbonate. The DCM layer was collected, dried over sodium sulfate, and evaporated to dryness, yielding 18 mg of the crude product (36% mass recovery).

2.11 Publications and acknowledgements

This work was conducted in collaboration with Brian Sun, Ashley Mahan, and Bob Li. This chapter was adapted from the publication below publication:

- **Pomfret, M. N**.; Sun, P. B.; Huang, Z.; Freund, A. C.; Miyoshi, T.; Golder, M. R.*

  Angew. Chem. Int. Ed. **2023**, *62*, e202301695

2.12 References

(1) Doering, W. von E.; Roth, W. R. A Rapidly Reversible Degenerate Cope Rearrangement. Bicyclo[5.1.0]Octa-2,5-Diene. *Tetrahedron* **1963**, *19* (5), 715–737. https://doi.org/10.1016/S0040-4020(01)99207-5.

(2) Schröder, G. Preparation and Properties of Tricyclo[3,3,2,04,6]Deca-2,7,9-Triene (Bullvalene). *Angew. Chemie Int. Ed. English* **1963**, *2* (8), 481–482. https://doi.org/10.1002/anie.196304814.

(3) Ferrer, S.; Echavarren, A. M. Synthesis of Barbaralones and Bullvalenes Made Easy by Gold Catalysis. *Angew. Chem., Int. Ed.* **2016**, *55*, 11178–11182. https://doi.org/10.1002/anie.201606101.

(4) Lippert, A. R.; Kaeobamrung, J.; Bode, J. W. Synthesis of Oligosubstituted Bullvalones : Shapeshifting Molecules Under Basic Conditions. *J. Am. Chem. Soc.* **2006**, 14738–14739. https://doi.org/10.1021/ja063900+.
(5) Lippert, A. R.; Naganawa, A.; Keleshian, V. L.; Bode, J. W. Synthesis of Phototrappable Shape-Shifting Molecules for Adaptive Guest Binding. *J. Am. Chem. Soc.* **2010**, *132* (44), 15790–15799. https://doi.org/10.1021/ja107314p.
(6) Teichert, J. F.; Mazunin, D.; Bode, J. W. Chemical Sensing of Polyols with Shapeshifting Boronic Acids as a Self-Contained Sensor Array. *J. Am. Chem. Soc.* **2013**, *135* (30), 11314–11321. https://doi.org/10.1021/ja404981q.
(7) Bismillah, A. N.; Sturala, J.; Chapin, B. M.; Yufit, D. S.; Hodgkinson, P.; McGonigal, P. R. Shape-Selective Crystallisation of Fluxional Carbon Cages. *Chem. Sci.* **2018**, *9* (46), 8631–8636. https://doi.org/10.1039/C8SC04303E.
(8) Yahiaoui, O.; Pašteka, L. F.; Judeel, B.; Fallon, T. Synthesis and Analysis of Substituted Bullvalenes. *Angew. Chemie Int. Ed.* **2018**, *57* (10), 2570–2574. https://doi.org/10.1002/anie.201712157.
(9) Patel, H.; Tran, T. H.; Sumby, C.; Fallon, T. Boronate Ester Bullvalenes. *J. Am. Chem. Soc.* **2020**, *142* (8), 3680–3685. https://doi.org/10.1021/jacs.9b12930.
(10) Birvé, A. P.; Patel, H. D.; Price, J. R.; Bloch, W. M.; Fallon, T. Guest-Dependent Isomer Convergence of a Permanently Fluxional Coordination Cage. *Angew. Chem. Int. Ed.* **2022**, *61* (9), e202115468. https://doi.org/10.1002/anie.202115468.
(11) Darzi, E. R.; White, B. M.; Loventhal, L. K.; Zakharov, L. N.; Jasti, R. An Operationally Simple and Mild Oxidative Homocoupling of Aryl Boronic Esters To Access Conformationally Constrained Macrocycles. *J. Am. Chem. Soc.* **2017**, *139* (8), 3106–3114. https://doi.org/10.1021/jacs.6b12658.
(12) Patel, H. D.; Gaggl, S.; Pašteka, L. F.; Fallon, T. Ambimodal Pericyclic Rearrangements of Dialkenyl-Bullvalenes Give Tetrahydro-1,8-Ethenoheptalenes. *Org. Lett.* **2022**, *24* (1), 319–323. https://doi.org/10.1021/acs.orglett.1c03984.
(13) Sardon, H.; Pascual, A.; Mecerreyes, D.; Taton, D.; Cramail, H.; Hedrick, J. L. Synthesis of Polyurethanes Using Organocatalysis: A Perspective. *Macromolecules* **2015**, *48* (10), 3153–3165. https://doi.org/10.1021/acs.macromol.5b00384.
(14) De Souza, F. M.; Kahol, P. K.; Gupta, R. K. Introduction to Polyurethane Chemistry. *ACS Symp. Ser.* **2021**, *1380*, 1–24. https://doi.org/10.1021/bk-2021-1380.ch001.
(15) Bossion, A.; Heifferon, K. V.; Meabe, L.; Zivic, N.; Taton, D.; Hedrick, J. L.; Long, T. E.; Sardon, H. Opportunities for Organocatalysis in Polymer Synthesis via Step-Growth Methods. *Prog. Polym. Sci.* **2019**, *90*, 164–210. https://doi.org/10.1016/j.progpolymsci.2018.11.003.
(16) Dohmen, C.; Ihmels, H.; Paululat, T. The Journey to Fluorescent Bullvalenes: Pitfalls and Prospects. *European J. Org. Chem.* **2022**, *2022* (45). https://doi.org/10.1002/ejoc.202201172.
(17) Yu, W.; Maynard, E.; Chiaradia, V.; Arno, M. C.; Dove, A. P. Aliphatic Polycarbonates from Cyclic Carbonate Monomers and Their Application as Biomaterials. *Chem. Rev.* **2021**, *121* (18), 10865–10907. https://doi.org/10.1021/acs.chemrev.0c00883.
(18) Sun, J.; Aly, K. I.; Kuckling, D. A Novel One-Pot Process for the Preparation of Linear and Hyperbranched Polycarbonates of Various Diols and Triols Using Dimethyl Carbonate. *RSC Adv.* **2017**, *7* (21), 12550–12560. https://doi.org/10.1039/c7ra01317e.
(19) Hilt, G.; Lüers, S. Cobalt(I)-Catalyzed 1,4-Hydrovinylation Reactions of 1,3-Dienes with

Functionalized Terminal Alkenes under Mild Conditions. *Synthesis (Stuttg).* **2002**, No. 5, 609–618. https://doi.org/10.1055/s-2002-23549.

(20) Schröder, G.; Oth, J. F. M. Recent Chemistry of Bullvalene. *Angew. Chemie Int. Ed. English* **1967**, *6* (5), 414–423. https://doi.org/10.1002/anie.196704141.

(21) Trætteberg, M.; Kozhushkov, S. I.; Yufit, D. S.; de Meijere, A. The Structure of Tricyclo[3.3.2.02.8]Decane (Hexahydrobullvalene) - A Gas-Phase Electron Diffraction (GED) Study. *J. Mol. Struct.* **2008**, *885* (1–3), 18–22. https://doi.org/10.1016/j.molstruc.2007.09.028.

(22) Mitschke, N.; Christoffers, J.; Wilkes, H. A Straightforward Synthesis of Trideuterated α-Terpinene for Mechanistic Studies. *European J. Org. Chem.* **2020**, *2020* (31), 4893–4899. https://doi.org/10.1002/ejoc.202000684.

(23) Dong, J.; Liu, Y.; Cui, Y. Chiral Porous Organic Frameworks for Asymmetric Heterogeneous Catalysis and Gas Chromatographic Separation. *Chem. Commun.* **2014**, *50* (95), 14949–14952. https://doi.org/10.1039/c4cc07648f.

(24) Bonn, A. G.; Yushchenko, O.; Vauthey, E.; Wenger, O. S. Photoinduced Electron Transfer in an Anthraquinone-[Ru(Bpy)3]2+-Oligotriarylamine-[Ru(Bpy)3]2+-Anthraquinone Pentad. *Inorg. Chem.* **2016**, *55* (6), 2894–2899. https://doi.org/10.1021/acs.inorgchem.5b02757.

(25) Mosset, P.; Grée, R. Indium-Catalyzed Friedel-Crafts Alkylation of Monosubstituted Benzenes by 1-Bromoadamantane. *Synlett* **2013**, *24* (9), 1142–1146. https://doi.org/10.1055/s-0032-1316909.

Chapter 3. Mechanistic studies of cyclic benzylidene catalysts facilitating REMP

3.1 Background

Cyclic polymers are a fascinating emerging macromolecular topology due to their unique properties compared to their linear counterparts.[1,2] Because of their lack of chain ends, cyclic polymers exhibit decreased viscosity,[3] interesting self-assembly properties,[4–7] enhanced stability,[8,9] and unexpected thermal properties.[10,11] With more methods of making these polymers and understanding of their structure-function relationship, potential applications include electronics,[12,13] drug delivery,[14,15] and nanolithography.[5] Methods of making these polymers include acyclic ring closure of linear polymers and ring expansion polymerization techniques (REP).[16] REP is advantageous in making large quantities of cyclic polymers in high purity because the cyclic topology is retained throughout the polymerization, thus avoiding entropic penalties involved in ring closure. One of the first examples of REP is ring expansion metathesis polymerization (REMP), which uses tethered variations of metathesis catalysts to polymerize strained cyclic olefin monomers.[17,18] Tethered W[19,20] and Mo[21] complexes can polymerize alkenes and alkynes, but have low functional group tolerance. Based on the success of Grubbs' catalysts in ring opening metathesis polymerization (ROMP) to make linear poly(olefins), Grubbs' and Furster developed a series of novel tethered Ru alkylidene REMP catalysts (Figure 3.1).[22,23] However, these complexes have not been optimized to the extent that ROMP catalystss like Grubbs **G2** and **G3** have.[24–29] Our group recently developed a tethered Ru benzylidene complex that displayed improved molecular weight control and stability[30]; using a more labile ancillary ligand in these complexes increased initiation rate and eliminates molecular weight evolution.[31] Despite these improvements, many mechanistic questions about REMP still remain.

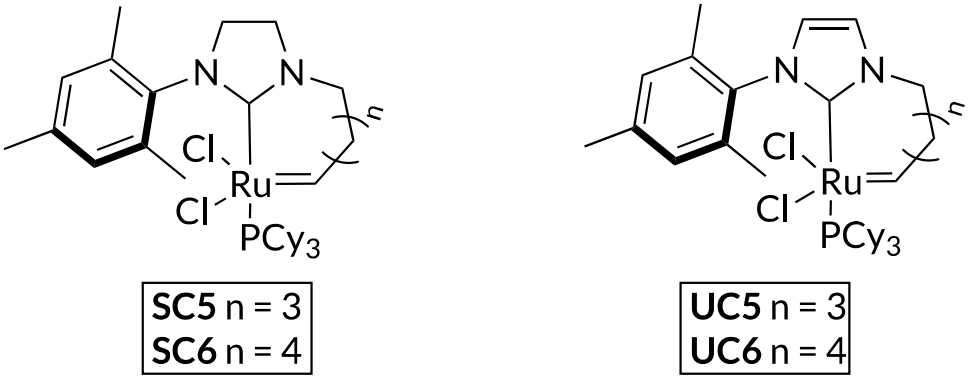

Figure 3.1. Structures of Grubbs' tethered alkylidene complexes

REMP is made up of five mechanistic steps: initiation (k_i), propagation (k_p), and three possible chain transfer events (Figure 3.2).[32] Initiation and propagation occur when strained olefin monomer undergoes metathesis with the Ru carbene. Initiation efficiency dictates how many polymers are formed and their size, and propagation is driven by release of monomer ring strain. Once polymers are formed, three possible chain transfer events can occur; backbiting to the benzylidene results in catalyst release (k_r) while non-selective backbiting (k_b) results in the formation of a smaller polymer and an unknown Ru alkylidene species. If the Ru containing macrocycle undergoes metathesis with another polymer chain fusion (k_f) can occur, producing a larger Ru macrocycle. The relative rates of each step will dictate the overall molecular weight growth profile and the final average polymer molecular weight. When initiation is slower than propagation, large polymers are formed with wide dispersities. If catalyst release is favored over propagation, the reaction will show a step-growth-like polymerization profile. On the other hand, if propagation is favored over catalyst release the polymerization will resemble a chain-growth profile. Unlike ROMP, REMP shows significant molecular weight evolution after all monomer is

consumed, which is governed by chain transfer events. Once all monomer is consumed, dominant backbiting will result in a molecular weight decrease, while chain fusion results in an increase in molecular weight. In these polymerizations, molecular weight evolution eventually stabilizes, suggesting that they are reaching a thermodynamic equilibrium.

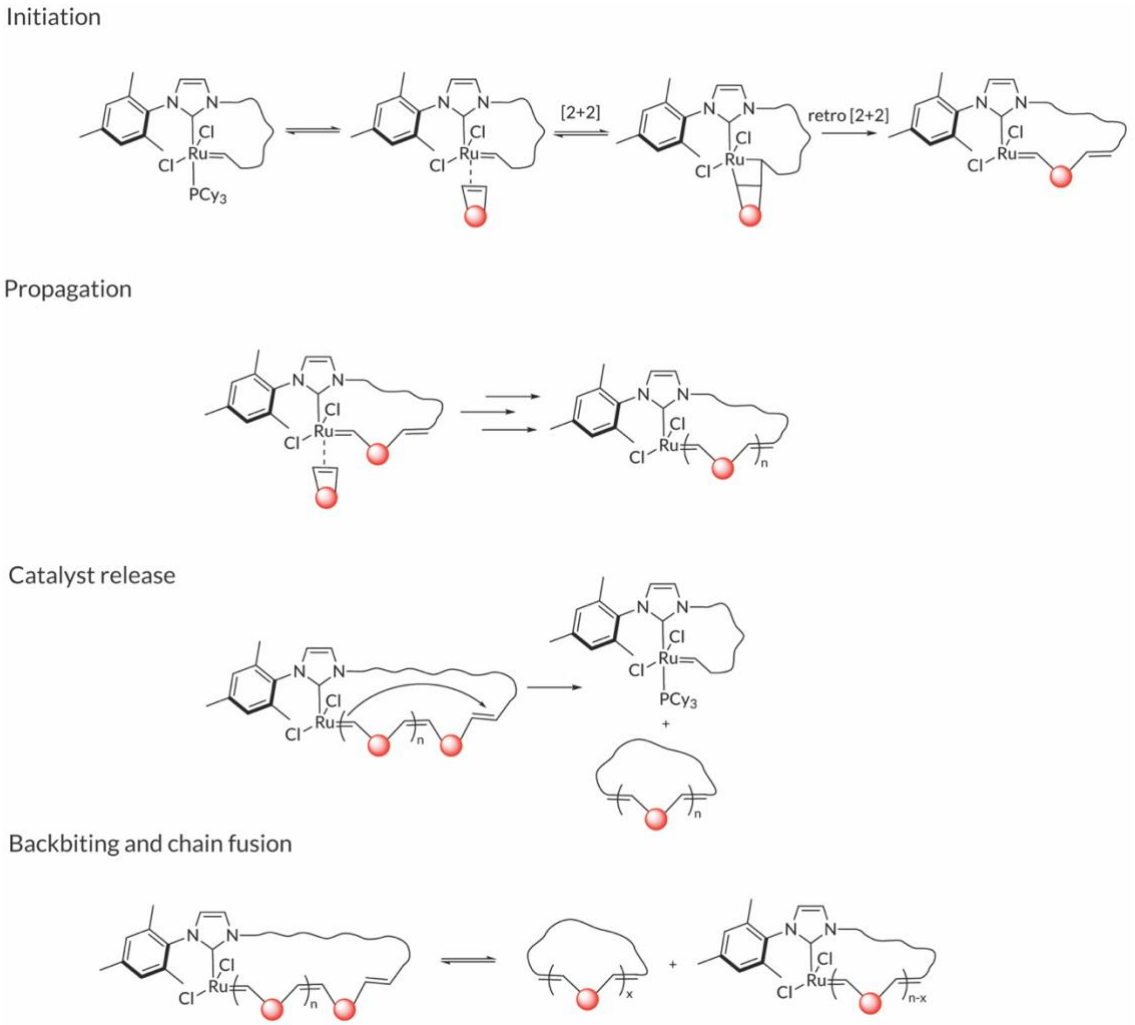

Figure 3.2. REMP mechanistic steps

Some mechanistic studies have been conducted using the Grubbs Ru alkylidene complexes investigating the favorability of catalyst release.[33] Acyclic analogs were synthesized of UC5, UC6, and UC7 catalysts and used to polymerize cyclooctene, and rates of cyclication were measured against rates of polymerization (Scheme 3.1)[33]. With a shorter tether (UC5), cyclization was shown

to be favored over polymerization, as mole fractions of acyclic UC5 decreased and cyclic UC5 formed over the course of the reaction (Figure 3.3).[33] An almost undetectable amounts of Ru were present in the polymeric species showing that UC5 favors catalyst release. UC6 and UC7 showed slow cyclization and thus favored catalyst incorporation. Incorporation of catalyst into purified polymer was also investigated, showing that longer tether lengths favored re-incorporation and shorter ones did not. The Ru alkylidene species always seemed to equilibrate to a final molecular weight that was independent of feed ratio, which indicates that the macrocycles reach a thermodynamic equilibrium. However, final equilibrium molecular weight appears to change with feed ratio of the Ru benzylidene catalysts and monomer, showing that the mechanistic intricacies are likely quite different between **CB6** and Grubbs' REMP catalysts.

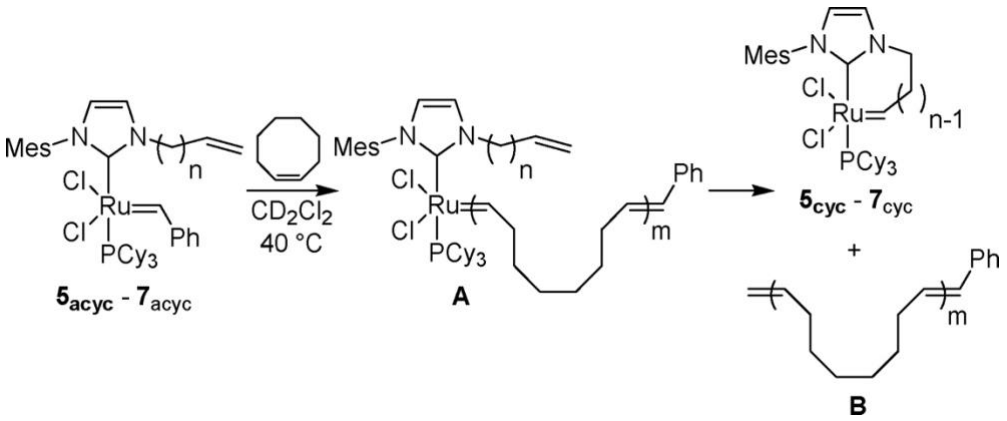

Scheme 3.1. Mechanistic studies using ring-opened analogs of UC5, UC6, and UC7 to determine Ru incorporation and catalyst release during REMP. Reprinted (adapted) with permission from Boydston, A. J.; Xia, Y.; Kornfield, J. A.; Gorodetskaya, I. A.; Grubbs, R. H. Cyclic Ruthenium-Alkylidene Catalysts for Ring-Expansion Metathesis Polymerization. *J. Am. Chem. Soc.* **2008**, *130* (11), 12775–12782. https://doi.org/10.1021/ja8037849 . Copyright 2008 American Chemical Society.

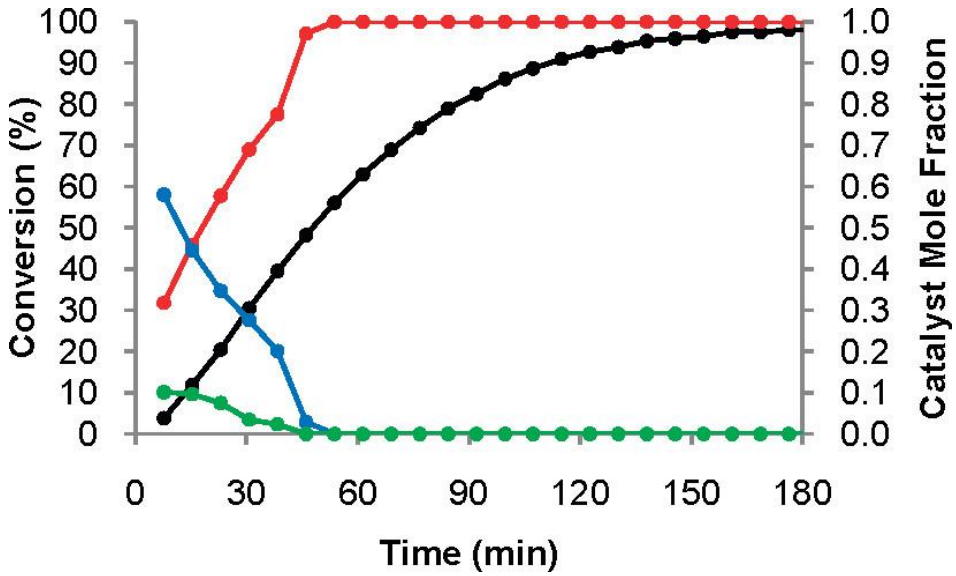

Figure 3.3. Data collected using mechanistic studies highlighted in Scheme 3.1 using UC5. Black: conversion of COE to PCOE using acyclic UC5; Red: mole fraction of cyliclized UC5; Blue: mole fraction acyclic UC5; Green: mole fraction of acyclic UC5 incorporated into PCOE (structure A in scheme 3.1). Reprinted (adapted) with permission from Boydston, A. J.; Xia, Y.; Kornfield, J. A.; Gorodetskaya, I. A.; Grubbs, R. H. Cyclic Ruthenium-Alkylidene Catalysts for Ring-Expansion Metathesis Polymerization. *J. Am. Chem. Soc.* **2008**, *130* (11), 12775–12782. https://doi.org/10.1021/ja8037849. Copyright 2008 American Chemical Society.

The novel cyclic benzylidene species, **CB6**, would be expected to show different behavior to the Grubbs REMP catalysts due to increased steric bulk, stability, and reactivity at the active site. In our previous work, we have observed that polymerization profiles of **CB6** are indeed distinct; monomer consumption is faster in **CB6**, with full conversion happening in two minutes compared to the Ru alkylidenes which take 4 hours to reach full conversion. Additionally, **CB6** demonstrated increased control over molecular weight, with final size appearing to vary with feed ratio, suggesting a chain-growth-like polymerization profile. However, significant molecular weight

evolution occurs over the course of 6-8 hours indicating that chain transfer events occur long after monomer is consumed. However, more mechanistic investigation needs to be done on the Ru benzylidene catalysts to determine how changes in structure can affect rates of different REMP events and provide insight on future catalytic design.

Herein, we conduct mechanistic studies for REMP of norbornenes using **CB6**. First, we conduct mechanistic studies monitoring benzylidene consumption over the course of the polymerization and when **CB6** is subject to excess linear alkene. Reincorporation of **CB6** into purified cyclic polymers and the resulting molecular weight evolution was also studied, revealing that molecular weight equilibrium can be shifted even after molecular weight stabilization is reached. Finally, concentration dependence on cyclic polymer molecular weight was studied, providing important mechanistic insights on the **CB6** catalyzed REMP process.

3.2 Synthesis of CB6

CB6 was synthesized according to previously published procedure (Scheme 3.2).[31] An alkylation of 4-bromobenzaldehyde with dibromohexane was followed by an alkylation of bromo-3,5 dimethylpehol with intermediate . Next, Wittig olefination followed by BrettPhos G3 catalyzed CN coupling and cyclization formed the imidazolium salt precursor. Metathesis with **G1** followed by ligand exchange afforded **CB6** and *bis*-**CB6** byproduct. The dimer could be removed using preparatory GPC. The purity of **CB6** was confirmed by a lone benzylidene resonance using ^{1}H NMR and ^{13}C NMR along with high-resolution mass spectrometry.

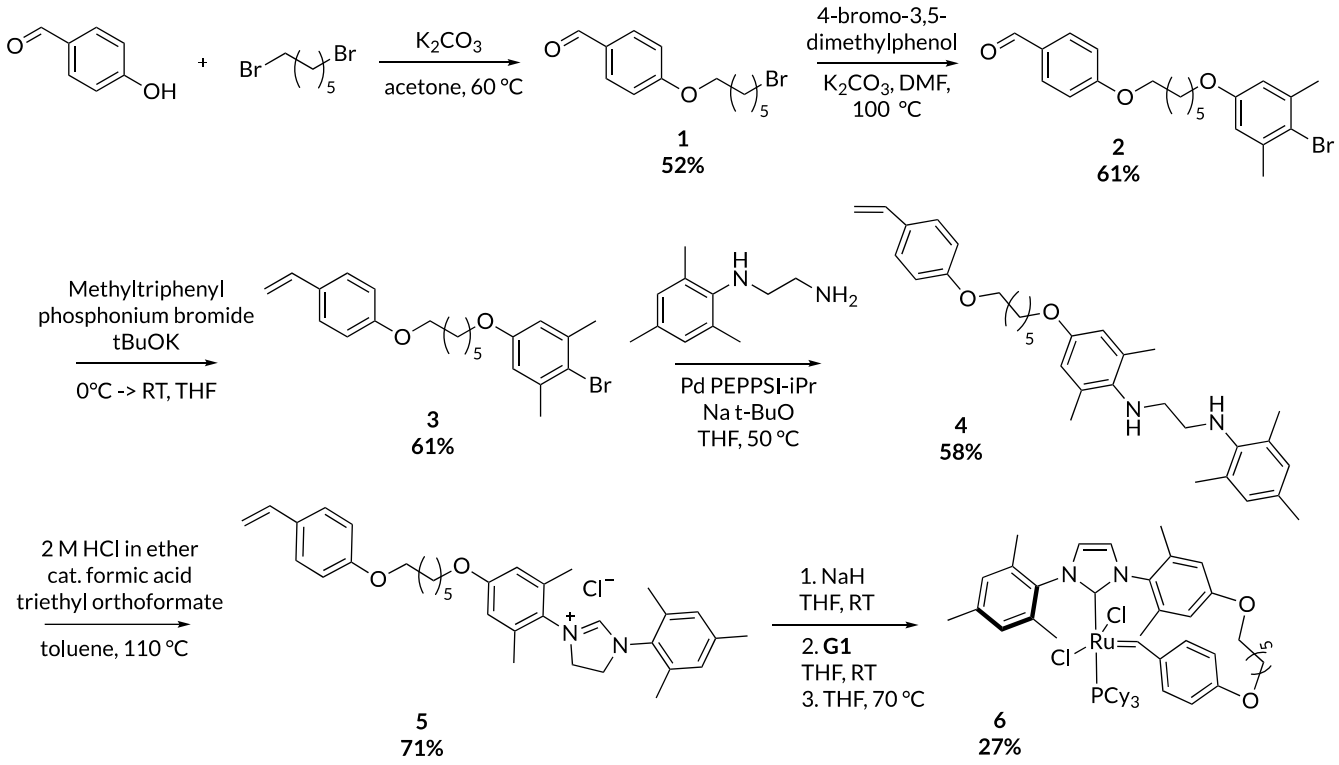

Scheme 3.2. Synthesis of **CB6**

3.3 Investigating concentration dependence of REMP

First, we wanted to investigate the mechanism of REMP by studying molecular weight dependence on the concentrations of monomer and catalyst. Previously, we observed that the final size of the cyclic polymers could be varied by changing the [monomer]:[catalyst] feed ratio, leading us to believe that these REMP reactions proceeded in a chain-growth manner. However, significant molecular weight decrease following full monomer conversion cannot be explained by a chain-growth mechanism. This behavior suggests that after the initiation and propagation phases, **CB6** is acting as a chain transfer agent (CTA) and facilitating 'pinching' of the macrocycles resulting in smaller rings. This process appears to be slower than polymerization, as it occurs over several hours where monomer consumption happens in minutes. Establishing a relationship between the concentrations of different components of the reaction and equilibrium molecular

weight could provide a mechanism to more accurately predict the size of polymers produced from a given reaction.

First, we decided to investigate the dependence of equilibrium molecular weight on the feed ratios of monomer to catalyst. We kept monomer concentration constant at 50 mM and varied catalyst concentration from 1.0 mM to 0.17 mM, targeting DP's of 50-300 (Table 3.1). Interestingly, these polymerizations showed an inverse dependence on catalyst concentration after molecular weight evolution, which is characteristic of a chain growth polymerization (Figure 3.4). However, all polymerizations significantly overshot the expected molecular weights based on feed ratio and had wide dispersities (approx. 1.5).

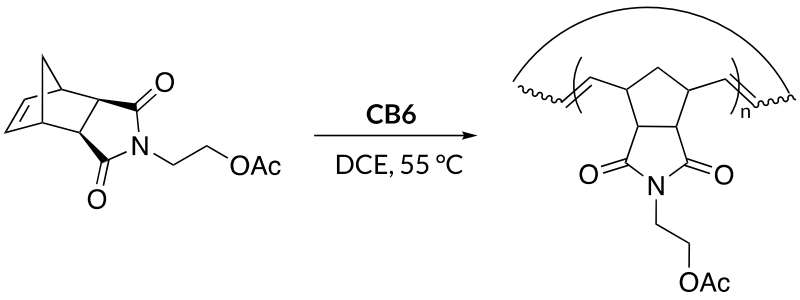

Scheme 3.3. Representative REMP scheme for concentration experiments.

CBX concentration (mM)	Monomer concentration (mM)	[Catalyst]:[monomer] feed ratio	Expected M_n[1] (kDa)	Experimental M_n (kDa)
1.0	50	1:50	12.4	33.9
0.50	50	1:100	24.9	62.2
0.25	50	1:200	49.8	182
0.17	50	1:300	74.7	365

Table 3.1. REMP dependence on **CB6** concentration with constant monomer concentration of 0.05 M. ([1]Based on monomer to catalyst feed ratio).

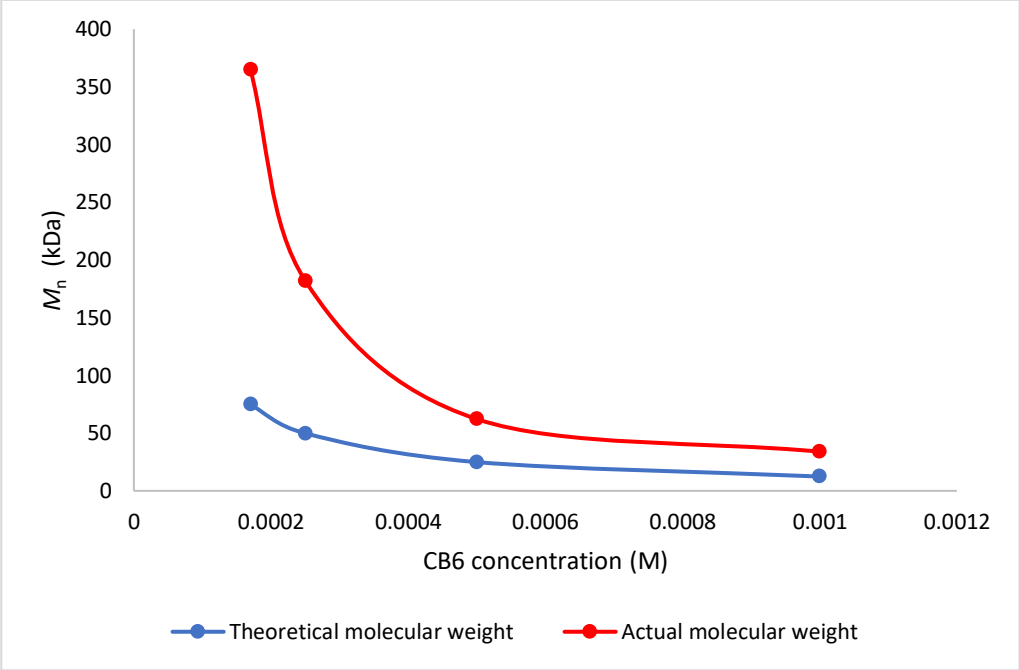

Figure 3.4. REMP shows an inverse dependence on **CB6** concentration

Next, we kept the catalyst concentration constant at 0.80 mM, but varied the monomer concentration to target DP's of 25-400 (Table 3.2). The final molecular weights after equilibration

showed a linear relationship with monomer concentration, but continued to significantly overshoot the target molecular weights based on a chain-growth polymerization model (Figure 3.5). These observations could be due to low catalyst efficiency, different rates of chain transfer events, or a combination of both factors.

CBX concentration (mM)	Monomer concentration (mM)	[catalyst]:[monomer] feed ratio	Expected M_n[1] (kDa)	Experimental M_n (kDa)
0.80	20	1:25	6.2	6.9
0.80	40	1:50	12.4	48.6
0.80	80	1:100	24.9	74.0
0.80	160	1:200	49.8	123
0.80	320	1:400	99.6	244

Table 3.2. REMP dependence on **CB6** concentration with constant monomer concentration of 0.05 M. ([1]Based on monomer to catalyst feed ratio).

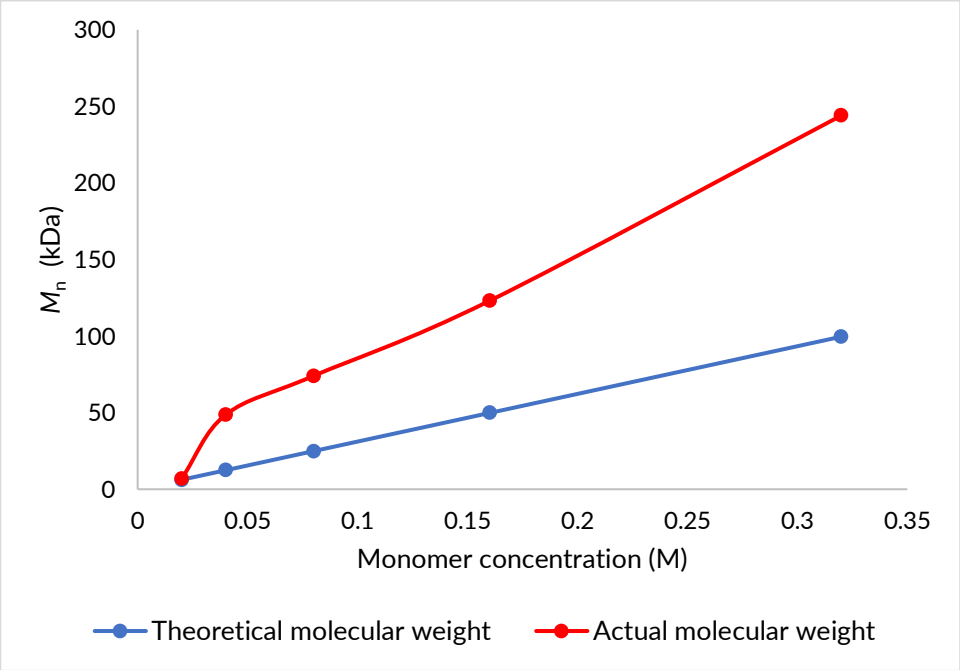

Figure 3.5. REMP shows a linear dependence on monomer concentration

To gain further insight on the concentration dependence of these polymerizations, we varied the overall reaction concentration while keeping the [catalyst]:[monomer] feed ratio constant (Table 3.3). Remarkably, we observed drastically different equilibrium molecular weights, despite having the same target molecular weights, which is inconsistent with a chain-growth model. These results suggest that chain transfer events play a role in determining the final molecular weight and that concentration affects the relative rates of these processes. For example, high concentrations could promote polymer fusion which would result in higher molecular weight polymers. This phenomenon opens up further possibilities of controlling polymer size; typically, high catalyst loading is needed to achieve lower molecular weight polymers. However, in our REMP experiments we can use dilute conditions to access lower molecular weight polymers

without having to use large amounts of **CB6** and reducing the amount of Ru impurities in the final products.

CBX concentration (mM)	Monomer concentration (mM)	[catalyst]:[monomer] feed ratio	Expected M_n[1] (kDa)	Experimental M_n (kDa)
0.16	50	1:300	74.7	395
0.032	10	1:300	74.7	224
0.016	5	1:300	74.7	136

[1]Based on monomer:catalyst feed ratio

Table 3.3. Equilibrium molecular weights of REMP reactions when overall reaction concentration is varied and [monomer]:[catalyst] feed ratios remain constant

From this data, we observe that individual rate dependence appears to mimic that of a chain growth polymerization, with an inverse dependence on catalyst concentration and a linear dependence on monomer concentration. However, the experiments varying the overall reaction concentration without changing the relative concentrations of monomer and catalyst provided insight that other chain transfer processes may also play a role in the outcomes of these polymerizations. When overall reaction concentration is changed, the polymer concentration will also change during the molecular weight evolution phase (after monomer is used up). Changes in polymer concentrations can shift the equilibrium of chain transfer events like fusion and backbiting, resulting in different polymer sizes. To decouple initiation and propagration rates from chain transfer, molecular weight evolution studies will be conducted at different overall concentrations while maintaining feed ratio constant. Observing differences in maximum

molecular weight and/or molecular weight evolution will provide insight on which processes are at play in determining the final molecular weight. Regardless, concentration dependence presents a mechanism of polymerization control that is not accessible via normal chain-growth methods.

3.4 Monitoring benzylidene consumption

After observing the interesting dependence of molecular weight on reaction concentration, we wanted to investigate the mechanism of molecular weight evolution and equilibration. First, we speculated that molecular weight evolution could stop due to catalyst death. To investigate this hypothesis, we monitored the solution-state thermal stability of CBX during the amount of time it typically takes for a REMP reaction to equilibrate. Compared to an internal standard (naphthalene), a slight decrease in the **CB6** benzylidene ^{1}H NMR peak (~13%) was observed over 24 hours, showing that full catalyst decomposition is not occurring under our reaction conditions (Figure 3.6).

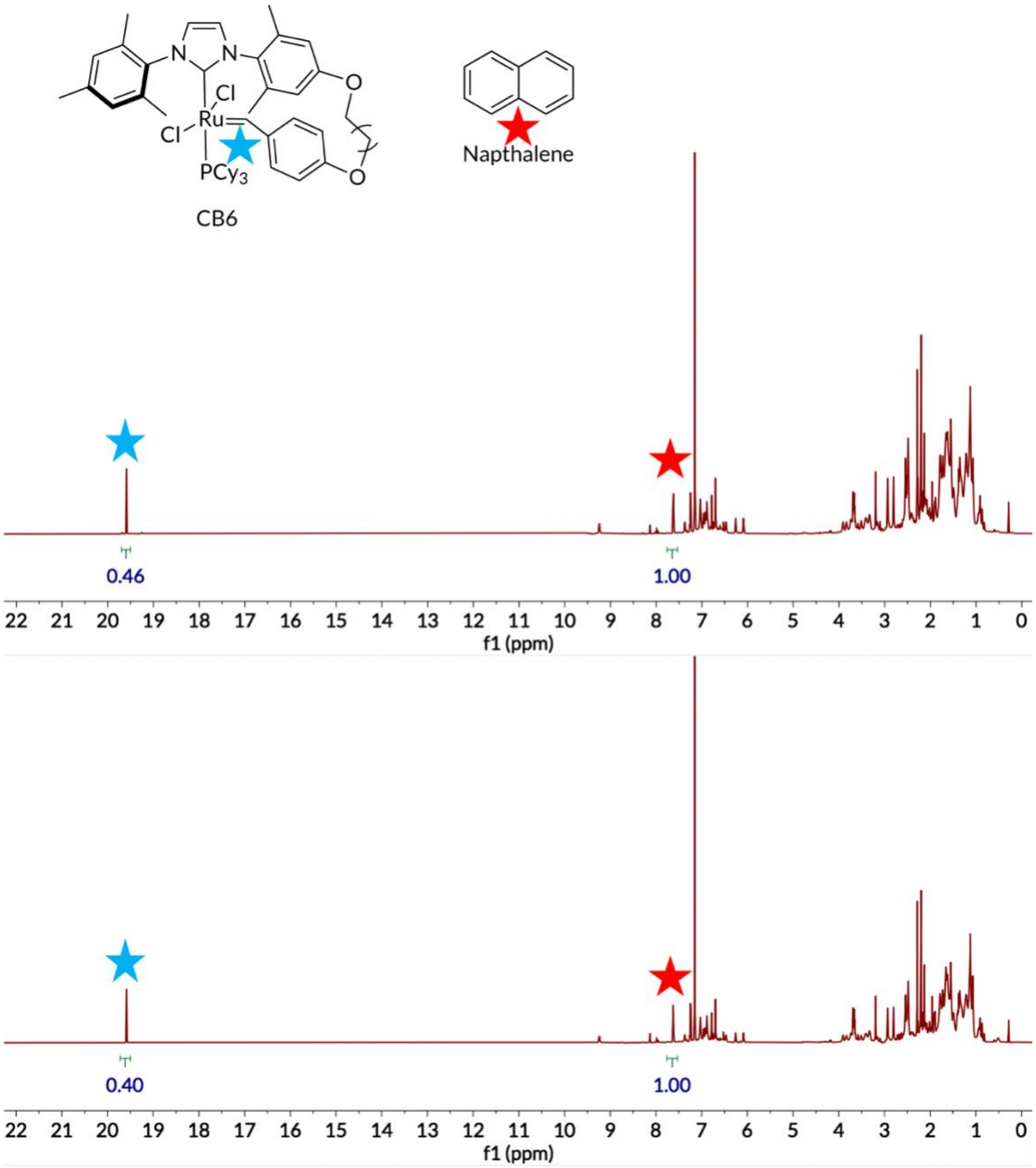

Figure 3.6. Measuring decomposition of the ^{1}H NMR (700 MHz) benzylidene peak (19.39 ppm) against the internal standard naphthalene (7.81 ppm) in C_6D_6.

Next, we hypothesized that **CB6** initiation is much slower than propagation, resulting in unreacted **CB6** after monomer consumption. We speculated that molecular weight evolution could be due to incorporation of uninitiated **CB6** into cyclic polymers and subsequent backbiting. We

attempted to measure the consumption of **CB6** by running the REMP reaction in an NMR tube and measuring the ^{1}H NMR peak over time against naphthalene as an internal standard. We hypothesized that because we could change the final molecular weight using feed ratios, that the catalyst would favor incorporation and as initiation occurs, the benzylidene peak should gradually diminish over time. Interestingly, in these reactions targeting DP = 20 by feed ratio, we did not see any changes in the benzylidene integration against the internal standard despite full monomer consumption (Figure 3.7). GPC analysis of the resulting polymer also shows a typical molecular weight for a 1:20 catalyst to monomer feed ratio. These observations suggest that either backbiting to **CB6** is occurring during REMP, or that a small undetectable amount of catalyst is driving the polymerization. However, the former is much more likely due to the fact that final molecular weight changes based on feed ratio and that the molecular weight evolution eventually stops, despite there still being catalyst in solution.

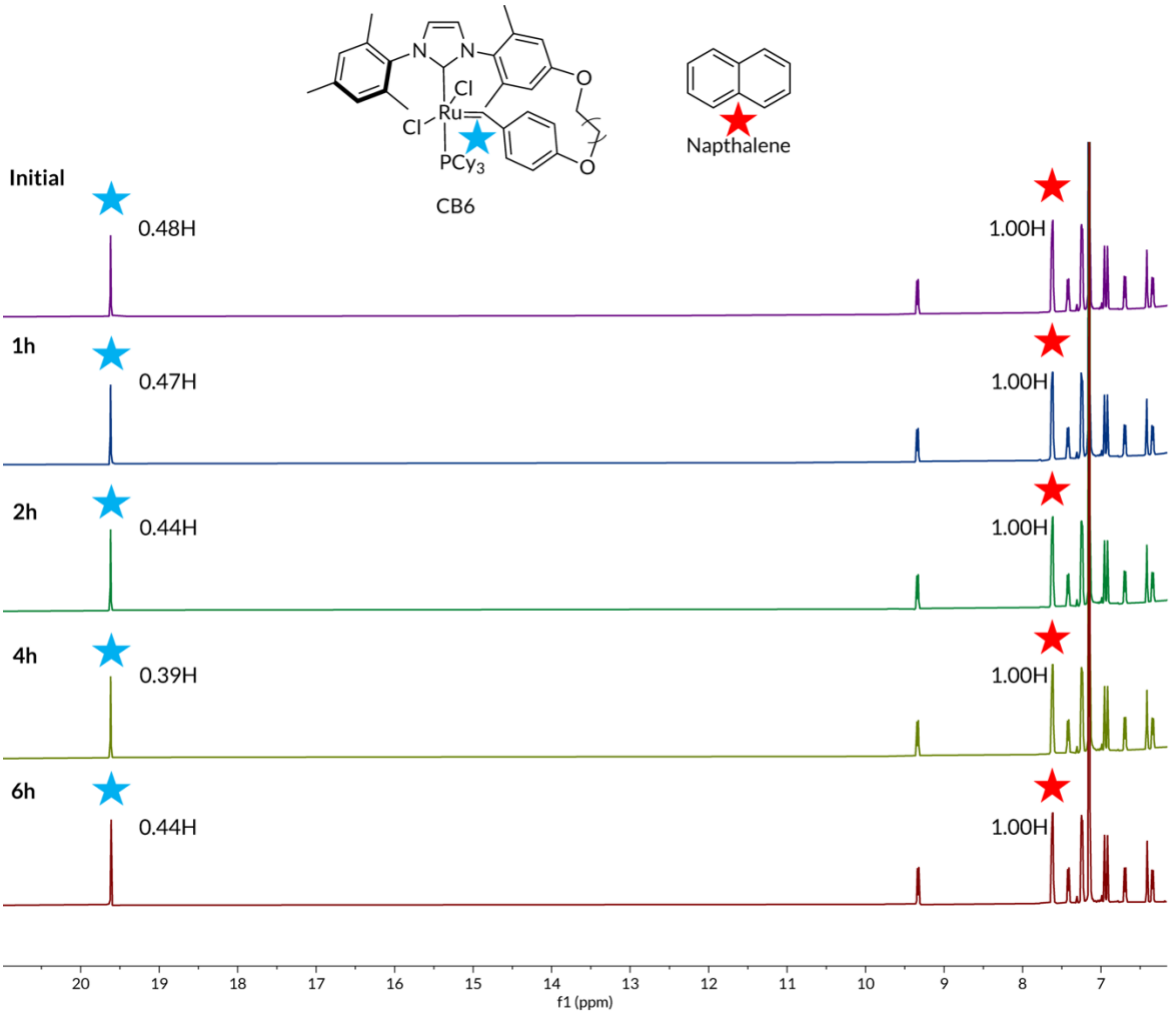

Figure 3.7. Measuring benzylidene consumption by ^{1}H NMR (700 MHz) in $CDCl_3$ over the course of a REMP reaction with target DP=20.

3.5 Resubjection of cyclic polymers to reaction conditions

To investigate the mechanism of **CB6** incorporation into cyclic polymers and determine if only a small amount of catalyst was driving all polymerization events, we wanted to determine if **CB6** could reincorporate into a cyclic polymer. Therefore, we resubjected cyclic polymers to a feed ratio that would target a molecular weight that is much lower than the original polymer, based on the amount of alkene present. For these experiments, we adjusted the feed ratios by varying

CB6 concentration and keeping alkene concentration constant at 0.05 M. Remarkably, we observed that the molecular weight after 24 hours shifted corresponding to the new feed ratio (Figure 3.8). These results reveal that **CB6** can enter the catalytic cycle not only through strained monomers, but can also insert into the unstrained alkenes of cyclic polymers. Additionally, we demonstrate that equilibrium molecular weight can be shifted by post-polymerization resubjection. These observations also corroborate our hypothesis that **CB6** is acting as a CTA during the molecular weight decrease phase, facilitating chain fusion and backbiting processes.

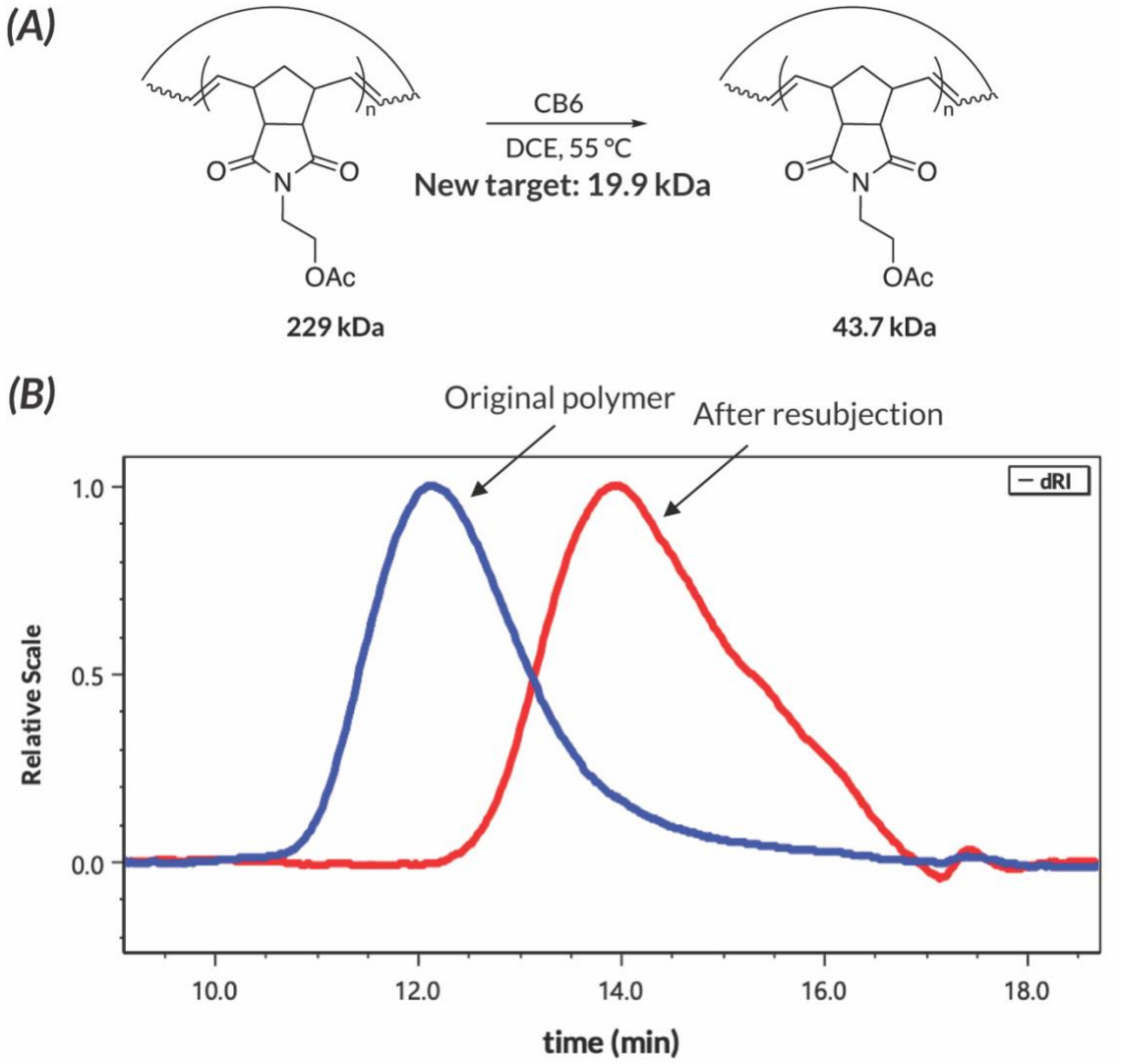

Figure 3.8. A) Resubjection experiment to target a lower molecular weight; B) GPC traces of polymers before and after resubjection to REMP conditions.

Based on these results, we speculated that cyclic copolymers could be made using this resubjection method. To verify this hypothesis, we resubjected a purified 360 kDa cyclic Poly(acetoxy norbornene) and benzyl norbornene monomer to REMP conditions. A feed ratio of 1:50 benzyl norbornene to catalyst was used, which corresponds to a molecular weight of 12.7 kDa in the case of benzyl norbornene homopolymerization (Figure 3.9A). Again, feed ratios were adjusted by

changing the concentration of **CB6** and keeping monomer concentration constant. Targeting a lower feed ratio with respect to benzyl norbornene compared to our initial polymer would allow us to differentiate between homopolymerization of benzyl norbornene and incorporation of benzyl norbornene monomer into the cyclic poly(acetoxy norbornene). Again, we observed **CB6** incorporation into the cyclic polymer through a monomodal GPC peak with a molecular weight of 43.7 kDa (Figure 3.9B) and further verified by ^{1}H NMR peaks confirming the presence of both aromatic and acetoxy groups within the cyclic polymer (Figure 3.9C). To gain further insight on these resubjection experiments, we observed molecular weight evolution as a function of time when resubjecting cyclic polymer to REMP conditions with additional monomer added (Figure 3.9). The molecular weight evolution profile was very similar to the initial polymerization; an initial fast increase in molecular weight followed by a slower decrease and eventual equilibration (Figure 3.10). All time points showed monomodal polymer GPC peaks, indicating that the benzyl norbornene monomers were being directly incorporated even before all monomer is used up. These results show that this method could be a novel and effective way of synthesizing cyclic random copolymers.

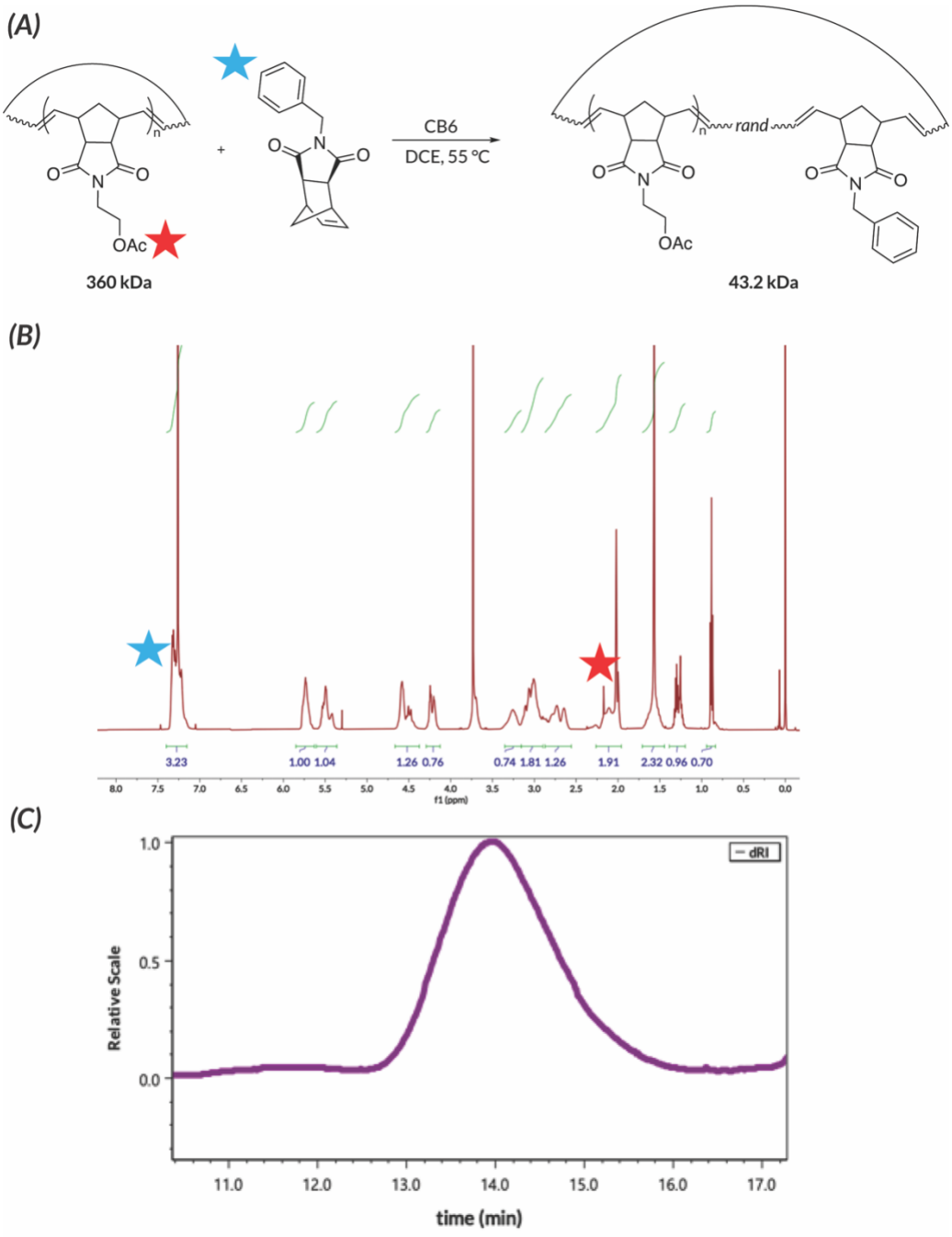

Figure 3.9. A) Resubjection of cyclic poly(acetoxy norbornene) to reactions conditions with additional monomer added; B) NMR of final polymer after molecular weight equilibration; C) GPC trace of final polymer after molecular weight equilibration.

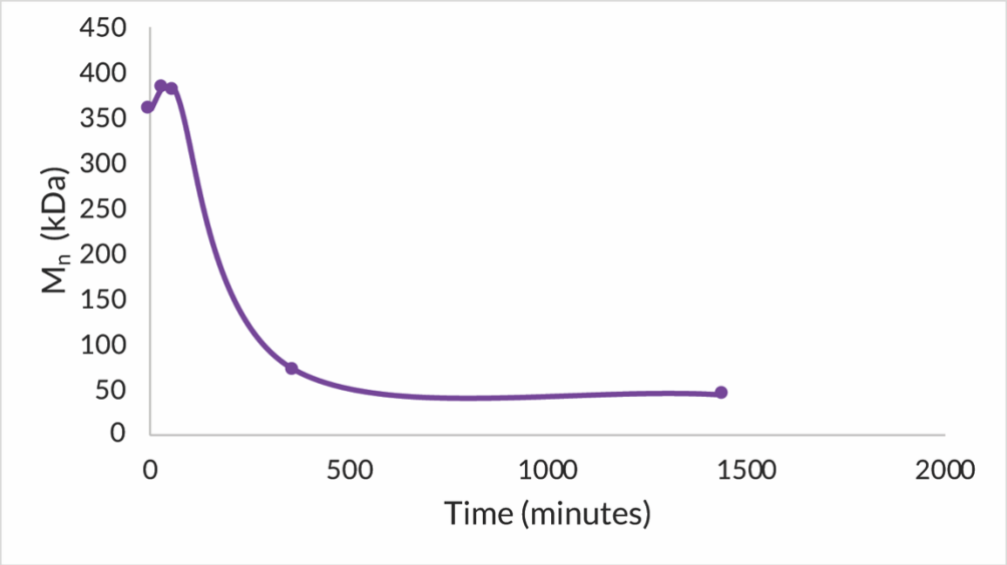

Figure 3.10. Molecular weight evolution after resubjection of poly(acetoxy norbornene) after resubjection to REMP conditions with additional benzyl norbornene monomer added.

3.6 Summary

From these mechanistic studies, we can conclude that **CB6** is acting as both a catalyst for polymerization and a chain transfer agent during the initial molecular weight growth and subsequent decline phases respectively. While monomer is being consumed, propagation is dominant as indicated by the rapid increase in molecular weight. Once all monomer is consumed, backbiting is dominant as molecular weight gradually decreases. As expected, propagation is faster than backbiting. Propagation is also shown to be faster than initiation due to the high molecular weights at 100% monomer conversion, indicating that only a small fraction of catalyst added resulted in growing chains. Through ^{1}H NMR studies, we were able to determine that **CB6** is not used up or decomposed throughout the reaction, and that we are able to shift the molecular weight

equilibrium after evolution stops. While this appears to be a chain-growth process by observing the change in molecular weight based on feed ratio, chain transfer events can also play a role in final polymer size based on REMP's unique concentration dependence.

Finally, resubjection experiments provided insight on some details regarding chain transfer mechanisms. First, we observed that **CB6** can insert into unstrained alkenes within a cyclic polymer, and the molecular weight of the resubjected polymers can be changed by varying the amount of catalyst added. Furthermore, additional monomer can be incorporated into the cyclic polymers, showing further evidence of both chain fusion and backbiting events occurring during molecular weight evolution. This finding also presents a novel method of post-polymerization modification to make cyclic random copolymers.

In conclusion, we conducted mechanistic studies that provided insight on the relative rates of REMP processes and the role of chain transfer in molecular weight evolution. Further advances in the mechanistic understand in REMP will lead to optimized catalyst design, further means of controlling polymerizations, and synthesis of novel cyclic materials.

3.7 Experimental

3.7.1 General considerations

All reagents were purchased from commercial suppliers and used as received unless otherwise noted. Glassware was flame dried or dried in an oven overnight at 120 ℃ before use. Degassed and anhydrous tetrahydrofuran (THF) and toluene were obtained from a JC Meyer solvent purification system. 1,2 dichloroethane (DCE) was dried over 3Å molecular sieves for at least 3 days and distilled before use. All moisture and air-sensitive reactions were performed under inert atmosphere (nitrogen) using standard Schlenk technique. SiliaFlash F60 (40-63 μm, 230-400 mesh) silica gel was used for column chromatography. Automated flash chromatography was

performed using a Yamazen Smart Flash AKROS system. Preparative gel permeation chromatography (prep-GPC) was performed using a Japan Analytical Industries LaboACE recycling preparative HPLC system equipped with JAIGEL-2.5HR and JAIGEL-3HR columns in series using chloroform (stabilized with 0.5% - 1.0% ethanol) as the mobile phase. ^{31}P NMR spectra were externally referenced to 85% H3PO4 (0.00 ppm).

NMR spectra were analyzed on MestreNova software. Chemical shifts are represented in parts per million (ppm); splitting patterns are assigned as s (singlet), d (doublet), t (triplet), q (quartet), p (quintet), m (multiplet), and br (broad); coupling constants, *J*, are reported in hertz (Hz).

High-resolution mass spectroscopy (HRMS) data were collected on an LTQ Orbitrap (ThermoScientific) operating in positive mode electrospray ionization. Instrument resolution was set to 60000 and elemental composition was confirmed by electrospray ionization HRMS. X-ray crystallography data was collected at –173 °C (100 K) on a Nonius Kappa CCD FR590 single crystal X-ray diffractometer, Mo-radiation. The data was integrated and scaled using SAINT, SADABS within the APEX2 software package by Bruker.

3.7.2 Synthesis of **CB6**

Synthesis of 4-((6-bromohexyl)oxy)benzaldehyde

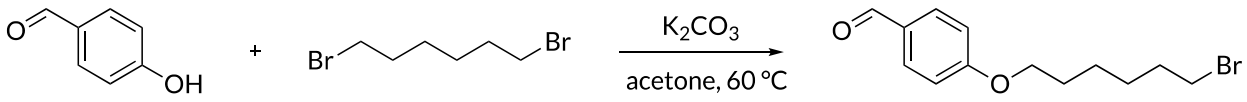

To a round bottom flask equipped with a stir bar and condenser was added 4-hydroxylaldehyde (10.0 g, 81.9 mmol), 1,6-dibromohexane (22.2 mL, 164 mmol), potassium carbonate (22.6 g, 164 mmol), and 200 mL acetone. The reaction stirred for 2 days at 60 °C open to air. The reaction was then cooled to room temperature, filtered through celite, and the filtrate was concentrated under

vacuum. The crude product was redissolved in 250 mL EtOAc and transferred to a separatory funnel. The ethyl acetate was washed with water (3 x 100 mL), brine (2 x 100 mL). The organic layer was then dried over sodium sulfate, filtered, and concentrated under vacuum. The crude yellow oil was eluted with a EtOAc/hexane (10-20%) solvent mixture on a silica column to yield 4-((6-bromohexyl)oxy)benzaldehyde as a white solid (10.3 g, 48.7%). ^{1}H

NMR (500 MHz, CDCl3): δ(ppm) 9.89 (s, 1H), 7.83 (d, J = 8.90 Hz, 2H), 6.99 (d, J = 8.77 Hz, 2H), 4.07 (td, J = 6.4, 4.4 Hz, 2H), 3.42 (td, J = 6.7, 4.7 Hz, 2H), 1.98 – 1.77 (overlap, 4H), 1.63 – 1.42 (overlap, 4H).

Synthesis of 4-((6-(4-bromo-3,5-dimethylphenoxy)hexyl)oxy)benzaldehyde

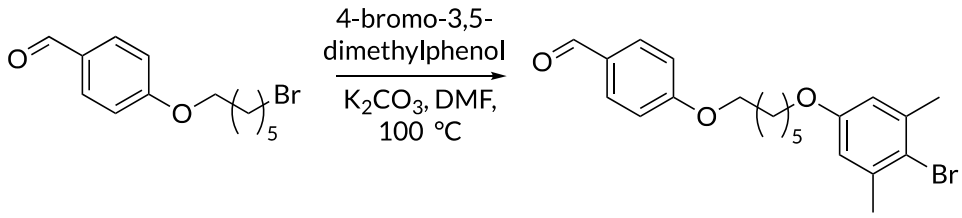

To a round bottom flask equipped with a stir bar and condenser was added 4-((6-bromohexyl)oxy)benzaldehyde (3.74 g, 13.1 mmol), 4-bromo-3,5- dimethylphenol (3.16 g, 15.7 mmol), potassium carbonate (3.08 g, 22.3 mmol), and DMF (120 mL) were added. The reaction mixture was stirred at 100 °C for 24 h. The reaction was cooled to room temperature, transferred to a separatory funnel then diluted with water (100 mL) and EtOAc (100 mL). The organic layer was collected and the water layer was extracted with ethyl acetate (3 x 50 mL). The organic layers were combined and washed with 5% lithium chloride solution (5 x 100 mL), water (2 x 50 mL), and brine (2 x 50 mL). The organic layer was dried over sodium sulfate, filtered, and concentrated under vacuum. The crude oil was crystallized by adding room temperature diethyl ether (40 mL)

and storing at 0 °C for 4 hours. The mixture was then filtered to yield 4-((6-(4-bromo-3,5-dimethylphenoxy)hexyl)oxy)benzaldehyde as pale brown crystals (3.79 g, 71%). ^{1}H NMR (500 MHz, CDCl3) δ 9.87 (s, 1H), 7.88 – 7.78 (d, J = 8.8 Hz, 2H), 7.03 – 6.94 (d, J = 8.8 Hz, 2H), 6.62 (s, 2H), 4.03 (t, J = 6.5 Hz, 2H), 3.41 (t, J = 6.4 Hz, 2H), 2.37 (s, 6H), 1.83 (overlap, 4H), 1.55 (overlap, 4H).

Synthesis of 2-bromo-1,3-dimethyl-5-((6-(4-vinylphenoxy)hexyl)oxy)benzene

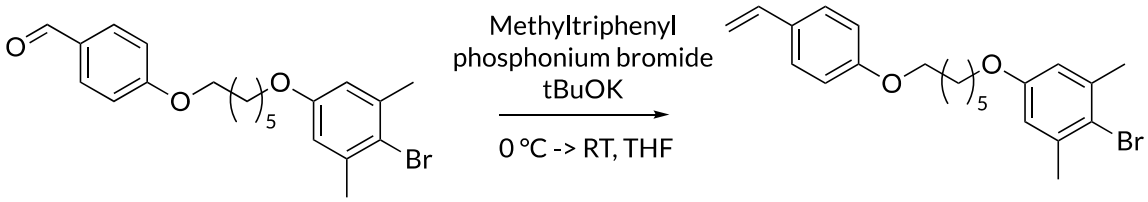

To a flame-dried Schlenk flask equipped with a stir bar was added methyltriphenylphosphonium bromide (4.01 g, 11.2 mmol), potassium tert-butoxide (2.10 g, 18.7 mmol). The flask was evacuated and refilled with nitrogen three times. Then, dry THF (37 mL) was added and the mixture stirred at 0 °C for 10 minutes. In a separate flame dried round bottom flask, 4-((6-(4-bromo-3,5-dimethylphenoxy)hexyl)oxy)benzaldehyde (3.79 g, 9.35 mmol) was dissolved in dry THF (45 mL) under nitrogen and transferred (via cannula) to the Schlenk flask. The mixture was stirred at 0 °C for 15 min then stirred at room temperature for 16 hours. Once the reaction was complete, the solution was quenched with methanol (40 mL). Solvent was evaporated under vacuum. The residue was dissolved in DCM (100 mL) and washed with water (3 x 30 mL), and brine (3 x 30 mL). The organic phase was then dried over sodium sulfate and concentrated under vacuum. The crude product was then loaded onto a silica column and the product was eluted with DCM/hexane (10-30%) to yield 2-bromo-1,3-dimethyl-5-((6-(4-vinylphenoxy)hexyl)oxy)benzene as a white solid (1.79 g, 47%). ^{1}H NMR (300 MHz, CDCl3) δ 7.32 (d, J = 8.8 Hz, 2H), 6.86 (d, J

= 8.8 Hz, 2H), 6.63 (overlap, 3H), 5.59 (dd, J = 17.7 Hz, 1H), 5.11 (dd, J = 11.0 Hz, 1H), overlap (m, 4H), 2.36 (s, 6H), 1.91 – 1.49 (overlap, 8H).

Synthesis of N-mesitylethane-1,2-diamine-HBr salt

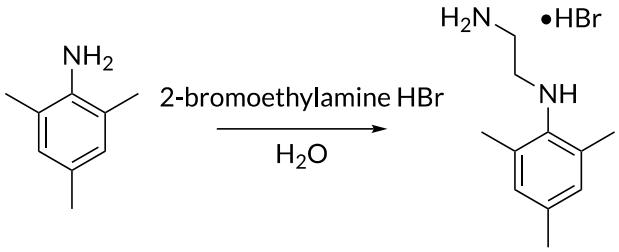

To a round bottom flask equipped with a stir bar and condenser was added 2,4,6-trimethyl aniline (31.2 mL, 222 mmol) and 2-bromoethylamine hydrobromide (22.7 g, 111 mmol). The solids were dissolved in 30.0 mL water. The mixture was stirred at 90 °C for 12 hours. The reaction was cooled to room temperature, transferred to a separatory funnel, and washed with EtOAc (5 x 30 mL). The aqueous layer was collected and concentrated under vacuum. The solid residue was crystallized from 300 mL hot (70 °C) EtOAc/methanol (2:1). The crystals were filtered and dried under vacuum to yield the N-mesitylethane-1,2-diamine-HBr salt as a white solid (22.0 g, 76.4%).

Synthesis of N-mesitylethane-1,2-diamine

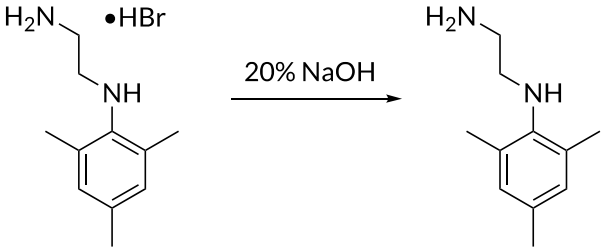

To a round bottom flask equipped with a stir bar was added SX (1.5 g, 5.79 mmol) and 20% aq. NaOH (45 mL). The solution was stirred for 30 min at room temperature. The solution was

transferred to a separatory funnel and extracted with DCM (3 x 40 mL). The combined organic layers were washed with water (15 mL x 3) and brine (15 mL x 2). The organic phase was dried over sodium sulfate and concentrated under vacuum to yield N-mesitylethane-1,2-diamine as a viscous yellow oil (800 mg, 77.5%). ^{1}H NMR (300 MHz, CDCl3) δ 6.81 (2, 2H), 3.01 – 2.84 (overlap, 4H), 2.25-2.22 (overlap, 9H).

Synthesis of N-(2,6-dimethyl-4-(4-(4-vinylphenoxy)butoxy)phenyl)-N-(3,4,5-trimethylphenyl)ethane-1,2-diamine

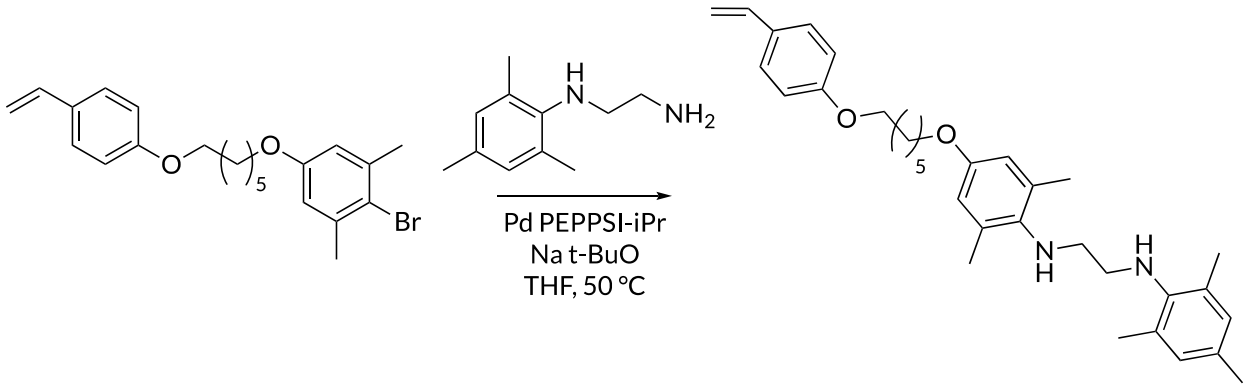

To a dry glass vial equipped with a stir bar was added 2-bromo-1,3-dimethyl-5-((6-(4-vinylphenoxy)hexyl)oxy)benzene (1.15 g, 3.06 mmol), sodium tert-butoxide (441 mg, 4.60 mmol), and Pd-PEPPSI-IPr (50.8 mg, 0.0736 mmol). To an additional dry glass vial, N-mesitylethane-1,2-diamine (765 mg, 4.29 mmol) was added. Both vials were added to a nitrogen-filled glovebox. To the vial containing Mes-diamine, dry THF was added (9.00 mL). The Mes-diamine solution was transferred to the other vial and was stirred at room temperature for 1 min. After 1 min, the vial was added to a preheated aluminum block at 60 °C and was stirred for an additional 2 min. The solution was then diluted with dry THF (9.00 mL). The reaction mixture was stirred overnight at 60 °C. The reaction was cooled to room temperature, filtered through neutral alumina, and concentrated under vacuum. The crude mixture was purified on a silica

column using EtOAc/hexane (0-20%) solvent mixture, eluting N-(2,6-dimethyl-4-(4-(4-vinylphenoxy)butoxy)phenyl)-N-(3,4,5- trimethylphenyl)ethane-1,2-diamine as a yellow solid (830 mg, 57.8%). ^{1}H NMR (500 MHz, CDCl3) δ 7.34 (d, J = 8.8 Hz, 2H), 6.88 – 6.81 (overlap, 4H), 6.66 (dd, J = 17.6, 10.9 Hz, 1H), 6.58 (s, 2H), 5.60 (d, J = 17.6 Hz, 1H), 5.11 (d, J = 10.9 Hz, 1H), 3.97 (t, J = 6.5 Hz, 2H), 3.91 (t, J = 6.4 Hz, 2H), 3.15-3.08 (overlap, 4H), 2.30 (s, 12H), 2.24 (s, 3H), 1.80 (overlap, 4H), 1.53 (overlap, 4H).

Synthesis of 3-(2,6-dimethyl-4-(4-(4-vinylphenoxy)butoxy)phenyl)-1-mesityl-4,5-dihydroimidazol-3-ium salt

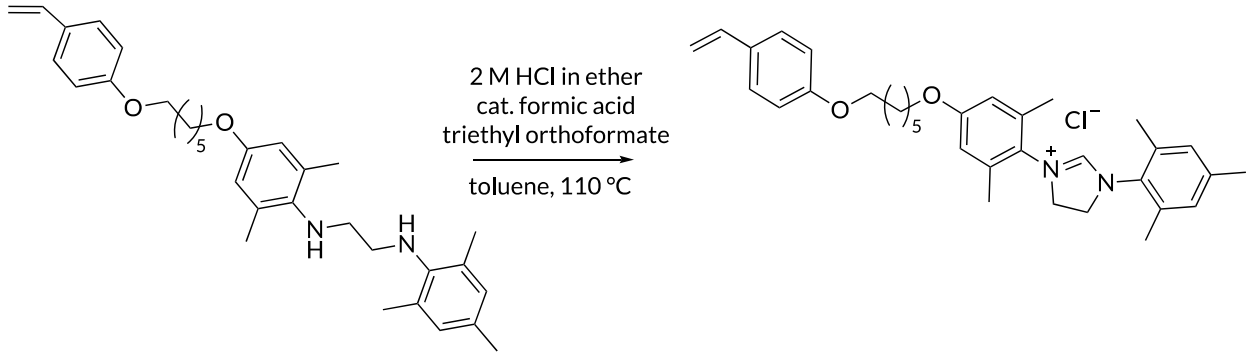

To a dry 25 mL Schlenk flask equipped with a stir bar was added N-(2,6-dimethyl-4-(4-(4-vinylphenoxy)butoxy)phenyl)-N-(3,4,5- trimethylphenyl)ethane-1,2-diamine (310 mg, 0.619 mmol) and ammonium chloride (66.2 mg, 1.23 mmol). The Schlenk flask was evacuated and refilled with nitrogen three times. The solids were dissolved in dry toluene (5.00 mL) and stirred for 10 minutes. Freshly distilled triethylorthoformate (3.74 mL, 24.8 mmol) followed by two drops of formic acid were added and the reaction stirred for 3.5 hours at 110 °C. The reaction mixture was then cooled to room temperature and evaporated to dryness. The crude mixture was purified on a silica column using methanol/DCM (0-10%) solvent mixture, eluting the 3-(2,6-dimethyl-4-(4-(4-vinylphenoxy)butoxy)phenyl)-1-mesityl-4,5-dihydroimidazol-3-ium salt as a white solid (239 mg, 82%). ^{1}H NMR (500 MHz, CDCl3) δ 9.14 (s, 1H), 7.36 – 7.30 (d, J = 8.7 Hz, 2H), 6.98

(s, 2H), 6.85 (d, J = 9.1 Hz, 2H), 6.65 (overlap, 3H), 5.60 (d, J = 17.6 Hz, 1H), 5.11 (d, J = 11.0, 1H), 4.52 (s, 4H), 3.96 (overlap, 4H), 1.81 (overlap, 4H), 1.54 (overlap, 4H).

Synthesis of CB6

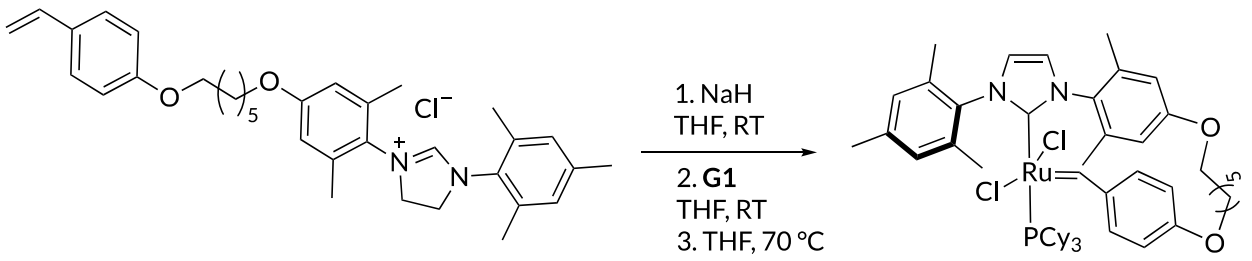

To a dry 20 mL vial was added 3-(2,6-dimethyl-4-(4-(4-vinylphenoxy)butoxy)phenyl)-1-mesityl-4,5-dihydroimidazol-3-ium salt (146 mg, 0.267 mmol) and sodium hydride (64.0 mg, 2.67 mmol) in a nitrogen filled glovebox. The solids were dissolved in dry THF (8.00 mL) and stirred at room temperature overnight. The next day, Grubbs 1st generation catalyst (220 mg, 0.269 mmol) was added to the reaction mixture and stirred at room temperature for an additional 90 minutes. Then, the reaction mixture was diluted with dry THF (100 mL) and stirred for 4 hours at 70 °C. The reaction mixture cooled to room temperature, filtered through celite, and evaporated to dryness. The reaction mixture was purified using pentane washes. The crude reaction mixture was suspended in pentanes (2 mL)nand sonicated for 5 minutes. The mixture was then centrifuged for 10 minutes at 3000 rpm and decanted. This wash procedure was repeated three times (or until the supernatant is colorless). The mixture was further purified using preparatory GPC to remove *bis*-**CB6**. The mixture was dissolved in HPLC grade chloroform (stabilized with 0.5-1% EtOH), filtered through an Aura MT 0.45 μm syringe filter, and purified via recycling prep-GPC (RI detection only). Solvent was removed under vacuum then further dried by sonication in diethyl ether followed by pentane to afford **CB6** as a light pink solid (75 mg, 38%). ^{1}H NMR (500 MHz,

C6D6) δ 19.39 (s, 1H), 9.39 (s, 1H), 7.32 (s, 1H), 6.96 (overlap, 2H), 6.92 (s, 2H), 6.47 (m, 2H), 5.91 (s, 1H), 3.99 (s, 1H), 3.65 (s, 1H), 3.50 – 3.12 (overlap, 6H), 2.95 (s, 3H), 2.78 (s, 3H), 2.62 (s, 3H), 2.53 (m, 3H), 2.42 (s, 3H), 2.20 (s, 3H), 1.77 (s, 3H), 1.72 – 0.99 (overlap, 38H).

3.7.3 REMP monomer synthesis

Synthesis of N-ethyl hydroxyl-exo-norbornene-2,3-dicarboximide

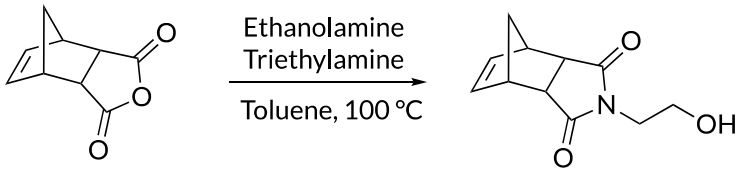

To a round bottom flask equipped with a stir bar was added cis-5-norbornene-exo-2,3-dicarboxylic anhydride (10.0 g, 60.9 mmol), ethanolamine (4.60 mL, 76.1 mmol), triethylamine (1.06 mL, 7.61 mmol), and dry toluene (160 mL). The reaction mixture stirred at reflux under nitrogen for 16 hours. The reaction mixture was cooled to room temperature, diluted with 100 mL ethyl acetate and transferred to a separatory funnel. The organic layer was washed with 10% HCl (2 x 40 mL), water (3 x 40 mL) and brine (2 x 40 mL). The organic layer was collected, dried over sodium sulfate, and evaporated to dryness yielding a white solid (4.65 g, 37%). ^{1}H NMR (500 MHz, CDCl3) δ 6.30 (s, 2H), 3.79 (t, J = 5.2 Hz, 2H), 3.72 (s, 2H), 3.30 (s, 2H), 2.73 (s, 2H), 2.07 (br, 1H), 1.55 (d, J = 9.9 Hz, 1H), 1.36 (d, J = 9.9 Hz, 1H).

Synthesis of N-ethyl acetoxy-exo-norbornene-2,3-dicarboximide (AcNb)

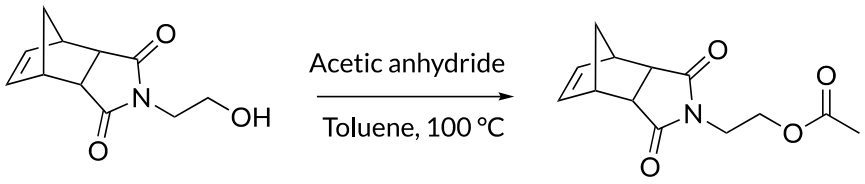

N-ethanol-exonorbornene-2,3-dicarboximide (1.6 g, 7.72 mmol), acetic anhydride (2.19 mL, 23.2 mmol), and 10 mL toluene were added to a flame dried flask equipped with a condenser. The reaction mixture stirred at reflux for 16 hours. The reaction mixture was then cooled to 0 °C then quenched by adding 40% methylamine in water (3 mL, 63.3 mmol) dropwise. The reaction mixture was transferred to a separatory funnel and diluted with 20 mL water. The mixture was extracted with ethyl acetate (3 x 20 mL). The organic layers were combined then washed with sodium carbonate (2 x 20 mL), water (3 x 20 mL) and brine (2 x 20 mL). The organic layer was dried over sodium sulfate and evaporated to dryness under vacuum. The crude product was further purified through column chromatography using a 2:1 hexane/EtOAc solvent mixture yielding AcNB as a viscous yellow oil (1.2 g, 78%). ^{1}H NMR (500 MHz, CDCl3) δ 6.29 (s, 1H), 4.23 (t, J = 5.2 Hz, 2H), 3.77 (t, J = 5.2 Hz, 2H), 3.29 (s, 2H), 2.71 (s, 2H), 2.00 (s, 3H), 1.53 (d, 9.8 Hz, 1H), 1.33 (d, J = 9.8 Hz, 1H).

Synthesis of N-benzyl-exo-norbornene-2,3-dicarboximide monomer (BnNb)

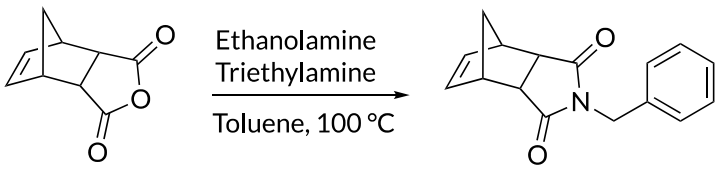

To a round bottom flask equipped with a stir bar was added cis-5-norbornene-exo-2,3-dicarboxylic anhydride (2.00 g, 12.2 mmol), benzylamine (1.42 mL, 13.4 mmol), triethylamine (1.87 mL, 13.4 mmol), and dry toluene (70 mL). The reaction mixture was stirred at reflux for 20 hr under nitrogen. The reaction mixture was cooled to temperature, evaporated to dryness, and redissolved in EtOAc (60 mL). The EtOAc was transferred to a separatory funnel and was washed with 10% HCl (2 x 30 mL), water (3 x 30 mL), and brine (2 x 30 mL). The organic phase was collected and dried with sodium sulfate. The filtered solution was concentrated under vacuum to yield a yellow solid. The solid was further purified by crystallization in DCM to obtain BnNb as a white solid (1.20 g, 39%). ^{1}H NMR (500 MHz, CDCl3) δ 7.39 (s, 0H), 7.34 – 7.22 (overlap, 5H), 6.28 (s, 2H), 4.62 (s, 2H), 3.25 (s, 2H), 2.68 (s, 2H), 1.42 (d, J = 9.9 Hz, 1H), 1.05 (d, J = 9.9 Hz, 1H).

3.7.4 Representative REMP procedures

Typical REMP polymerization with AcNB

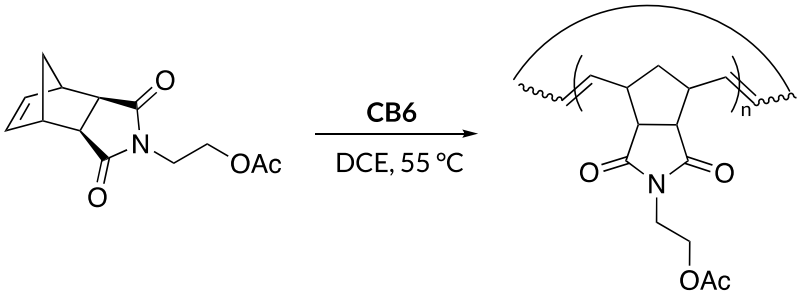

In a nitrogen filled glovebox, AcNB was added to a dry 8 mL vial with a stir bar. Monomer was dissolved in dry DCE and stirred for 5 minutes at 55 °C. A stock solution was prepared using 50 mg/mL **CB6** and an aliquot of this solution was added to monomer. Reactions stirred at 55 °C in the glovebox for at least 24 hours for molecular weight equilibration. The resulting polymers were

cooled to room temperature and filtered through neutral alumina. The resulting polymers were dissolved in chloroform, filtered through a 0.2 μm syringe filter, and analyzed by GPC-MALS-IV.

NMR studies

In a nitrogen filled glovebox, AcNb (10 mg, 0.0040 mmol) and naphthalene (1.2 mg, 0.0080 mmol) dissolved in deuterated DCE (0.800 mL) and transferred to an oven-dried screw-top NMR tube. A 50 mg/mL stock solution of **CB6** in DCE was prepared. An aliquot (0.038 mL, 0.0002 mmol) of the stock solution was added to the NMR tube. The NMR tube was capped, electrical taped, and an initial time point was taken using ^{1}H NMR at room temperature. The reaction mixture was heated to 55 °C in a sand bath and ^{1}H NMR spectra were taken about every hour for 6 hours, then an additional spectrum was taken at 24 hours. For analysis by GPC-MALS-IV, the reaction was transferred to a vial, evaporated to dryness, re-dissolved in chloroform and filtered through a 0.2 μm syringe filter.

Resubjection without additional monomer added

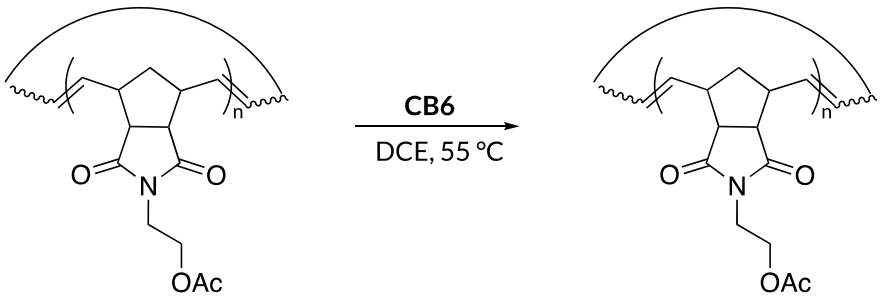

In a nitrogen-filled glovebox, polyAcNB (25 mg, M_n = 229 kDa) was dissolved in 2.45 mL DCE and stirred for 5 minutes at 55 °C. An aliquot of a 50 mg/mL **CB6** stock solution was added (23 μL, 0.0125 eq. per alkene) to the polymer vial. The reaction stirred at 55 °C in the glovebox overnight. The reactions were cooled to room temperature and filtered through neutral alumina.

The resulting polymers were dissolved in chloroform, filtered through a 0.2 μm syringe filter, and analyzed by GPC-MALS-IV.

Resubjection with additional monomer added

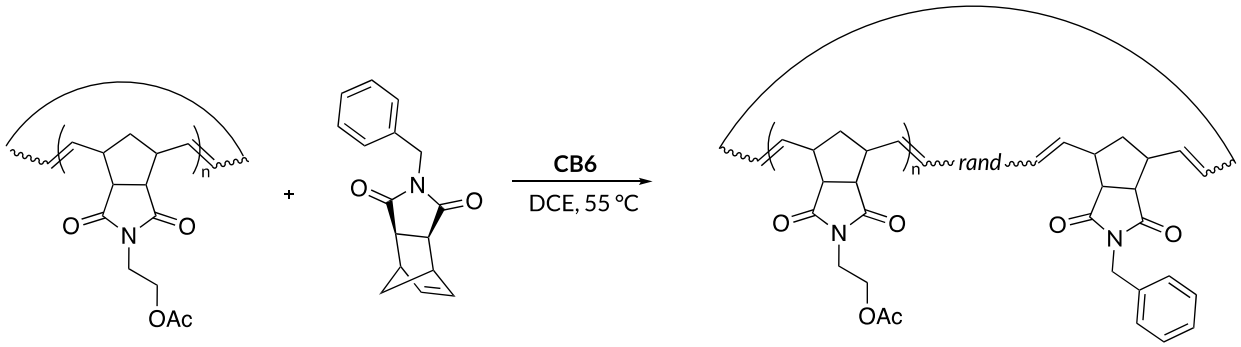

In a nitrogen-filled glovebox, polyAcNB (25 mg, M_n = 360 kDa) and BnNb (25 mg, 0.0988 mmol) were dissolved in 2.50 mL DCE and stirred for 5 minutes at 55 °C. An aliquot of a 50 mg/mL **CB6** stock solution was added (36 μL, 0.02 eq. with respect to BnNb) to the polymer vial. The reaction stirred at 55 °C in the glovebox overnight. The reactions were cooled to room temperature and filtered through neutral alumina. The resulting polymers were dissolved in chloroform, filtered through a 0.2 μm syringe filter, and analyzed by GPC-MALS-IV.

3.8 Acknowledgements and publications

This work was conducted in collaboration with Nick Serck, Lucy Miller, and Bob Li. This chapter was adapted from the publication below publication:

- **Pomfret, M. N**.; Serck, N. P.; Miller, L. P.; Li, B.; Golder, M. R.* *Manuscript in preparation.*

3.9 References

(1) Kricheldorf, H. R. Cyclic Polymers: Synthetic Strategies and Physical Properties. *J. Polym. Sci. Part A Polym. Chem.* **2010**, *48* (2), 251–284. https://doi.org/10.1002/pola.23755.

(2) Haque, F. M.; Grayson, S. M. The Synthesis, Properties and Potential Applications of Cyclic Polymers. *Nat. Chem.* **2020**, *12*, 433–444. https://doi.org/10.1038/s41557-020-0440-5.

(3) Jeong, Y.; Jin, Y.; Chang, T.; Uhlik, F.; Roovers, J. Intrinsic Viscosity of Cyclic Polystyrene. *Macromolecules* **2017**, *50* (19), 7770–7776. https://doi.org/10.1021/acs.macromol.7b01511.

(4) Trachsel, L.; Romio, M.; Grob, B.; Zenobi-Wong, M.; Spencer, N. D.; Ramakrishna, S. N.; Benetti, E. M. Functional Nanoassemblies of Cyclic Polymers Show Amplified Responsiveness and Enhanced Protein-Binding Ability. *ACS Nano* **2020**, *14* (8), 10054–10067. https://doi.org/10.1021/acsnano.0c03239.

(5) Poelma, J. E.; Ono, K.; Miyajima, D.; Aida, T.; Satoh, K.; Hawker, C. J. Cyclic Block Copolymers for Controlling Feature Sizes in Block Copolymer Lithography. *ACS Nano* **2012**, *6* (12), 10845–10854. https://doi.org/10.1021/nn304217y.

(6) Xiao, L.; Qu, L.; Zhu, W.; Wu, Y.; Liu, Z.; Zhang, K. Donut-Shaped Nanoparticles Templated by Cyclic Bottlebrush Polymers. *Macromolecules* **2017**, *50* (17), 6762–6770. https://doi.org/10.1021/acs.macromol.7b01512.

(7) Pal, D.; Garrison, J. B.; Miao, Z.; Diodati, L. E.; Veige, A. S.; Sumerlin, B. S. Nanobowls from Amphiphilic Core-Shell Cyclic Bottlebrush Polymers. *Macromolecules* **2022**, *55* (17), 7446–7453. https://doi.org/10.1021/acs.macromol.2c01232.

(8) Honda, S.; Yamamoto, T.; Tezuka, Y. Topology-Directed Control on Thermal Stability: Micelles Formed from Linear and Cyclized Amphiphilic Block Copolymers. *J. Am. Chem. Soc.* **2010**, *132* (30), 10251–10253. https://doi.org/10.1021/ja104691j.

(9) Yamamoto, T. Synthesis of Cyclic Polymers and Topology Effects on Their Diffusion and Thermal Properties. *Polym. J.* **2013**, *45* (7), 711–717. https://doi.org/10.1038/pj.2012.213.

(10) Kammiyada, H.; Ouchi, M.; Sawamoto, M. A Study on Physical Properties of Cyclic Poly(Vinyl Ether)s Synthesized via Ring-Expansion Cationic Polymerization. *Macromolecules* **2017**, *50* (3), 841–848. https://doi.org/10.1021/acs.macromol.6b02704.

(11) Wang, J.; Li, Z.; Pérez, R. A.; Müller, A. J.; Zhang, B.; Grayson, S. M.; Hu, W. Comparing Crystallization Rates between Linear and Cyclic Poly(Epsilon-Caprolactones) via Fast-Scan Chip-Calorimeter Measurements. *Polymer (Guildf).* **2015**, *63*, 34–40. https://doi.org/10.1016/j.polymer.2015.02.039.

(12) Miao, Z.; Esper, A. M.; Nadif, S. S.; Gonsales, S. A.; Sumerlin, B. S.; Veige, A. S. Semi-Conducting Cyclic Copolymers of Acetylene and Propyne. *React. Funct. Polym.* **2021**, *169* (August), 105088. https://doi.org/10.1016/j.reactfunctpolym.2021.105088.

(13) Lidster, B. J.; Behrendt, J. M.; Turner, M. L. Monotelechelic Poly(p-Phenylenevinylene)s by Ring Opening Metathesis Polymerisation. *Chem. Commun.* **2014**, *50* (80), 11867–11870. https://doi.org/10.1039/c4cc05118a.

(14) Golba, B.; Benetti, E. M.; De Geest, B. G. Biomaterials Applications of Cyclic Polymers. *Biomaterials* **2021**, *267* (June 2020), 120468. https://doi.org/10.1016/j.biomaterials.2020.120468.

(15) Chen, B.; Jerger, K.; Fréchet, J. M. J.; Szoka, F. C. The Influence of Polymer Topology on

Pharmacokinetics: Differences between Cyclic and Linear PEGylated Poly(Acrylic Acid) Comb Polymers. *J. Control. Release* **2009**, *140* (3), 203–209. https://doi.org/10.1016/j.jconrel.2009.05.021.

(16) Wang, T.-W.; Golder, M. R. Advancing Macromolecular Hoop Construction: Recent Developments in Synthetic Cyclic Polymer Chemistry. *Polym. Chem.* **2021**, *12*, 958–969. https://doi.org/10.1039/d0py01655a.

(17) Morrison, C. M.; Golder, M. R. Ring-Expansion Metathesis Polymerization Initiator Design for the Synthesis of Cyclic Polymers. *Synlett* **2022**, *33* (08), 699–704. https://doi.org/10.1055/s-0041-1737802.

(18) Edwards, J. P.; Wolf, W. J.; Grubbs, R. H. The Synthesis of Cyclic Polymers by Olefin Metathesis: Achievements and Challenges. *J. Polym. Sci. Part A Polym. Chem.* **2019**, *57* (3), 228–242. https://doi.org/10.1002/pola.29253.

(19) Jakhar, V.; Pal, D.; Ghiviriga, I.; Abboud, K. A.; Lester, D. W.; Sumerlin, B. S.; Veige, A. S. Tethered Tungsten-Alkylidenes for the Synthesis of Cyclic Polynorbornene via Ring Expansion Metathesis: Unprecedented Stereoselectivity and Trapping of Key Catalytic Intermediates. *J. Am. Chem. Soc.* **2021**, *143* (2), 1235–1246. https://doi.org/10.1021/jacs.0c12248.

(20) Roland, C. D.; Li, H.; Abboud, K. A.; Wagener, K. B.; Veige, A. S. Cyclic Polymers from Alkynes. *Nat. Chem.* **2016**, *8*, 791–796. https://doi.org/10.1038/nchem.2516.

(21) Mandal, U.; Ghiviriga, I.; Abboud, K. A.; Lester, D. W.; Veige, A. S. Double Tethered Metallacyclobutane Catalyst for Cyclic Polymer Synthesis. *J. Am. Chem. Soc.* **2021**, *143* (41), 17276–17283. https://doi.org/10.1021/jacs.1c08806.

(22) Bielawski, C. W.; Benitez, D.; Grubbs, R. H. An "Endless" Route to Cyclic Polymers. *Science (80-.).* **2002**, *297* (5589), 2041–2044. https://doi.org/10.1126/science.1075401.

(23) Bielawski, C. W.; Benitez, D.; Grubbs, R. H. Synthesis of Cyclic Polybutadiene via Ring-Opening Metathesis Polymerization: The Importance of Removing Trace Linear Contaminants. *J. Am. Chem. Soc.* **2003**, *125* (28), 8424–8425. https://doi.org/10.1021/ja034524l.

(24) Masoud, S. M.; Mailyan, A. K.; Dorcet, V.; Roisnel, T.; Dixneuf, P. H.; Bruneau, C.; Osipov, S. N. Metathesis Catalysts with Fluorinated Unsymmetrical NHC Ligands. *Organometallics* **2015**, *34* (11), 2305–2313. https://doi.org/10.1021/om501077w.

(25) Fürstner, A.; Ackermann, L.; Gabor, B.; Goddard, R.; Lehmann, C. W.; Mynott, R.; Stelzer, F.; Thiel, O. R. Comparative Investigation of Ruthenium-Based Metathesis Catalysts Bearing N-Heterocyclic Carbene (NHC) Ligands. *Chem. - A Eur. J.* **2001**, *7* (15), 3236–3253. https://doi.org/10.1002/1521-3765(20010803)7:15<3236::AID-CHEM3236>3.0.CO;2-S.

(26) Teator, A. J.; Bielawski, C. W. Remote Control Grubbs Catalysts That Modulate Ring-Opening Metathesis Polymerizations. *J. Polym. Sci. Part A Polym. Chem.* **2017**, *55* (18), 2949–2960. https://doi.org/10.1002/pola.28665.

(27) Yang, H. C.; Huang, Y. C.; Lan, Y. K.; Luh, T. Y.; Zhao, Y.; Truhlar, D. G. Carbene Rotamer Switching Explains the Reverse Trans Effect in Forming the Grubbs Second-Generation Olefin Metathesis Catalyst. *Organometallics* **2011**, *30* (15), 4196–4200. https://doi.org/10.1021/om200529m.

(28) Scholl, M.; Ding, S.; Lee, C. W.; Grubbs, R. H. Synthesis and Activity of a New Generation of Ruthenium-Based Olefin Metathesis Catalysts Coordinated with 1,3-Dimesityl-4,5-Dihydroimidazol-2-Ylidene Ligands. *Org. Lett.* **1999**, *1* (6), 953–956.

https://doi.org/10.1021/ol990909q.
(29) Hong, S. H.; Grubbs, R. H. Highly Active Water-Soluble Olefin Metathesis Catalyst. *J. Am. Chem. Soc.* **2006**, *128* (11), 3508–3509. https://doi.org/10.1021/ja058451c.
(30) Wang, T.-W.; Huang, P.-R.; Chow, J. L.; Kaminsky, W.; Golder, M. R. A Cyclic Ruthenium Benzylidene Initiator Platform Enhances Reactivity for Ring-Expansion Metathesis Polymerization. *J. Am. Chem. Soc.* **2021**, *143* (19), 7314–7319. https://doi.org/10.1021/jacs.1c03491.
(31) Levenson, A. M.; Morrison, C. M.; Huang, P.-R.; Wang, T.-W.; Carter-Schwendler, Z.; Golder, M. R. Ancillary Ligand Lability Improves Control in Cyclic Ruthenium Benzylidene Initiated Ring-Expansion Metathesis Polymerizations. *ACS Macro Lett.* **2023**, 1286–1292. https://doi.org/10.1021/acsmacrolett.3c00520.
(32) Xia, Y.; Boydston, A. J.; Yao, Y.; Kornfield, J. A.; Gorodetskaya, I. A.; Spiess, H. W.; Grubbs, R. H. Ring-Expansion Metathesis Polymerization: Catalyst-Dependent Polymerization Profiles. *J. Am. Chem. Soc.* **2009**, *131* (7), 2670–2677. https://doi.org/10.1021/ja808296a.
(33) Boydston, A. J.; Xia, Y.; Kornfield, J. A.; Gorodetskaya, I. A.; Grubbs, R. H. Cyclic Ruthenium-Alkylidene Catalysts for Ring-Expansion Metathesis Polymerization. *J. Am. Chem. Soc.* **2008**, *130* (11), 12775–12782. https://doi.org/10.1021/ja8037849.

Chapter 4: Cyclic Benzylidene Catalyst Design

4.1 Background

Cyclic polymers are a captivating macromolecular topology due to their unique physical properties compared to their linear counterparts.[1,2] These polymers have emerging applications in emerging applications in biomaterials,[3,4] drug delivery,[5,6] sustainability[7] and are useful for studying the fundamental structure/function relationship in macromolecules. However, the full potential of cyclic polymers has not yet been realized due to challenges in synthesis and purity of these materials.[8] These polymers can be accessed through either acyclic ring closure or ring expansion methods; the latter is desirable because cyclic topology is retained throughout the polymerization.[9,10]

Ring expansion metathesis polymerization (REMP) is one of the most versatile ways to access cyclic polymers in high yields and high purity (Figure 4.1).[11] This technique is based on ring opening metathesis polymerization (ROMP), which is a popular and widespread method of making linear olefin polymers from strained cyclic olefin monomers. W[12–14] and Mo[15] catalysts can polymerize both alkenes and alkynes, but have low functional group tolerance.

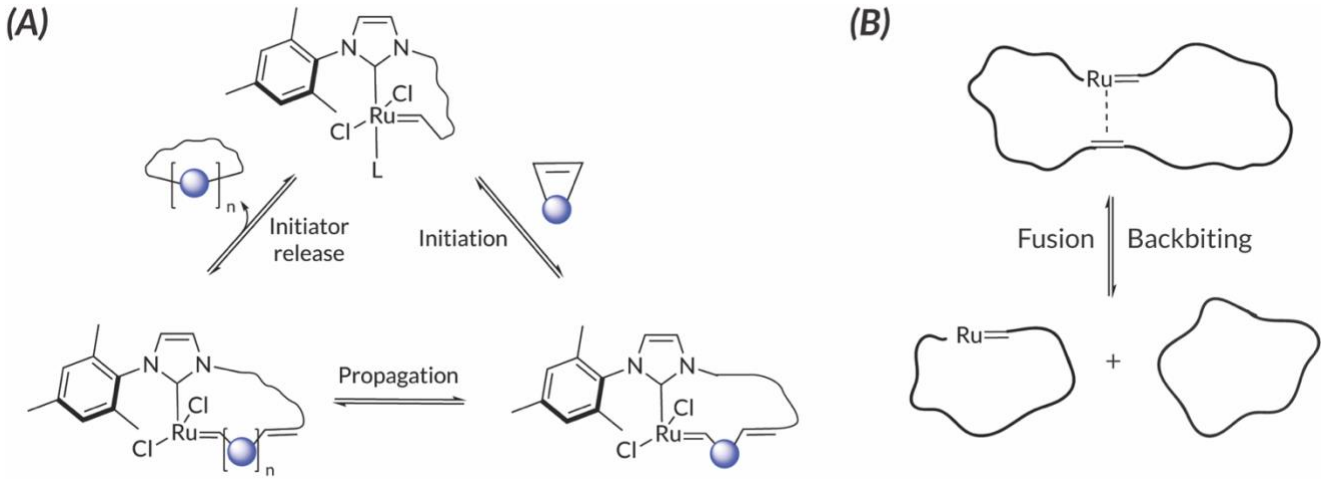

Figure 4.1. A) General REMP mechanism; B) Fusion and backbiting REMP chain transfer events

Early Ru based catalysts were developed by Grubbs and Fürstner as cyclic variants of ROMP catalysts **G1** and **G2**.[16–18] Different versions of these catalysts were developed with variations in tether length and saturation of the NHC.[19] Initiation rates of Grubbs' complexes were also investigated by measuring rate of catalyst consumption with excess butyl vinyl ether; in this case, it was observed that initiation rate was faster in five-carbon tethers than six carbon tethers in both saturated and unsaturated compounds. Tether length was not shown to have an effect on polymerization rate because once multiple monomers are incorporated into the macrocycle, a single carbon difference in the tether will have negligible effects on further monomer incorporation. However, NHC electronics were observed to dictate propagation rate; saturated compounds displayed faster polymerization rates than their unsaturated counterparts. While tether length does not affect polymerization rate, it did dictate the molecular weight evolution profile of the polymers by controlling the rate of catalyst release (Figure 4.2).[19] Five carbon tethered alkylidenes showed an initially slow increase in molecular weight then a sharp increase at >90% conversion, showing that these complexes favor catalyst release and a step-

growth like polymerization profile. On the other hand, the six carbon tethers had a chain-growth-like polymerization, showing that it favored propagation over catalyst release. However, REMP catalysts have not been optimized to the same extent that ROMP catalysts have, resulting in lagging progress in the development of cyclic polymers.

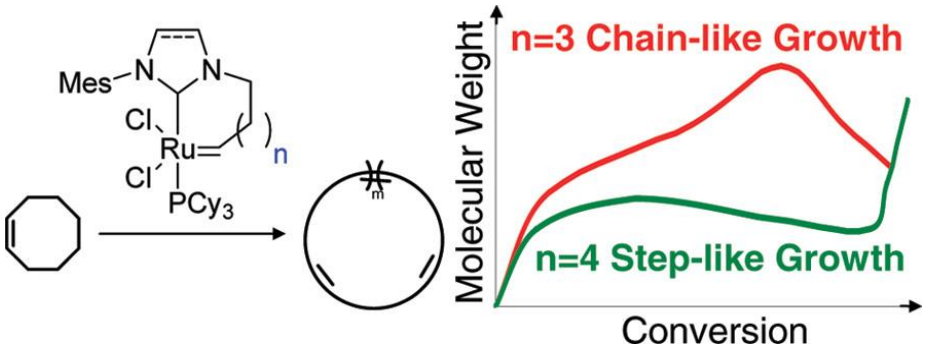

Figure 4.2. Differences in molecular weight evolution profiles in Grubbs' cyclic catalysts with 5 and 6 carbon tethers. Reprinted (adapted) with permission from Xia, Y.; Boydston, A. J.; Yao, Y.; Kornfield, J. A.; Gorodetskaya, I. A.; Spiess, H. W.; Grubbs, R. H. Ring-Expansion Metathesis Polymerization: Catalyst-Dependent Polymerization Profiles. *J. Am. Chem. Soc.* **2009**, *131* (7), 2670–2677. https://doi.org/10.1021/ja808296a. Copyright 2009 American Chemical Society.

REMP catalysts contain a tether, a structural aspect that has not been present in ROMP mechanistic studies. While variations in tether length have been studied in Grubbs' alkylidene catalysts, these changes would be expected to have a different effect on our Ru benzylidne complex **CB6** (Figure 4.3).[20,21] Increased steric bulk results in differences in ring strain and bond angles of the NHC, carbene, and phosphine, all of which could alter initiation rates. The

increased steric bulk also may require a longer tether to achieve the optimal catalyst conformation for efficient initiation of the REMP process.

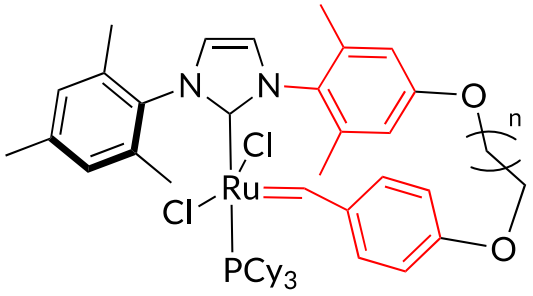

Figure 4.3. CBX structure (X = number of carbons in tether) with differences from Grubbs' cyclic alkylidene catalysts highlighted in red.

Herein, we synthesize a series of **CBX** (X = number of carbons in tether) REMP catalysts ranging from X = 4-7 and study their stabilities and molecular weight control. To gain insight on how tether length affects the rate of each REMP event, we measured molecular weight evolution as a function of time. Overall, we establish that REMP rates can be tuned through small modifications in catalyst design.

4.2 Synthesis of CBX catalysts

CBX catalysts were synthesized according to our previously published procedure.[21] To achieve the desired tether length, 4-hydroxybenzaldehyde was alkylated with dibromobutane, dibromopentane, or dibromohexane for **CB4**, **CB5**, and **CB6** respectively. 4-Bromo-3,5-dimethylphenol was then alkylated using the step 1 product. These steps were followed by Wittig olefination, PdBrettPhos catalyzed CN coupling, and formation of the imidazolium salt using ammonium chloride, triethylorthoformate, and catalytic formic acid. The imidazolium salt

precursor could then be deprotonated with sodium hydride, followed by cross metathesis and diluted for ligand exchange with Grubbs G1 in one pot, affording the **CBX** catalyst. Consistent yields were observed across all steps among the three catalysts. Bis-**CBX** dimer byproduct was observed for all three catalysts and removed using preparatory-GPC (prep-GPC). Increased dimer byproduct was formed when higher concentrations were used during the ligand exchange step or at extended reaction times for the cross metathesis. Attempts were made at synthesizing CB7, however bis-CB7 was the only product formed as indicated by high resolution mass spectroscopy (HRMS) and a single high molecular weight peak on prep-GPC. Future efforts will be made to optimize the reaction conditions to access catalysts with longer tethers.

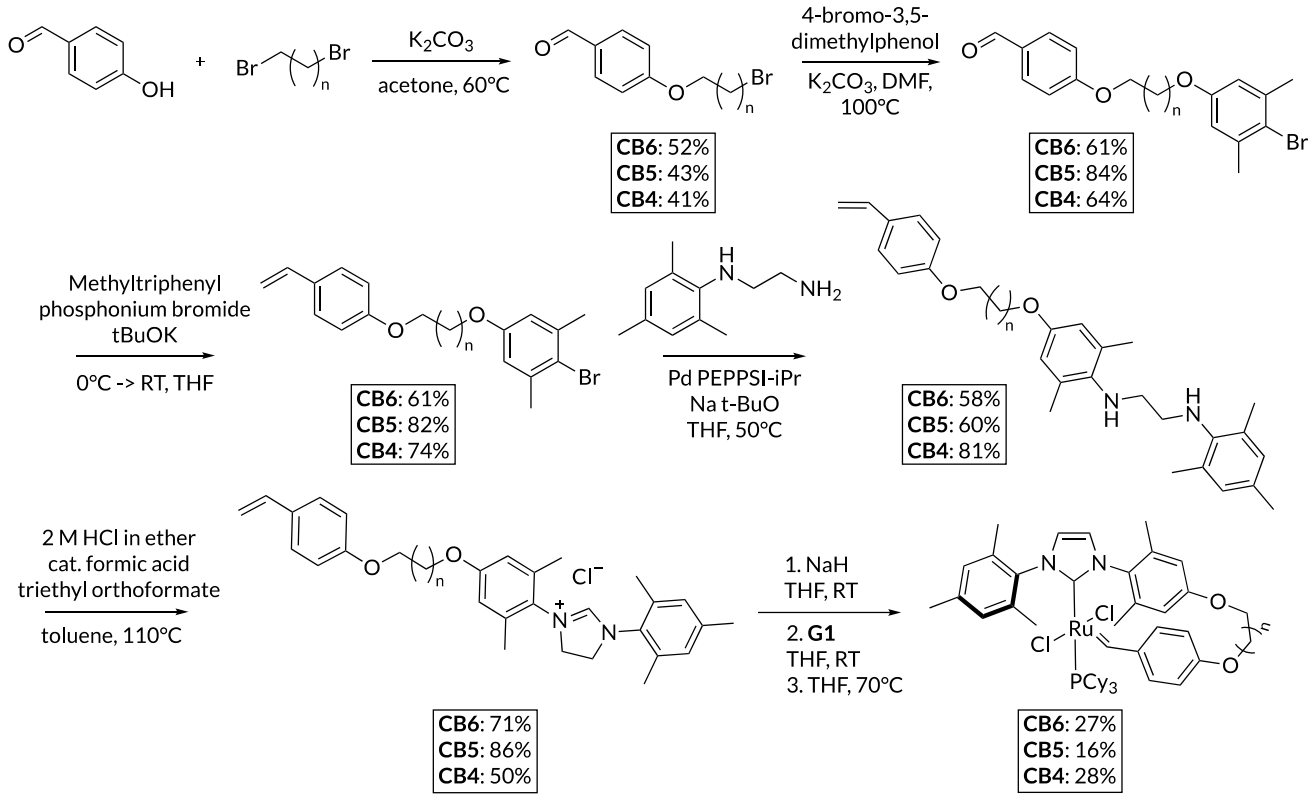

Scheme 4.1. Synthesis of **CB4**, **CB5** and **CB6**

4.3 Characterization of CBX catalysts

The formation of **CBX** was confirmed by the presence of a sole benzylidene proton by ^{1}H NMR (Figure 4.4) and ^{13}C NMR. HRMS spectra also confirmed the presence of each catalyst. The structures of our catalysts were further elucidated by solid state X-ray analysis of **CBX** crystals, revealing several differences between Grubbs' **G2** ROMP catalyst crystal structure[22] and **CBX**. For example, the phosphine-Ru-NHC bond angle is offset by ~3.5 degrees in **G2** complexes compared to **CBX**; this small difference could play a role in initiation, as phosphine dissociation is an important step. Interestingly, in **G2** the benzylidene is offset from the Cl spectator ligand by about 11°, where in **CB4** and **CB6**[20] it is close to planar (-1.67° and 0.04° respectively. We also observed several structural differences among the different tether lengths, specifically in the dihedral angles of the NHC relative to the catalytic active sit. In **G2** and **CB6**, the N1-C1 bond of the NHC is almost planar to the carbene, where in **CB4** the N1-C1 bond is offset by about 18°. We speculate that this geometric discrepancy could be due to lack of conformational flexibility in shorter tethers, which would lead to differences in reactivity. Therefore, molecular weight evolution profiles will likely differ between catalysts with differently sized tethers. Future attempts will be made to obtain a crystal structure of **CB5**.

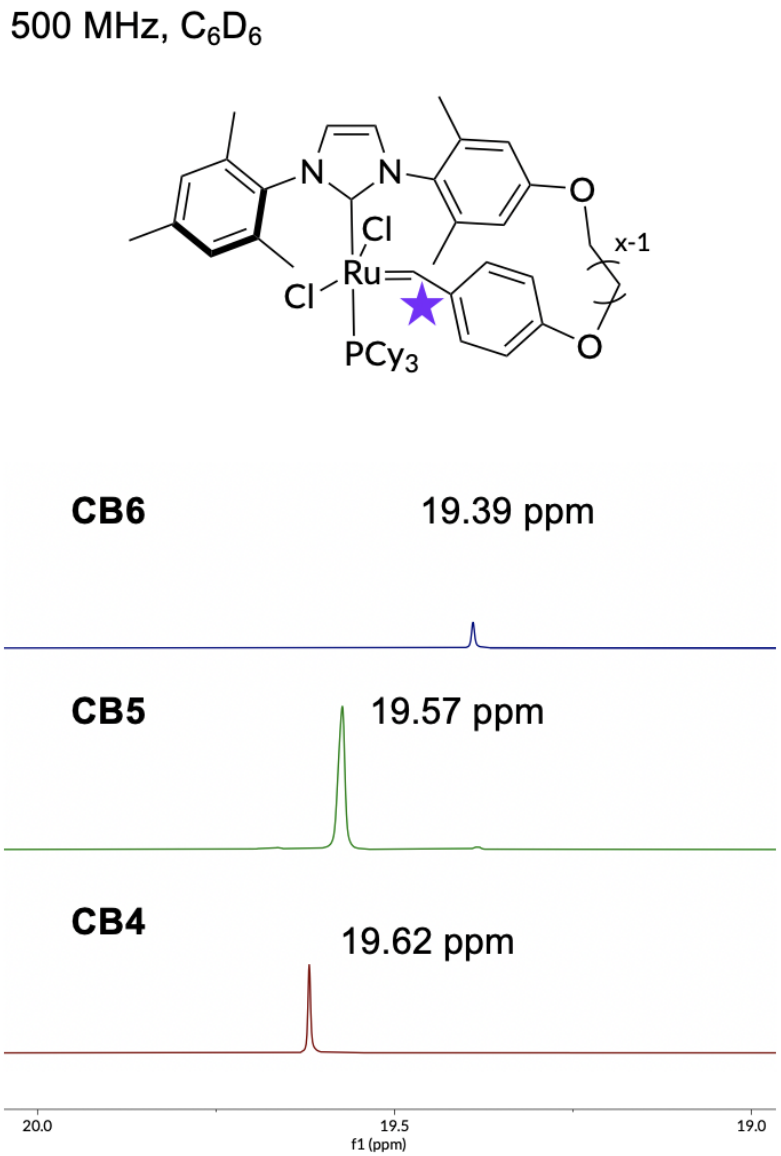

Figure 4.4. Chemical shifts of the benzylidene resonance by ^{1}H NMR are slightly varied between **CB6**, **CB5**, and **CB4**

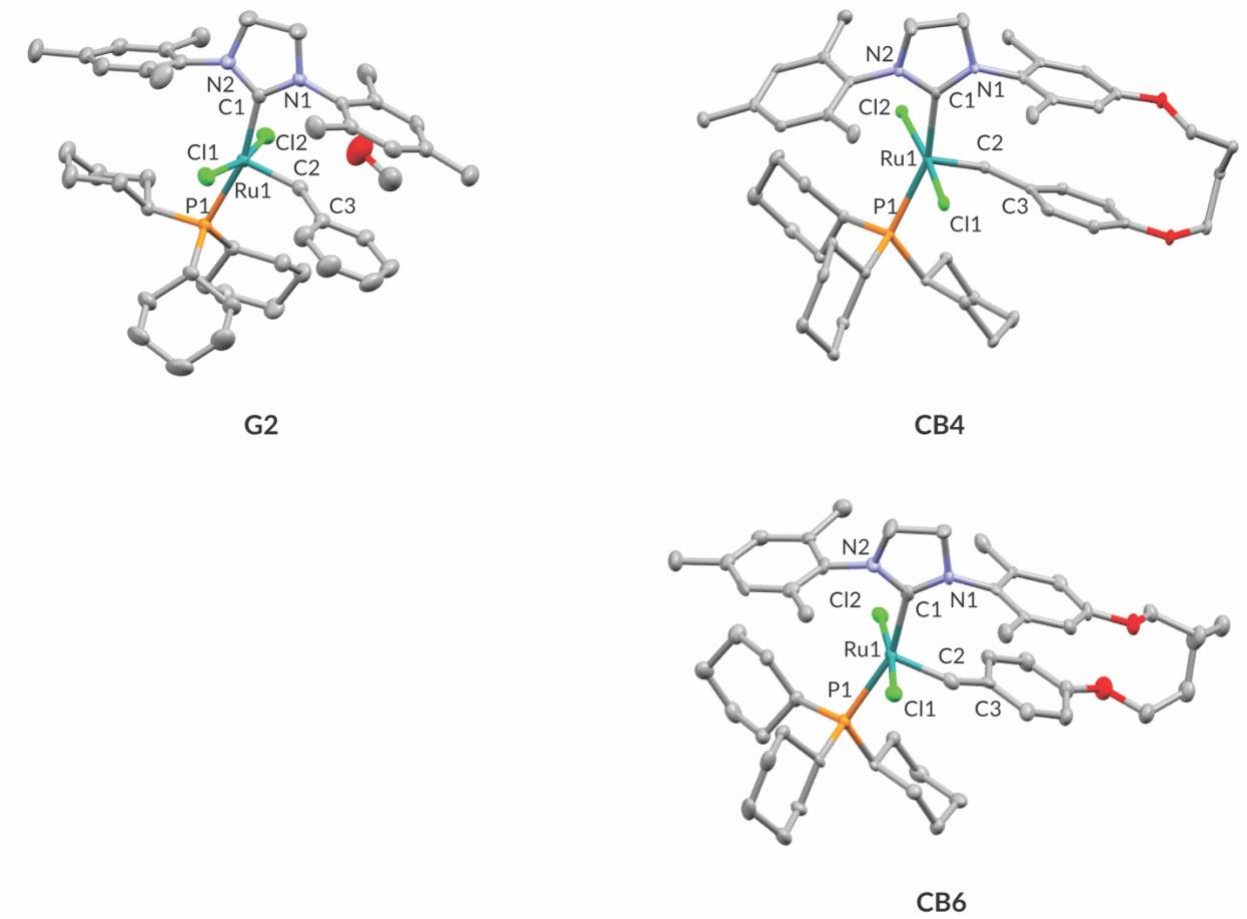

Figure 4.5. CBX and **G2** crystal structures with numbering schemes

Bond angles (deg)	CB4	CB6	G2
C1-Ru1-P1	159.36	159.86	164.31
N1-C1-Ru1	132.02	130.95	129.10
N2-C1-Ru1	121.21	121.11	124.21
N1-C1-N2	106.73	107.16	106.69
Ru1-C2-C3	139.96	139.64	137.04
Cl1-Ru1-C2	100.13	101.29	87.78
Cl2-Ru1-C2	87.56	85.30	104.53

Table 4.1. Comparison of bond angles between **CB4**, **CB6**, and **G2**

Dihedral angles (deg)	CB4	CB6	G2
N2-C1-Ru1-P1	166.90	162.20	172.75
N1-C1-Ru-C2	17.80	5.85	3.44

Table 4.2. Comparison of dihedral angles between **CB4**, **CB6**, and **G2**

4.4 Thermal stability and initiation kinetics of CBX

First, we investigated the effect of structural differences in **CBX** on their thermal stability in solution using ^{1}H NMR studies. To accomplish this, we dissolved each **CBX** in 0.5 mL C_6D_6, heated to 55 °C, and measured the integration of the benzylidene peak over time against an internal standard. Surprisingly, all **CBX** catalysts were remarkably stable in solution at the reaction temperature, showing minimal changes in relative integration over 24 hours. These observations indicate that all three catalysts are relatively stable throughout the course of the reaction, despite geometric and reactivity differences.

Catalyst	Int. benzylidene (initial)	Int. benzylidene (24h)
CB4	1.00	0.89
CB5	1.00	0.83
CB6	1.00	0.87

Table 4.3. CBX thermal stability studies in C_6D_6; benzylidene peaks are integrated against naphthalene as an internal standard.

4.5 Polymerization control and molecular weight evolution

To determine the molecular weight control of **CBX** polymerizations, REMP reactions were set up with each catalyst targeting DP = 100, 200, and 300 based on the feed ratio of [monomer]:[catalyst]. Acetoxy norbornene was chosen as a monomer for these reactions due to ease of synthesis and good solubility of polymeric products in chloroform for characterization (Scheme 4.2).

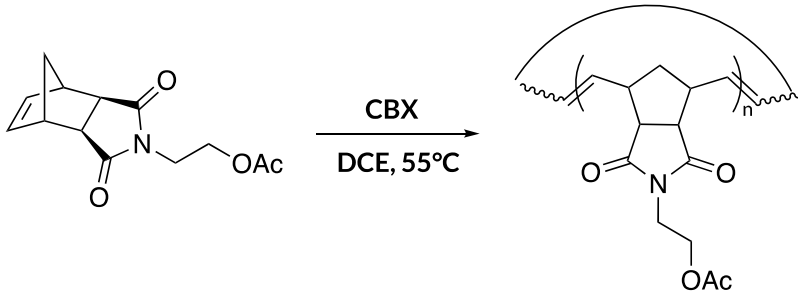

Scheme 4.2. CBX catalyzed polymerization of AcNB

In these experiments, monomer concentration was kept constant at 0.05 M and catalyst concentrations were varied to access target feed ratios. This way, any differences between the polymerizations can be directly attributed to catalyst concentration. While all catalysts gave higher molecular weights than would be expected from a chain-growth model, **CB6** consistently showed the lowest molecular weights of the three catalysts (Table 4.4). **CB4** showed the produced the largest polymers at each given catalyst concentration, with resulting polymers 10 times bigger than would be expected from a chain-growth model. These results suggest that catalysts with different tether lengths have different dependence on **CBX** concentration for final molecular weight, showing that initiation and/or catalyst release rates vary among the catalysts. Propagation rate should not be affected by tether length, because once a growing macrocycle is formed, differences in tether size will be negligible.

Catalyst	[catalyst]:[monomer]	Experimental M_n (Kda)	Đ
CB4	1:100	229	1.4
CB4	1:200	412	1.6
CB4	1:300	486	1.5
CB5	1:100	77.5	1.8
CB5	1:200	259	1.5
CB5	1:300	460	1.5
CB6	1:100	51.6	1.8
CB6	1:200	210	1.5
CB6	1:300	351	1.4

Table 4.4. Polymerization control data as measured by GPC-MALS-IV-RI

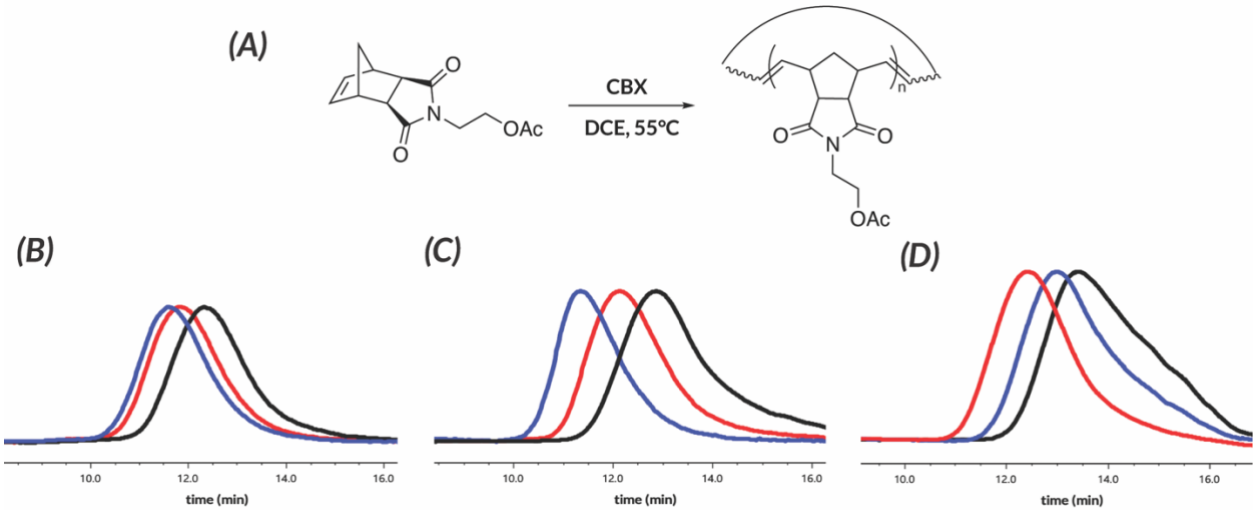

Figure 4.6. A) Representative scheme for **CBX** initiated REMP of acetoxy norbornene; B) GPC traces for **CB4** catalyzed REMP; C) GPC traces for **CB5** catalyzed REMP; D) GPC traces for **CB6** catalyzed REMP

To further understand the differences in polymerization control, we conducted time studies for REMP of acetoxy norbornene to determine the molecular weight evolution profiles of these catalysts. Across all catalysts, a sharp increase in molecular weight was observed followed by a gradual decrease in molecular weight over 6-10 hours; maximum molecular weight occurs when all monomer is consumed. The growth stage of the polymerization is governed by initiation and rapid monomer propagation driven by monomer ring strain, where the molecular weight decrease stage of the polymerization is governed by chain transfer events. Propagation is faster than chain transfer in all cases, as evidenced by rapid monomer consumption and chain growth, then slower molecular weight decrease. During the chain transfer events, molecular weight decreases showing that backbiting is dominant over chain fusion. Because the shape of the evolution profile is similar among all three catalysts, we surmise that in all catalysts, propagation rate is faster than both initiation and chain transfer.

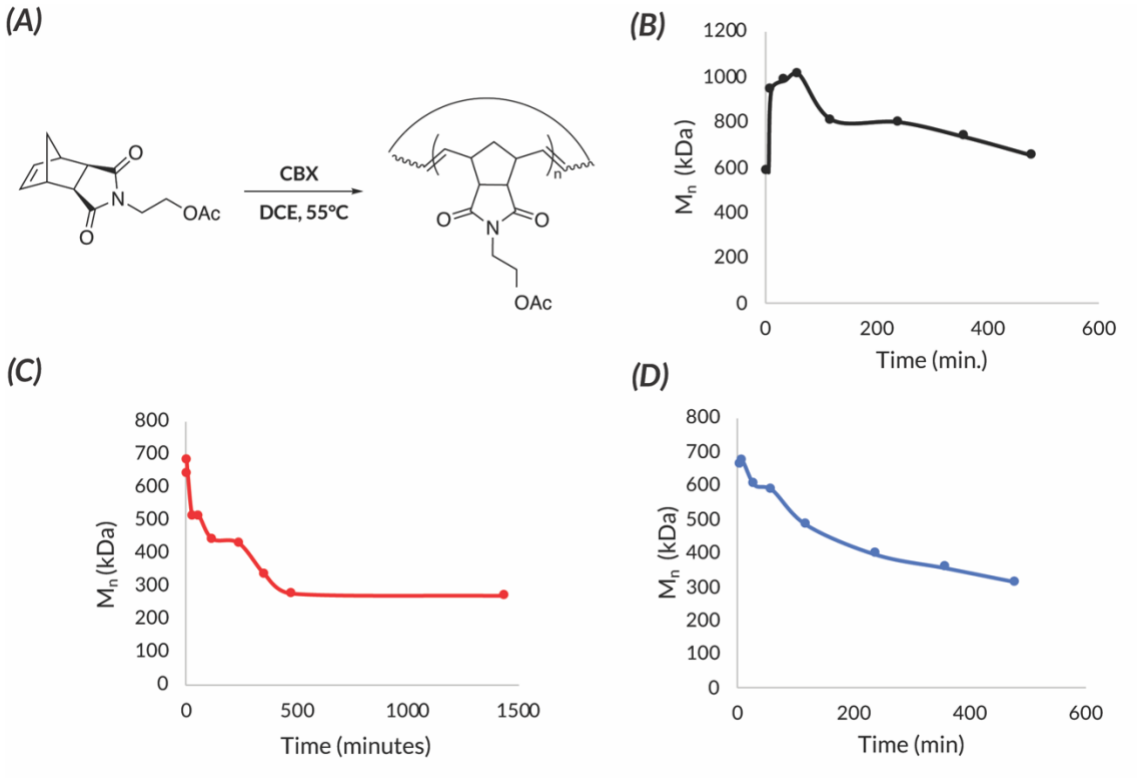

Figure 4.7. A) Representative REMP scheme of acetoxy norbornene using **CBX**. All polymerizations are run at 0.05 M monomer concentration with a catalyst to monomer feed ratio of 1:200; B) Molecular weight evolution profile of acetoxy norbornene REMP using **CB4**; C) Molecular weight evolution profile of acetoxy norbornene REMP using **CB5**; D) Molecular weight evolution profile of acetoxy norbornene REMP using **CB6**

CB4 had the highest peak molecular weight, indicating that it had the slowest initiation rate among the three catalysts. **CB5** and **CB6** showed similar initiation rates with number average molecular weights at 669 kDa and 672 kDa respectively at peak molecular weight. Interestingly, peak molecular weight was reached much later in **CB4** (1 hour) than in **CB5** (10 minutes) or **CB6** (2 minutes). This discrepancy could be due to sluggish initiation or a higher rate of chain fusion compared to catalyst release compared to the other two catalysts. Based on

this data, longer tethers with more conformational freedom result in increased molecular weight control, making it easier to access lower molecular weight cyclic polymers.

4.6 Summary

In summary, we have synthesized a series of **CBX** catalysts to investigate structure-function relationship in REMP. We found that catalysts with longer tethers have faster initiation rates and more molecular weight control than catalysts with shorter tethers. Crystal structures provide a possible reason for this discrepancy; in **G2** and **CB6**, the NHC and carbene are almost copolanar coplanar. In **CB4**, the NHC is twisted significantly out of plane with the carbene compared to its longer-tethered counterparts. Lack of conformational freedom in catalysts with shorter tethers likely distort the geometry of these complexes, forcing it into a sub-optimal geometry for phosphine dissociation and/or the first metathesis event. All three catalysts are similar in that they experience significant chain transfer events, leading to molecular weight evolution over several hours. All three catalysts favored a non-incorporated catalytic resting state as evidenced by ^{1}H NMR experiments and quenching experiments with ethyl vinyl ether. Future efforts will go into further structural optimization of **CBX** complexes. Further exploration of these structures include changing NHC electronics, making complexes with longer tethers (>6 carbons), and altering benzylidene electronics using electron withdrawing or electron donating groups.

4.7 Experimental

4.7.1 General considerations

All reagents were purchased from commercial suppliers and used as received unless otherwise noted. Glassware was flame dried or dried in an oven overnight at 120 ℃ before use. Degassed and anhydrous tetrahydrofuran (THF) and toluene were obtained from a JC Meyer solvent purification system. 1,2 dichloroethane (DCE) was dried over 3Å molecular sieves for at least 3 days and distilled before use. All moisture and air-sensitive reactions were performed under inert atmosphere (nitrogen) using standard Schlenk technique. SiliaFlash F60 (40-63 μm, 230-400 mesh) silica gel was used for column chromatography. Automated flash chromatography was performed using a Yamazen Smart Flash AKROS system. Preparative gel permeation chromatography (prep-GPC) was performed using a Japan Analytical Industries LaboACE recycling preparative HPLC system equipped with JAIGEL-2.5HR and JAIGEL-3HR columns in series using chloroform (stabilized with 0.5% - 1.0% ethanol) as the mobile phase. ^{31}P NMR spectra were externally referenced to 85% H3PO4 (0.00 ppm).

NMR spectra were analyzed on MestreNova software. Chemical shifts are represented in parts per million (ppm); splitting patterns are assigned as s (singlet), d (doublet), t (triplet), q (quartet), p (quintet), m (multiplet), and br (broad); coupling constants, *J*, are reported in hertz (Hz).
High-resolution mass spectroscopy (HRMS) data were collected on an LTQ Orbitrap (ThermoScientific) operating in positive mode electrospray ionization. Instrument resolution was set to 60000 and elemental composition was confirmed by electrospray ionization HRMS. X-ray crystallography data was collected at –173 ℃ (100 K) on a Nonius Kappa CCD FR590 single

crystal X-ray diffractometer, Mo-radiation. The data was integrated and scaled using SAINT, SADABS within the APEX2 software package by Bruker.

4.7.2 **CBX** synthesis

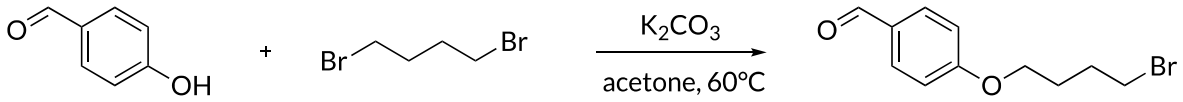

Synthesis of 4-((6-bromobutyl)oxy)benzaldehyde

To a round bottom flask equipped with a stir bar and condenser was added 4-hydroxylaldehyde (10.0 g, 81.9 mmol), 1,6-dibromobutane (19.6 mL, 164 mmol), potassium carbonate (22.6 g, 164 mmol), and 200 mL acetone. The reaction stirred for 2 days at 60 °C open to air. The reaction was then cooled to room temperature, filtered through celite, and the filtrate was concentrated under vacuum. The crude product was redissolved in 250 mL EtOAc and transferred to a separatory funnel. The ethyl acetate was washed with water (3 x 100 mL), brine (2 x 100 mL). The organic layer was then dried over sodium sulfate, filtered, and concentrated under vacuum. The crude yellow oil was eluted with a EtOAc/hexane (10-20%) solvent mixture on a silica column to yield 4-((6-bromobutyl)oxy)benzaldehyde as a white solid (8.99 g, 40.9%). ^{1}H NMR (300 MHz, CDCl3) δ 9.88 (s, 1H), 7.83 (d, J = 8.8 Hz, 2H), 6.99 (d, J = 8.7 Hz, 2H), 4.08 (td, J = 5.5, 3.3 Hz, 2H), 3.52 – 3.46 (td, 2H), 2.09 – 1.97 (overlap, 6H).

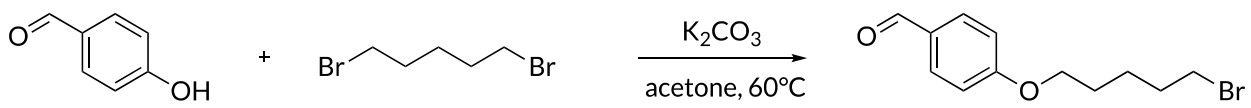

Synthesis of 4-((6-bromopentyl)oxy)benzaldehyde

To a round bottom flask equipped with a stir bar and condenser was added 4-hydroxylaldehyde (5.00 g, 40.9 mmol), 1,6-dibromopentane (10.5 mL, 81.9 mmol), potassium carbonate (11.3 g, 81.9 mmol), and 100 mL acetone. The reaction stirred for 2 days at 60 °C open to air. The reaction was then cooled to room temperature, filtered through celite, and the filtrate was concentrated under vacuum. The crude product was redissolved in 250 mL EtOAc and transferred to a separatory funnel. The ethyl acetate was washed with water (3 x 100 mL), brine (2 x 100 mL). The organic layer was then dried over sodium sulfate, filtered, and concentrated under vacuum. The crude yellow oil was eluted with a EtOAc/hexane (10-20%) solvent mixture on a silica column to yield 4-((6-bromopentyl)oxy)benzaldehyde as a white solid (4.84 g, 43.6%). ^{1}H NMR (300 MHz, CDCl3) δ 9.88 (s, 1H), 7.83 (d, J = 8.7 Hz, 2H), 6.99 (d, J = 9.0 Hz, 2H), 4.08 (dt, J = 6.8, 3.2 Hz, 4H), 3.45 (td, J = 6.4, 2.9 Hz, 2H), 2.08 – 1.77 (overlap, 4H), 1.65 (overlap, 3H).

Synthesis of 4-((6-bromohexyl)oxy)benzaldehyde

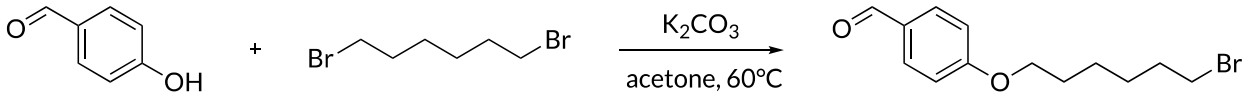

To a round bottom flask equipped with a stir bar and condenser was added 4-hydroxylaldehyde (10.0 g, 81.9 mmol), 1,6-dibromohexane (22.2 mL, 164 mmol), potassium carbonate (22.6 g, 164 mmol), and 200 mL acetone. The reaction stirred for 2 days at 60 °C open to air. The reaction was then cooled to room temperature, filtered through celite, and the filtrate was concentrated under vacuum. The crude product was redissolved in 250 mL EtOAc and transferred to a separatory funnel. The ethyl acetate was washed with water (3 x 100 mL), brine (2 x 100 mL). The organic

layer was then dried over sodium sulfate, filtered, and concentrated under vacuum. The crude yellow oil was eluted with a EtOAc/hexane (10-20%) solvent mixture on a silica column to yield 4-((6-bromohexyl)oxy)benzaldehyde as a white solid (10.3 g, 48.7%). ^{1}H NMR (500 MHz, CDCl3): δ(ppm) 9.89 (s, 1H), 7.83 (d, J = 8.90 Hz, 2H), 6.99 (d, J = 8.77 Hz, 2H), 4.07 (td, J = 6.4, 4.4 Hz, 2H), 3.42 (td, J = 6.7, 4.7 Hz, 2H), 1.98 – 1.77 (overlap, 4H), 1.63 – 1.42 (overlap, 4H).

General procedures for CBX synthesis

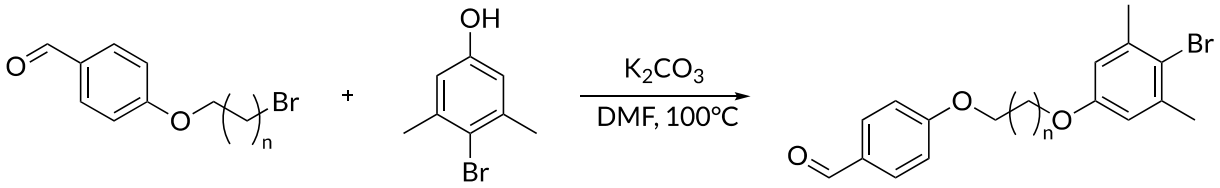

To a round bottom flask equipped with a stir bar and condenser was added **1** (1.00 eq.), 4-bromo-3,5- dimethylphenol (1.20 eq.), potassium carbonate (1.70 eq.) and DMF were added (0.108 M reaction concentration based on **1**). The reaction mixture was stirred at 100 °C for 24 h. The reaction was cooled to room temperature, transferred to a separatory funnel then diluted with 100 mL water and 100 mL EtOAc. The organic layer was collected and the water layer was extracted with ethyl acetate (3 x 50 mL). The organic layers were combined and washed with 5% lithium chloride solution (5 x 100 mL), water (2 x 50 mL), and brine (2 x 50 mL). The organic layer was dried over sodium sulfate, filtered, and concentrated under vacuum. The crude oil was crystallized by adding room temperature diethyl ether (40 mL) and storing at 0 °C for 4 hours. The mixture was then filtered to yield **2** as pale brown crystals.

n = 3

Yield: 8.74 g, 63.9%

^{1}H NMR (500 MHz, CDCl3) δ 9.89 (s, 1H), 7.86 – 7.80 (d, J = 8.7 Hz, 2H), 7.02 – 6.96 (d, J = 8.7 Hz, 2H), 6.64 (s, 2H), 4.12 (t, J = 5.9 Hz, 2H), 4.00 (t, J = 5.8 Hz, 2H), 2.37 (s, 6H), 2.06 – 1.92 (overlap, 4H).

n = 4

Yield: 7.55 g, 84.1%

^{1}H NMR (500 MHz, CDCl3) δ 9.88 (s, 1H), 7.86 – 7.79 (d, J = 8.7 Hz, 2H), 7.02 – 6.95 (d, J = 8.8 Hz) 2H), 6.64 (s, 2H), 4.07 (t, J = 6.4 Hz, 2H), 3.95 (t, J = 6.3 Hz, 2H), 2.37 (s, 6H), 1.94 – 1.80 (overlap, 4H), 1.71 – 1.61 (overlap, 2H).

n = 5

Yield: 3.79 g, 74%

^{1}H NMR (500 MHz, CDCl3) δ 9.87 (s, 1H), 7.88 – 7.78 (d, J = 8.8 Hz, 2H), 7.03 – 6.94 (d, J = 8.8 Hz, 2H), 6.62 (s, 2H), 4.03 (t, J = 6.5 Hz, 2H), 3.41 (t, J = 6.4 Hz, 2H), 2.37 (s, 6H), 1.83 (overlap, 4H), 1.55 (overlap, 4H).

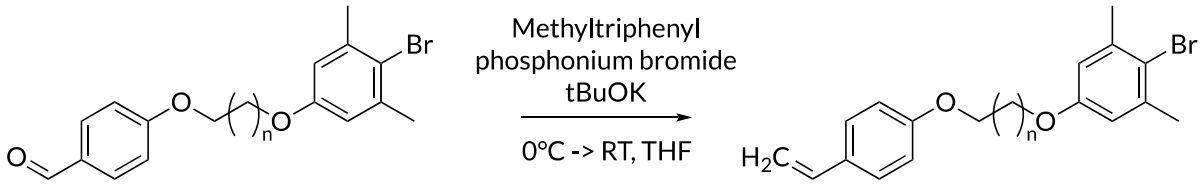

To a flame-dried Schlenk flask equipped with a stir bar was added methyltriphenylphosphonium bromide (1.20 eq.), potassium tert-butoxide (2.00 eq.). The flask was evacuated and refilled with nitrogen three times. Then, dry THF (0.224 M based on methyltriphenylphosphonium bromide) was added and the mixture stirred at 0 °C for 10 minutes. In a separate flame dried round bottom

flask, **2** (1.00 eq.) was dissolved in dry THF (0.465 M based on **2**) under nitrogen and transferred (via cannula) to the Schlenk flask. The mixture was stirred at 0 °C for 15 min then stirred at room temperature for 16 hours. Once the reaction was complete, the solution was quenched with methanol (40 mL). Solvent was evaporated under vacuum. The residue was dissolved in DCM (100 mL) and washed with water (3 x 30 mL), and brine (3 x 30 mL). The organic phase was then dried over sodium sulfate and concentrated under vacuum. The crude product was then loaded onto a silica column and the product was eluted with DCM/hexane (10-30%) to yield **3** as a white solid.

n = 3

Yield: 1.49 g, 74.9%

^{1}H NMR (300 MHz, CDCl3) δ 7.39 – 7.21 (d, J = 8.7, 2H), 6.90 – 6.79 (d, 8.7, 1H), 6.63 (overlap, 3H), 5.61 (dd, J = 17.5 Hz, 1H), 5.18 – 5.05 (dd, J = 11 Hz, 1H), 4.01 (overlap, 4H), 2.37 (s, 6H), 2.00 – 1.90 (overlap, 4H), 1.54 (overlap, 2H).

n = 4

Yield: 1.57 g, 81.8%

^{1}H NMR (500 MHz, CDCl3) δ 7.36 – 7.30 (d, J = 8.7 Hz, 2H), 6.88 – 6.81 (d, J = 8.7 Hz, 1H), 6.70 – 6.61 (overlap, 3H), 5.60 (dd, J = 17.6 Hz, 1H), 5.12 (dd, J = 10.9 Hz, 1H), 4.02 – 3.91 (overlap, 2H), 2.37 (s, 6H), 1.90 – 1.79 (overlap, 4H), 1.69 – 1.59 (overlap, 2H).

n = 5

Yield: 1.79 g, 51.0%

^{1}H NMR (300 MHz, CDCl3) δ 7.32 (d, J = 8.8 Hz, 2H), 6.86 (d, J = 8.8 Hz, 2H), 6.63 (overlap, 3H), 5.59 (dd, J = 17.7 Hz, 1H), 5.11 (dd, J = 11.0 Hz, 1H), 4.01 (overlap, 4H), 2.36 (s, 6H), 1.91 – 1.49 (overlap, 8H).

Synthesis of N-mesitylethane-1,2-diamine-HBr salt

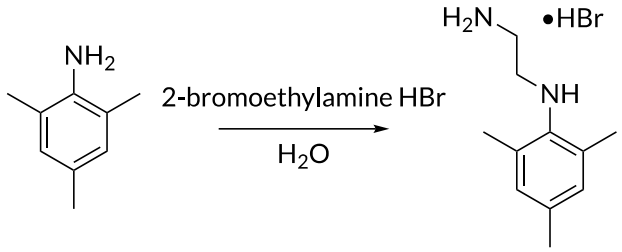

To a round bottom flask equipped with a stir bar and condenser was added 2,4,6-trimethyl aniline (31.2 mL, 222 mmol) and 2-bromoethylamine hydrobromide (22.7 g, 111 mmol). The solids were dissolved in 30.0 mL water. The mixture was stirred at 90 °C for 12 hours. The reaction was cooled to room temperature, transferred to a separatory funnel, and washed with EtOAc (5 x 30 mL). The aqueous layer was collected and concentrated under vacuum. The solid residue was crystallized from 300 mL hot (70 °C) EtOAc/methanol (2:1). The crystals were filtered and dried under vacuum to yield N-mesitylethane-1,2-diamine-HBr salt as a white solid (22.0 g, 76.4%).

Synthesis of N-mesitylethane-1,2-diamine

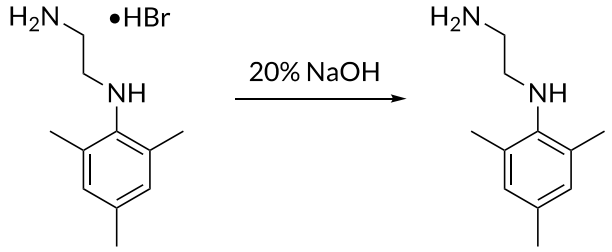

To a round bottom flask equipped with a stir bar was added the N-mesitylethane-1,2-diamine-HBr salt (1.5 g, 5.79 mmol) and 20% aq. NaOH (45 mL). The solution was stirred for 30 min at room temperature. The solution was transferred to a separatory funnel and extracted with DCM (3 x 40 mL). The combined organic layers were washed with water (15 mL x 3) and brine (15 mL x 2). The organic phase was dried over sodium sulfate and concentrated under vacuum to yield N-mesitylethane-1,2-diamine as a viscous yellow oil (800 mg, 77.5%). ^{1}H NMR (300 MHz, CDCl3) δ 6.81 (2, 2H), 3.01 – 2.84 (overlap, 4H), 2.25-2.22 (overlap, 9H).

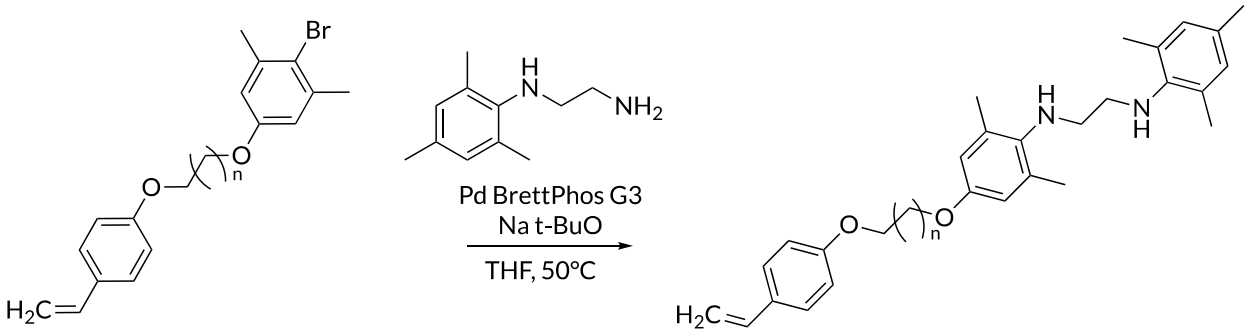

To a dry glass vial equipped with a stir bar was added **3** (1.00 eq.), sodium tert-butoxide (1.50 eq.), and Pd-PEPPSI-IPr (0.05 eq.). To an additional dry glass vial, Mes-diamine (1.40 eq.) was added. Both vials were added to a nitrogen-filled glovebox. To the vial containing Mes-diamine, THF was added (0.443 M based on **3**). The Mes-diamine solution was transferred to the other vial and was stirred at room temperature for 1 min. After 1 min, the vial was added to a preheated aluminum block at 60 °C and was stirred for an additional 2 min. The solution was then diluted with THF (diluted to 0.224 M based on **3**). The reaction mixture was stirred overnight at 60 °C. The reaction was cooled to room temperature, filtered through neutral

alumina, and concentrated under vacuum. The crude mixture was purified on a silica column using EtOAc/hexane (0-20%) solvent mixture, eluting **4** as a yellow solid.

n = 3

Yield: 3.00 g, 74.5%

^{1}H NMR (500 MHz, CDCl3) δ 7.37 – 7.30 (m, 2H), 6.89 – 6.81 (overlap, 4H), 6.58 (s, 1H), 5.60 (d, J = 17.6, 1H), 5.12 (d, J = 10.9 Hz, 1H), 4.06 – 3.97 (t, J = 6.4 Hz, 2H), 4.00 – 3.94 (t, J = 6.4 Hz, 2H), 3.15-3.08 (overlap, 4H), 2.29 (s, 12H), 1.95 (overlap, 4H).

n = 4

Yield: 1.12 g, 89%

^{1}H NMR (500 MHz, CDCl3) δ 7.36 – 7.30 (m, 1H), 6.88 – 6.81 (overlap, 4H), 6.65 (s, 1H), 6.58 (s, 1H), 5.60 (d, J = 17.6 Hz, 1H), 5.11 (d, J = 10.9 Hz, 1H), 4.01 – 3.89 (t, J = 6.4 Hz, 2H), 3.19 – 3.00 (overlap, 4H), 2.28 (overlap, 12H), 1.83 (overlap, 4H), 1.68 – 1.58 (overlap, 2H).

n = 5

Yield: 0.830 g, 57.8%

^{1}H NMR (500 MHz, CDCl3) δ 7.34 (d, J = 8.8 Hz, 2H), 6.88 – 6.81 (overlap, 4H), 6.66 (dd, J = 17.6, 10.9 Hz, 1H), 6.58 (s, 2H), 5.60 (d, J = 17.6 Hz, 1H), 5.11 (d, J = 10.9 Hz, 1H), 3.97 (t, J = 6.5 Hz, 2H), 3.91 (t, J = 6.4 Hz, 2H), 3.15-3.08 (overlap, 4H), 2.30 (s, 12H), 2.24 (s, 3H), 1.80 (overlap, 4H), 1.53 (overlap, 4H).

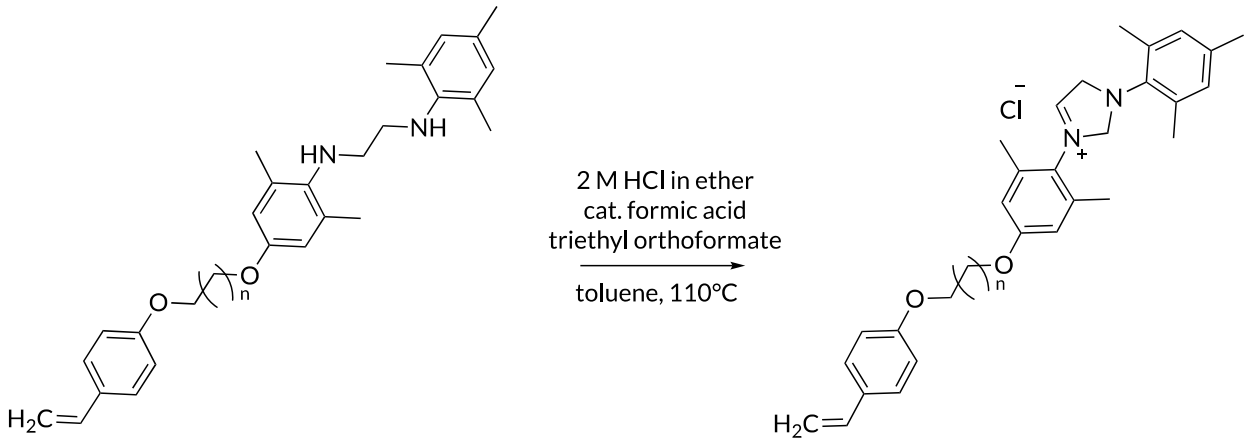

To a dry 25 mL Schlenk flask equipped with a stir bar was added **4** and ammonium chloride. The Schlenk flask was evacuated and refilled with nitrogen three times. The solids were dissolved in dry toluene (xx mL) and stirred for 10 minutes. Freshly distilled triethylorthoformate (xx mL, XX mmol) followed by two drops of formic acid were added and the reaction stirred for 3.5 hours at 110 °C. The reaction mixture was then cooled to room temperature and evaporated to dryness. The crude mixture was purified on a silica column using methanol/DCM (0-10%) solvent mixture, eluting **5** as a white solid.

n = 3

Yield: 293 mg, 82%

^{1}H NMR (500 MHz, CDCl3) δ 9.13 (s, 1H), 7.34 (m, 2H), 6.97 (s, 2H), 6.89 – 6.83 (m, 2H), 6.66 (overlap, 3H), 5.60 (d, J = 17.5 Hz, 1H), 5.12 (d, J = 10.9 Hz, 1H), 4.02 (overlap, 4H), 2.40 (s, 12H), 1.99 – 1.91 (overlap, 4H).

n = 4

Yield: 383 mg, 86%

^{1}H NMR (500 MHz, CDCl3) δ 9.25 (s, 1H), 7.37 – 7.30 (m, 2H), 6.98 (s, 2H), 6.88 – 6.82 (m, 2H), 6.65 (overlap, 3H), 5.60 (d, J = 17.6 Hz, 1H), 5.11 (d, J = 10.8 Hz, 1H), 3.96 (overlap, 4H), 1.81 (overlap, 4H), 1.56 – 1.51 (overlap, 2H).

n = 5

Yield: 510 mg, 61%

^{1}H NMR (500 MHz, CDCl3) δ 9.14 (s, 1H), 7.36 – 7.30 (d, J = 8.7 Hz, 2H), 6.98 (s, 2H), 6.85 (d, J = 9.1 Hz, 2H), 6.65 (overlap, 3H), 5.60 (d, J = 17.6 Hz, 1H), 5.11 (d, J = 11.0, 1H), 4.52 (s, 4H), 3.96 (overlap, 4H), 1.81 (overlap, 4H), 1.54 (overlap, 4H).

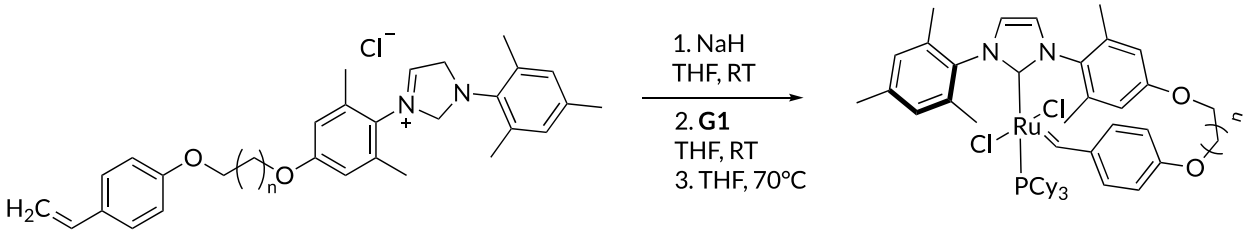

To a dry 20 mL vial was added **5** and sodium hydride (10.0 eq.) in a nitrogen filled glovebox. The solids were dissolved in dry THF (0.026 M based on **5**) and stirred at room temperature overnight. The next day, Grubbs 1st generation catalyst was added to the reaction mixture and stirred at room temperature for an additional 90 minutes. Then, the reaction mixture was diluted with dry THF (diluted to 0.0018 M based on **5**) and stirred for 4 hours at 70 °C. The reaction mixture cooled to room temperature, filtered through celite, and evaporated to dryness. The reaction mixture was purified using pentane washes. The crude reaction mixture was suspended in pentanes (2 mL) and sonicated for 5 minutes. The mixture was then centrifuged for 10 minutes at 3000 rpm and decanted. This wash procedure was repeated three times (or until the

supernatant is colorless). The mixture was further purified using preparatory GPC to remove *bis*-**CB6**. The mixture was dissolved in HPLC grade chloroform (stabilized with 0.5-1% EtOH), filtered through an Aura MT 0.45 μm syringe filter, and purified via recycling prep-GPC (RI detection only). Solvent was removed under vacuum then further dried by sonication in diethyl ether followed by pentane to afford **CBX** as a light pink solid.

n = 3

Yield: 20.0 mg, 28%

^{1}H NMR (500 MHz, C_6D_6) δ 19.24 (s, 1H), 9.50 (s, 1H), 7.24 (d, J = 8.7 Hz, 1H), 6.97 (s, 1H), 6.69 (overlap, 6H), 5.79 (s, 1H), 3.74 (s, 3H), 3.44 (s, 5H), 2.96 – 2.90 (m, 7H), 2.76 – 2.66 (m, 7H), 2.52 (s, 3H), 2.33 (s, 3H), 1.74-1.12 (overlap, 38H), .

n = 4

Yield: 70.0 mg, 16%

^{1}H NMR (500 MHz, C_6D_6) δ 19.57 (s, 1H), 9.24 (d, J = 8.8 Hz, 1H), 7.37 (d, J = 8.4 Hz, 1H), 6.92 (overlap, 2H), 6.70 (s, 1H), 6.46 (m, 2H), 6.26 (s, 1H), 6.09 (s, 1H), 3.87 – 3.79 (overlap, 2H), 3.46 – 3.27 (overlap, 6H), 2.93 (s, 3H), 2.80 (s, 3H), 2.56 – 2.47 (overlap, 12H), 1.57-0.99 (overlap, 38H).

n = 5

Yield: 75 mg, 38%

^{1}H NMR (500 MHz, C_6D_6) δ 19.39 (s, 1H), 9.39 (s, 1H), 7.32 (s, 1H), 6.96 (overlap, 2H), 6.92 (s, 2H), 6.47 (m, 2H), 5.91 (s, 1H), 3.99 (s, 1H), 3.65 (s, 1H), 3.50 – 3.12 (overlap, 6H), 2.95 (s, 3H), 2.78 (s, 3H), 2.62 (s, 3H), 2.53 (m, 3H), 2.42 (s, 3H), 2.20 (s, 3H), 1.77 (s, 3H), 1.72 – 0.99 (overlap, 38H).

REMP monomer synthesis

Synthesis of N-ethyl hydroxyl-exo-norbornene-2,3-dicarboximide

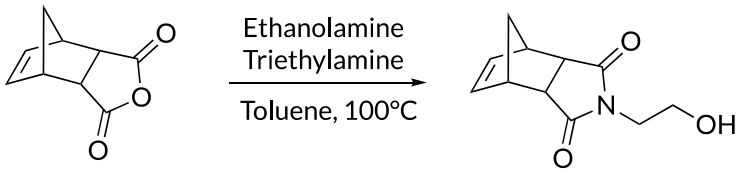

To a round bottom flask equipped with a stir bar was added cis-5-norbornene-exo-2,3-dicarboxylic anhydride (10.0 g, 60.9 mmol), ethanolamine (4.60 mL, 76.1 mmol), triethylamine (1.06 mL, 7.61 mmol), and dry toluene (160 mL). The reaction mixture stirred at reflux under nitrogen for 16 hours. The reaction mixture was cooled to room temperature, diluted with 100 mL ethyl acetate and transferred to a separatory funnel. The organic layer was washed with 10% HCl (2 x 40 mL), water (3 x 40 mL) and brine (2 x 40 mL). The organic layer was collected, dried over sodium sulfate, and evaporated to dryness yielding a white solid (4.65 g, 37%). ^{1}H NMR (500 MHz, CDCl3) δ 6.30 (s, 2H), 3.79 (t, J = 5.2 Hz, 2H), 3.72 (s, 2H), 3.30 (s, 2H), 2.73 (s, 2H), 2.07 (br, 1H), 1.55 (d, J = 9.9 Hz, 1H), 1.36 (d, J = 9.9 Hz, 1H).

Synthesis of N-ethyl acetoxy-exo-norbornene-2,3-dicarboximide (AcNb)

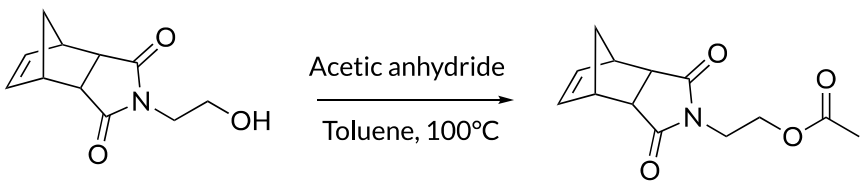

N-ethanol-exonorbornene-2,3-dicarboximide (1.6 g, 7.72 mmol), acetic anhydride (2.19 mL, 23.2 mmol), and 10 mL toluene were added to a flame dried flask equipped with a condenser. The reaction mixture stirred at reflux for 16 hours. The reaction mixture was then cooled to 0 °C then quenched by adding 40% methylamine in water (3 mL, 63.3 mmol) dropwise. The reaction mixture was transferred to a separatory funnel and diluted with 20 mL water. The mixture was extracted with ethyl acetate (3 x 20 mL). The organic layers were combined then washed with sodium carbonate (2 x 20 mL), water (3 x 20 mL) and brine (2 x 20 mL). The organic layer was dried over sodium sulfate and evaporated to dryness under vacuum. The crude product was further purified through column chromatography using a 2:1 hexane/EtOAc solvent mixture yielding AcNB as a viscous yellow oil (1.2 g, 78%). ^{1}H NMR (500 MHz, CDCl3) δ 6.29 (s, 1H), 4.23 (t, J = 5.2 Hz, 2H), 3.77 (t, J = 5.2 Hz, 2H), 3.29 (s, 2H), 2.71 (s, 2H), 2.00 (s, 3H), 1.53 (d, 9.8 Hz, 1H), 1.33 (d, J = 9.8 Hz, 1H).

4.7.3 General procedures for REMP of **CB4**, **CB5**, and **CB6**

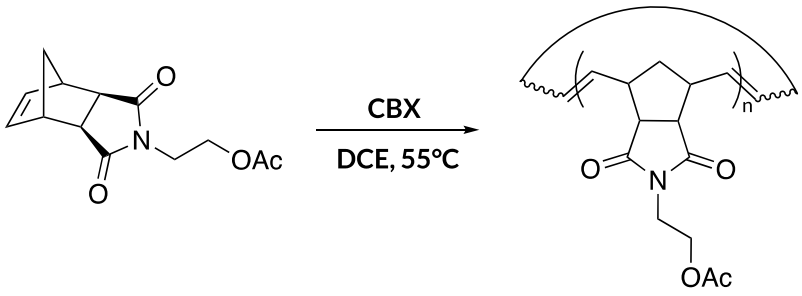

Example for DP = 200 with **CB4**

In a nitrogen filled glovebox, AcNB (100 mg, 402 mmol) was added to a dry 20 mL vial with a stir bar. Monomer was dissolved in dry DCE (9.98 mL) and stirred for 5 minutes at 55 °C. A

stock solution was prepared using 50 mg/mL **CB4** and an aliquot (0.046 mL) of this solution was added to monomer. Reactions stirred at 55 °C in the glovebox for at least 24 hours for molecular weight equilibration. The resulting polymers were cooled to room temperature and filtered through neutral alumina. The resulting polymers were dissolved in chloroform, filtered through a 0.2 μm syringe filter, and analyzed by GPC-MALS-IV.

For all polymerizations, monomer concentration was kept constant at 0.05 M.

For time studies, all reactions were set up according to the above procedure with a target DP of 200 for all three catalysts. Time points were taken by removing a 1 mL aliquot of the reaction mixture, transferring to a new vial, and filtering through neutral alumina. Polymers were characterized by GPC-MALS-IV as described above.

4.7.4 X-ray crystallography data

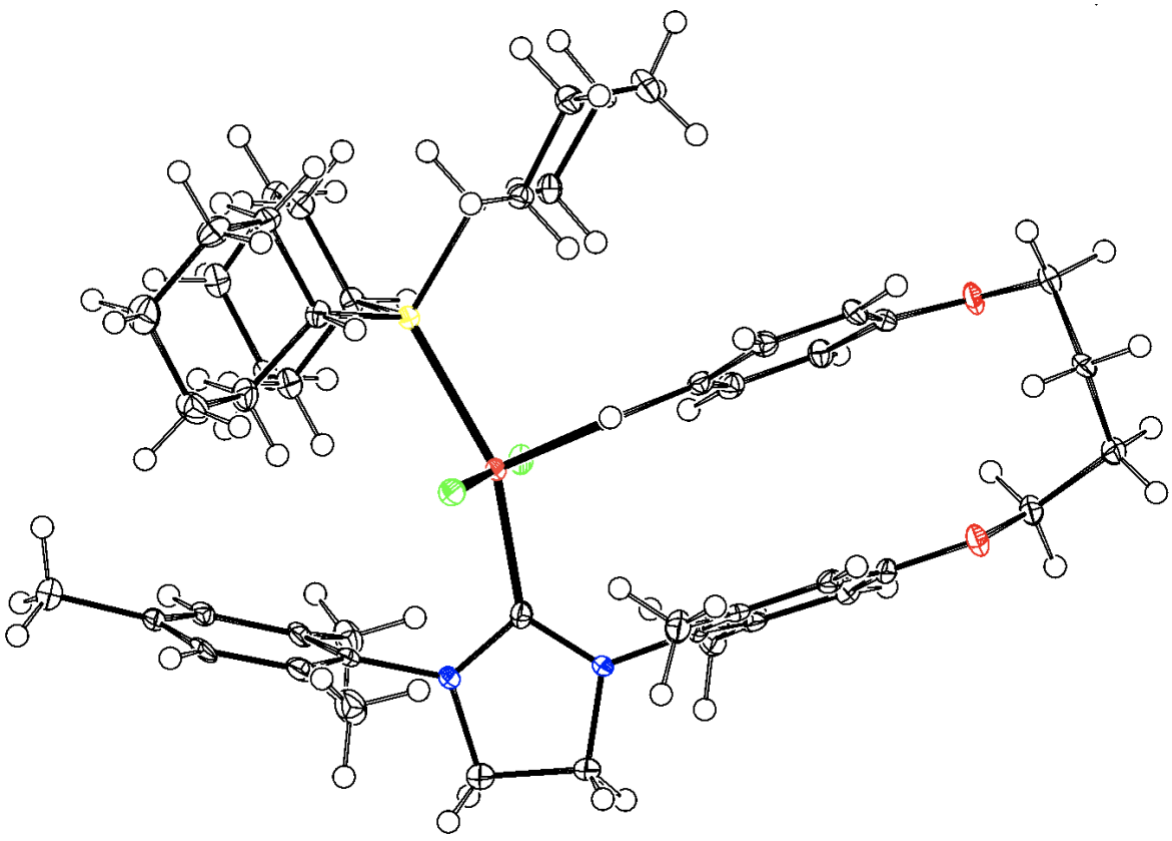

Identification code	shelx	
Empirical formula	C49 H69 Cl2 N2 O2 P Ru	
Formula weight	921.00	
Temperature	100(2) K	
Wavelength	0.71073 Å	
Crystal system	Triclinic	
Space group	P -1	
Unit cell dimensions	a = 9.6650(9) Å	α= 95.202(5)°.
	b = 12.3870(11) Å	β= 91.981(5)°.
	c = 18.7203(19) Å	γ = 93.218(5)°.
Volume	2226.7(4) $Å^3$	
Z	2	
Density (calculated)	1.374 Mg/m^3	
Absorption coefficient	0.549 mm^{-1}	
F(000)	972	
Crystal size	0.070 x 0.050 x 0.030 mm^3	
Theta range for data collection	1.093 to 26.471°.	
Index ranges	-12<=h<=12, -15<=k<=15, -23<=l<=23	
Reflections collected	18186	
Independent reflections	9151 [R(int) = 0.0642]	
Completeness to theta = 25.242°	100.0 %	
Refinement method	Full-matrix least-squares on F^2	
Data / restraints / parameters	9151 / 0 / 519	
Goodness-of-fit on F^2	1.005	
Final R indices [I>2sigma(I)]	R1 = 0.0407, wR2 = 0.0815	
R indices (all data)	R1 = 0.0691, wR2 = 0.0907	
Largest diff. peak and hole	0.473 and -0.684 $e.Å^{-3}$	

4.8 Publication and acknowledgements

This work was conducted in collaboration with Nick Serck, Lucy Miller, and Bob Li. Computational work was done in collaboration with Osvaldo Gutierrez. This chapter was adapted from the publication below publication:

- **Pomfret, M. N**.; Serck, N. P.; Miller, L. P.; Li, B.; Gomez, A. R.; Gutierrez, O.*; Golder, M. R.* *Manuscript in preparation.*

4.9 References

(1) Chen, C.; Weil, T. Cyclic Polymers: Synthesis, Characteristics, and Emerging Applications. *Nanoscale Horizons* **2022**, *7* (10), 1121–1135. https://doi.org/10.1039/d2nh00242f.

(2) Haque, F. M.; Grayson, S. M. The Synthesis, Properties and Potential Applications of Cyclic Polymers. *Nat. Chem.* **2020**, *12*, 433–444. https://doi.org/10.1038/s41557-020-0440-5.

(3) Tu, X. Y.; Liu, M. Z.; Wei, H. Recent Progress on Cyclic Polymers: Synthesis, Bioproperties, and Biomedical Applications. *J. Polym. Sci. Part A Polym. Chem.* **2016**, *54* (11), 1447–1458. https://doi.org/10.1002/pola.28051.

(4) Golba, B.; Benetti, E. M.; De Geest, B. G. Biomaterials Applications of Cyclic Polymers. *Biomaterials* **2021**, *267* (June 2020), 120468. https://doi.org/10.1016/j.biomaterials.2020.120468.

(5) Chen, B.; Jerger, K.; Fréchet, J. M. J.; Szoka, F. C. The Influence of Polymer Topology on Pharmacokinetics: Differences between Cyclic and Linear PEGylated Poly(Acrylic Acid) Comb Polymers. *J. Control. Release* **2009**, *140* (3), 203–209. https://doi.org/10.1016/j.jconrel.2009.05.021.

(6) Ma, W.; Kang, G. Y.; Sun, L.; Meng, C.; Liu, Y.; Zheng, Z.; Jiang, M. C.; Wang, D.; Pun, S. H.; Yu, C. Y.; Wei, H. Multicyclic Topology-Enhanced Anticancer Drug Delivery. *J. Control. Release* **2022**, *345* (February), 278–291. https://doi.org/10.1016/j.jconrel.2022.03.018.

(7) Kaitz, J. A.; Diesendruck, C. E.; Moore, J. S. End Group Characterization of Poly(Phthalaldehyde): Surprising Discovery of a Reversible, Cationic Macrocyclization Mechanism. *J. Am. Chem. Soc.* **2013**, *135* (34), 12755–12761. https://doi.org/10.1021/ja405628g.

(8) Edwards, J. P.; Wolf, W. J.; Grubbs, R. H. The Synthesis of Cyclic Polymers by Olefin Metathesis: Achievements and Challenges. *J. Polym. Sci. Part A Polym. Chem.* **2019**, *57* (3), 228–242. https://doi.org/10.1002/pola.29253.

(9) Ochs, J.; Pagnacco, C. A.; Barroso-Bujans, F. Macrocyclic Polymers: Synthesis, Purification, Properties and Applications. *Prog. Polym. Sci.* **2022**, *134*, 101606. https://doi.org/https://doi.org/10.1016/j.progpolymsci.2022.101606.

(10) Wang, T.; Golder, M. R. Advancing Macromolecular Hoop Construction: Recent Developments in Synthetic Cyclic Polymer Chemistry. *Polym. Chem.* **2021**, *12*, 958–969. https://doi.org/10.1039/d0py01655a.

(11) Morrison, C. M.; Golder, M. R. Ring-Expansion Metathesis Polymerization Initiator Design for the Synthesis of Cyclic Polymers. *Synlett* **2022**, *33* (08), 699–704. https://doi.org/10.1055/s-0041-1737802.

(12) Miao, Z.; Gonsales, S. A.; Ehm, C.; Mentink-Vigier, F.; Bowers, C. R.; Sumerlin, B. S.;

Veige, A. S. Cyclic Polyacetylene. *Nat. Chem.* **2021**, *13* (8), 792–799. https://doi.org/10.1038/s41557-021-00713-2.
(13) Nadif, S. S.; Kubo, T.; Gonsales, S. A.; VenkatRamani, S.; Ghiviriga, I.; Sumerlin, B. S.; Veige, A. S. Introducing "Ynene" Metathesis: Ring-Expansion Metathesis Polymerization Leads to Highly Cis and Syndiotactic Cyclic Polymers of Norbornene. *J. Am. Chem. Soc.* **2016**, *138* (20), 6408–6411. https://doi.org/10.1021/jacs.6b03247.
(14) Roland, C. D.; Li, H.; Abboud, K. A.; Wagener, K. B.; Veige, A. S. Cyclic Polymers from Alkynes. *Nat. Chem.* **2016**, *8*, 791–796. https://doi.org/10.1038/nchem.2516.
(15) Mandal, U.; Ghiviriga, I.; Abboud, K. A.; Lester, D. W.; Veige, A. S. Double Tethered Metallacyclobutane Catalyst for Cyclic Polymer Synthesis. *J. Am. Chem. Soc.* **2021**, *143* (41), 17276–17283. https://doi.org/10.1021/jacs.1c08806.
(16) Bielawski, C. W.; Benitez, D.; Grubbs, R. H. An "Endless" Route to Cyclic Polymers. *Science (80-.).* **2002**, *297* (5589), 2041–2044. https://doi.org/10.1126/science.1075401.
(17) Bielawski, C. W.; Benitez, D.; Grubbs, R. H. Synthesis of Cyclic Polybutadiene via Ring-Opening Metathesis Polymerization: The Importance of Removing Trace Linear Contaminants. *J. Am. Chem. Soc.* **2003**, *125* (28), 8424–8425. https://doi.org/10.1021/ja034524l.
(18) Boydston, A. J.; Xia, Y.; Kornfield, J. A.; Gorodetskaya, I. A.; Grubbs, R. H. Cyclic Ruthenium-Alkylidene Catalysts for Ring-Expansion Metathesis Polymerization. *J. Am. Chem. Soc.* **2008**, *130* (11), 12775–12782. https://doi.org/10.1021/ja8037849.
(19) Xia, Y.; Boydston, A. J.; Yao, Y.; Kornfield, J. A.; Gorodetskaya, I. A.; Spiess, H. W.; Grubbs, R. H. Ring-Expansion Metathesis Polymerization: Catalyst-Dependent Polymerization Profiles. *J. Am. Chem. Soc.* **2009**, *131* (7), 2670–2677. https://doi.org/10.1021/ja808296a.
(20) Wang, T.-W.; Huang, P.-R.; Chow, J. L.; Kaminsky, W.; Golder, M. R. A Cyclic Ruthenium Benzylidene Initiator Platform Enhances Reactivity for Ring-Expansion Metathesis Polymerization. *J. Am. Chem. Soc.* **2021**, *143* (19), 7314–7319. https://doi.org/10.1021/jacs.1c03491.
(21) Levenson, A. M.; Morrison, C. M.; Huang, P.-R.; Wang, T.-W.; Carter-Schwendler, Z.; Golder, M. R. Ancillary Ligand Lability Improves Control in Cyclic Ruthenium Benzylidene Initiated Ring-Expansion Metathesis Polymerizations. *ACS Macro Lett.* **2023**, 1286–1292. https://doi.org/10.1021/acsmacrolett.3c00520.
(22) Lehman, S. E.; Wagener, K. B. Synthesis of Ruthenium Olefin Metathesis Catalysts with Linear Alkyl Carbene Complexes. *Organometallics* **2005**, *24* (7), 1477–1482. https://doi.org/10.1021/om049176q.